ICSNC 2020

The Fifteenth International Conference on Systems and Networks Communications

ISBN: 978-1-61208-828-0

October 18 -22, 2020

ICSNC 2020 Editors

Jorge Cobb, The University of Texas at Dallas, USA

Abdallah A. Alshehri, Petroleum Scientist, Saudi Aramco, Saudi Arabia

Klemens Katterbauer, Deep Learning Specialist, Saudi Aramco, Saudi Arabia

ICSNC 2020

Forward

The Fifteenth International Conference on Systems and Networks Communications (ICSNC 2020), held on October 18 - 22, 2020, continued a series of events covering a broad spectrum of systems and networks related topics.

As a multi-track event, ICSNC 2020 served as a forum for researchers from the academia and the industry, professionals, standard developers, policy makers and practitioners to exchange ideas. The conference covered fundamentals on wireless, high-speed, mobile and Ad hoc networks, security, policy based systems and education systems. Topics targeted design, implementation, testing, use cases, tools, and lessons learnt for such networks and systems

The conference had the following tracks:

- TRENDS: Advanced features
- WINET: Wireless networks
- HSNET: High speed networks
- SENET: Sensor networks
- MHNET: Mobile and Ad hoc networks
- AP2PS: Advances in P2P Systems
- MESH: Advances in Mesh Networks
- VENET: Vehicular networks
- RFID: Radio-frequency identification systems
- SESYS: Security systems
- MCSYS: Multimedia communications systems
- POSYS: Policy-based systems
- PESYS: Pervasive education system

We welcomed technical papers presenting research and practical results, position papers addressing the pros and cons of specific proposals, such as those being discussed in the standard forums or in industry consortiums, survey papers addressing the key problems and solutions on any of the above topics, short papers on work in progress, and panel proposals.

We take here the opportunity to warmly thank all the members of the ICSNC 2020 technical program committee as well as the numerous reviewers. The creation of such a broad and high quality conference program would not have been possible without their involvement. We also kindly thank all the authors that dedicated much of their time and efforts to contribute to the ICSNC 2020. We truly believe that thanks to all these efforts, the final conference program consists of top quality contributions.

This event could also not have been a reality without the support of many individuals, organizations and sponsors. We also gratefully thank the members of the ICSNC 2020 organizing committee for their help in handling the logistics and for their work that is making this professional meeting a success. We gratefully appreciate to the technical program committee co-chairs that contributed to identify the appropriate groups to submit contributions.

We hope the ICSNC 2020 was a successful international forum for the exchange of ideas and results between academia and industry and to promote further progress in networking and systems communications research.

ICSNC 2020 Publicity Chair

Lorena Parra, Universitat Politecnica de Valencia, Spain

ICSNC 2020

Committee

ICSNC 2020 Publicity Chair

Lorena Parra, Universitat Politecnica de Valencia, Spain

ICSNC 2020 Technical Program Committee

Ahmed M. Abdelmoniem, KAUST, Saudi Arabia
Baadache Abderrahmane, University of Benyoucef Benkhadda, Algeria
Ishtiaq Ahmad, University of South Australia, Australia
Francisco Airton Silva, Universidade Federal do Piauí, Brazil
Abdelkaher Ait Abdelouahad, Chouaib Doukkali University, Morocco
Alper Akarsu, HAVELSAN, Turkey
Lina Alfantoukh, King Faisal Specialist Hospital & Research Centre, Riyadh, Saudi Arabia
Reem Alshahrani, Taif University, Saudi Arabia
Abdallah A. Alshehri, Saudi Aramco, Dhahran, Saudi Arabia
Sarah Al-Shareeda, University of Bahrain, Bahrain
Mourad Amad, Bouira University, Algeria
Muhammad Sohaib Ayub, Lahore University of Management Sciences (LUMS), Pakistan
V. Balasubramanian, Arizona State University, USA
Ilija Basicevic, University of Novi Sad, Serbia
Mohamed Benmohammed, University Constantine2, Algeria
Robert Bestak, Czech Technical University in Prague, Czech Republic
Muhammad Danial Bin Zakaria, Universiti Sultan Zainal Abidin, Malaysia
Eugen Borcoci, University "Politehnica"of Bucharest (UPB), Romania
Christos Bouras, University of Patras, Greece
An Braeken, Vrije Universiteit Brussel, Belgium
Uwe Breitenbücher, University of Stuttgart, Germany
Francesco Buccafurri, University of Reggio Calabria, Italy
Dumitru Dan Burdescu, University of Craiova, Romania
Dalton Cézane Gomes Valadares, Federal Institute of Pernambuco (IFPE), Brazil
Hao Che, University of Texas at Arlington, USA
Fuxiang Chen, DeepSearch Inc., Korea
Enrique Chirivella-Perez, University of the West of Scotland, UK
Dickson K.W. Chiu, University of Hong Kong, Hong Kong
Domenico Ciuonzo, University of Naples "Federico II", Italy
Monireh Dabaghchian, George Mason University, USA
Vincenzo De Angelis, University of Reggio Calabria, Italy
Katja Gilly de la Sierra-Llamazares, Universidad Miguel Hernández, Spain
Mehmet Demirci, Karadeniz Technical University, Turkey
Luis Diez, University of Cantabria, Spain
Mustapha Djeddou, National Polytechnic School, Algiers, Algeria

Copyright Information

For your reference, this is the text governing the copyright release for material published by IARIA.

The copyright release is a transfer of publication rights, which allows IARIA and its partners to drive the dissemination of the published material. This allows IARIA to give articles increased visibility via distribution, inclusion in libraries, and arrangements for submission to indexes.

I, the undersigned, declare that the article is original, and that I represent the authors of this article in the copyright release matters. If this work has been done as work-for-hire, I have obtained all necessary clearances to execute a copyright release. I hereby irrevocably transfer exclusive copyright for this material to IARIA. I give IARIA permission or reproduce the work in any media format such as, but not limited to, print, digital, or electronic. I give IARIA permission to distribute the materials without restriction to any institutions or individuals. I give IARIA permission to submit the work for inclusion in article repositories as IARIA sees fit.

I, the undersigned, declare that to the best of my knowledge, the article is does not contain libelous or otherwise unlawful contents or invading the right of privacy or infringing on a proprietary right.

Following the copyright release, any circulated version of the article must bear the copyright notice and any header and footer information that IARIA applies to the published article.

IARIA grants royalty-free permission to the authors to disseminate the work, under the above provisions, for any academic, commercial, or industrial use. IARIA grants royalty-free permission to any individuals or institutions to make the article available electronically, online, or in print.

IARIA acknowledges that rights to any algorithm, process, procedure, apparatus, or articles of manufacture remain with the authors and their employers.

I, the undersigned, understand that IARIA will not be liable, in contract, tort (including, without limitation, negligence), pre-contract or other representations (other than fraudulent misrepresentations) or otherwise in connection with the publication of my work.

Exception to the above is made for work-for-hire performed while employed by the government. In that case, copyright to the material remains with the said government. The rightful owners (authors and government entity) grant unlimited and unrestricted permission to IARIA, IARIA's contractors, and IARIA's partners to further distribute the work.

Table of Contents

Media Content Delivery Protocols Performance and Reliability Evaluation in Cellular Mobile Networks

Kirill Krinkin, Igor Dronnikov
Saint Petersburg Electrotechnical University "LETI"
Saint-Petersburg, Russia
email: kirill@krinkin.com, dronnikovigor@gmail.com

***Abstract*—Currently, tens of millions of devices around the world communicate with each other via cellular networks. In this paper, we study the stability of network content delivery protocols to the effects of network interference. To conduct the research, a tool was developed that allows testing of protocols, such as TCP, UDP and QUIC. The analysis and comparison of the obtained test results was carried out. In the conclusion, the best protocols for the content delivery were shown.**

Keywords—Network content delivery protocols; network performance; network reliability; interference; TCP; UDP; QUIC; rtt; packet loss; bandwidth.

I. INTRODUCTION

It is difficult to imagine the modern world without means of communication. Every day, tens of millions of devices around the world communicate via computer networks. However, as the number of devices increases, so does the number of terms of use for these devices. So, some users of modern means of communication have a good stable connection, while other users may have problems connecting. An unstable network connection usually occurs when using wireless networks inside reinforced concrete buildings, or outside of large cities where the network infrastructure is not very well developed. As a result, device users may receive certain content with delays, or only partially - due to a connection failure.

At the same time, each network is organized according to the appropriate standards. All devices communicate according to the generally accepted Open Systems Interconnection model (OSI) standard, usually using the most popular transport protocols Transmission Control Protocol (TCP) or User Datagram Protocol (UDP). This is why any company that generates a large amount of traffic sooner or later thinks about what protocol it should use in its work, so that customers who would like to receive the content of this company, get it quickly and in full, regardless of the quality of connection on the client's device. Thus, the relevance of the problem lies in the complexity of choosing the appropriate protocol, since each protocol has its own set of features, in particular, different resistance to network interference. In accordance with this, it is necessary to study the stability of TCP and UDP protocols to the effects of network interference, as well as to compare them with the new protocol from Google - Quick UDP Internet Connections (QUIC) [1].

Most people [2] access social networks from mobile devices via cellular networks. The most common access pattern is the request media (image and video thumbnails) for the content feed. It motivated us to study the performance and reliability of the content delivery protocols via cellular networks (2G, 3G, 4G, Long-Term Evolution (LTE) etc).

In Section 2, a study of the current state of the problem was conducted, and works on this topic were studied. Section 3 describes network simulation using the developed tools and we provide a description of the protocols under test, including a brief description of how they work. In Section 4, we provide a description of the test cases during the experiment. Also, we give an analysis of the results obtained during the experiment.

II. RELATED WORKS

Since the problem described in the previous section has been relevant for a long period of time, there are a number of works describing the pros and cons of the TCP and UDP protocols, as well as their comparison. For example, AL-Dhief et al. [3] studied the performance of TCP and UDP protocols in order to identify the best protocol. In this work, attention is paid to such network parameters as delay, network throughput, delivery ratio of packets and packet loss ratios. The authors of this work tested the protocols on two scenarios and found that TCP is more efficient and reliable than UDP. The advantages of this work include detailed theoretical calculations, a description of the testing method and a test bench. This paper also describes the calculation of metrics and provides the resulting graphs. The disadvantages of this work include a small number of test scenarios - only changes in the speed parameters and data sizes were considered. In addition, parameters such as delay and packet loss are considered only as the results of the action of the two parameters being changed, and not as the cause.

Another paper, Coonjah et al. [4] examine the performance of TCP and UDP protocols inside TCP and UDP tunnels. The authors conclude that TCP in the UDP tunnel provides better latency. Also, in this work, a series of tests were performed, UDP traffic was sent inside the UDP tunnel and the TCP tunnel sequentially. The same tests were performed using TCP traffic. The advantages of the work include a detailed theoretical description of the protocols, as well as the test stand. This paper contains a detailed description of test scenarios and resulting graphs. Disadvantages include insufficient coverage of the impact on performance of other parameters, such as latency, packet

 ISBN: 978-1-61208-828-0

loss, and network speed, as well as the possible presence of network interference in the test stand using physical switching between devices.

The next paper, M. P. Sarma [5] considers the issue of performance evaluation based on modeling of transport layer protocols TCP and UDP using two popular queue management methods: Random Early Detection (RED) and Tail Drop. Performance is evaluated in terms of throughput, queue latency, packet drop rate, and bandwidth usage. In the conclusions, the author points out that the simulation results show that RED is superior to Tail Drop in terms of queue latency and packet drop rate. However, the performance of queue management algorithms also depends on the protocols they are applied to, TCP or UDP. The type of network topology, whether it is a shared UDP and TCP topology, or just one type of client topology also affects the performance of buffer management. For some applications, UDP using the RED queue will provide better performance, and for reliable packet delivery, TCP using the RED queue will be better than other protocols and queues in a high-speed Local Area Network (LAN). The positive aspects of this work include a detailed description of the work of queues and the test stand, as well as a detailed review of the results and the variability of test scenarios. The disadvantages of this work include that parameters such as delay and packet loss are considered only as side effects.

Another paper, S. A. Nor et al. [6] analyze the transport layer protocols that are used for video streaming. Furthermore, through simulation results, performed in Network Simulator – 3 (NS-3), the strength and weaknesses of TCP, Scalable TCP (SCTP), Datagram Congestion Control Protocol (DCCP) and UDP are presented that may give the idea of selecting the best protocols for the LTE environment. Also, this performance evaluation can provide a base to determine which protocol can be better for which metrics among the four, i.e., end to end delay, throughput, packet loss, and average jitter. The advantages of the work include good theoretical description of measurements and graphs for results. In addition, it would be interesting to see comparison with 2G, 3G, Wi-Fi, though it is not mentioned in paper state.

As seen in this section, despite the fact that the question of comparing the performance and resistance of TCP and UDP protocols to interference has been open for a long time, the results of the work still vary for different situations. Therefore, the task of studying the stability of protocols to the effects of cellular mobile networks interference is relevant.

III. EVALUATION APPROACH

The NetPacket Simulator tool [7] was developed to solve the problem of investigating the stability of protocols to network interference. This tool can be used to describe various network connection configurations and emulate possible network interference. For example, this tool can be used to see how the following parameters affect data transmission:

- RTT - round-trip time, the time it takes for the data packet to reach the recipient and the confirmation of receipt to reach the sender.
- Bandwidth - maximum data transfer speed over the network.
- Packet Loss - packet loss occurs when one or more data packets passing through the computer network do not reach their destination. Packet loss is caused by errors in data transmission, usually over wireless networks, or network congestion. Packet loss is measured as the percentage of lost packets relative to sent packets.
- Upload/Download rate - download speed is the speed at which data is transferred from the Internet to the user's computer. The upload speed is the speed of data transfer from the user's computer to the Internet. Internet companies often provide an asymmetric communication channel by default - loading is faster than return. The reason for this is that most people need to download information more. This allows the user to quickly download movies, music, and a large number of documents.
- Multiple clients - running multiple clients on the same network.

The developed tool works on the basis of virtual network drivers TUN/TAP. TUN/TAP is used to provide packet reception and transmission for user space programs. TUN (stands for network TUNnel) is a network layer device and TAP (stands for network TAP) is a link layer device. Both of them are virtual network kernel devices — this allows one to organize a virtual network within a single physical device, which eliminates the occurrence of uncontrolled network interference, if the network is organized between several physical devices.

Before conducting the experiment, it should be noted that the TCP data transfer protocol has a built-in implementation of data receipt verification and in case of loss of any packets, it will independently re-forward the lost data and guarantee their delivery. Therefore, a TCP connection can be organized directly "out of the box" - one just needs to describe the connection setup on the client and server and be sure of 100% data delivery.

In the case of the UDP data transfer protocol, the situation is different. Although a UDP connection can be set up right out of the box, UDP does not implement data receipt checks and does not guarantee that the client will receive them. Thus, if one needs to make sure that the data reached the client in its entirety or some part was lost, one must implement data integrity checks, re-forwarding, and other mechanisms oneself.

One of the add-ons for the UDP protocol with its own implementation of all mechanisms is QUIC. As shown in Figure 1, QUIC is located under HyperText Transfer Protocol 3 (HTTP/3). It partially replaces the HyperText Transfer Protocol Secure (HTTPS) and TCP layers, using UDP for packet generation. QUIC only supports secure data transfer, since Transport Layer Security (TLS) is fully embedded in QUIC.

 ISBN: 978-1-61208-828-0

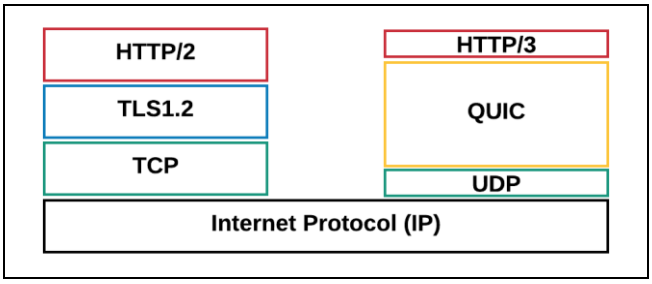

Figure 1. TCP and QUIC protocol stack

Since the purpose of our research is to compare the TCP, UDP and QUIC protocols, it is necessary to implement a full-fledged comparison for the UDP protocol, as well as mechanisms for establishing a connection, making up for losses, and confirming data receipt. This is because, for any potential use of the UDP protocol, it will be necessary to implement these mechanisms if the ultimate goal is guaranteed delivery of content to the client. Thus, our implementation of the self-made UDP (smUDP) protocol that will participate in testing will have the following mechanisms implemented: Error Correction, Pacing, Flow Control, and Congestion Control.

IV. EVALUATION

To study the stability of protocols to network interference, the following experimental scenarios were identified. Among network interference cases we selected: RTT, Bandwidth, Packet Loss, Upload/Download rate, and Congestion Control window size. These scenarios reflect the most popular network connections. The information for the scenarios was collected by studying the statistics of usage by real social network users [8]:

A. *Wi-Fi*

- RTT - 110 ms
- Packet Loss - 0.5%
- Bandwidth - 2.2 Mbit/s
- Upload/Download rate - 0.7
- Congestion Control window - 1 mbyte
- File Size - 50, 100, 250, 500, 1000 Kbytes

B. *LTE*

- RTT - 250 ms
- Packet Loss - 0.7%
- Bandwidth - 2.0 Mbit/s
- Upload/Download rate - 0.7
- Congestion Control window - 1 mbyte
- File Size - 50, 100, 250, 500, 1000 Kbytes

C. *3G*

- RTT - 550 ms
- Packet Loss - 0.5%
- Bandwidth - 1.0 Mbit/s
- Upload/Download rate - 0.7
- Congestion Control window - 1 mbyte
- File Size - 50, 100, 250, 500, 1000 Kbytes

D. *2G*

- RTT - 900 ms
- Packet Loss - 2.5%
- Bandwidth - 0.2 Mbit/s
- Upload/Download rate - 0.7
- Congestion Control window - 1 mbyte
- File Size - 50, 100, 250, 500, 1000 Kbytes

E. *RTT influence*

- RTT - 10, 50, 100, 250, 500, 750, 1000 ms
- Packet Loss - 0.5%
- Bandwidth - 2.2 Mbit/s
- Upload/Download rate - 0.7
- Congestion Control window - 1 mbyte
- File Size - 250 Kbytes

F. *Packet Loss influence*

- RTT - 100 ms
- Packet Loss - 0.5, 1.0, 1.5, 2.0, 2.5%
- Bandwidth - 2.2 Mbit/s
- Upload/Download rate - 0.7
- Congestion Control window - 1 mbyte
- File Size - 250 Kbytes

G. *Bandwidth influence*

- RTT - 100 ms
- Packet Loss - 0.5%
- Bandwidth - 0.2, 0.6, 1.0, 1.4, 1.8, 2.2 Mbit/s
- Upload/Download rate - 0.7
- Congestion Control window - 1 mbyte
- File Size - 4096 Kbytes

Based on these scenarios, network connection configurations were described and the average time required for query execution to get the required amount of data was measured. The average time per request was calculated based on data on the execution time of five repeated simulations.

After the experiments had been performed, the results were summarized in the following Tables I - VII:

TABLE I. WI-FI

File Size, kbytes	smUDP, ms	QUIC, ms	TCP, ms
5	137	373	206
100	163	492	538
250	234	597	1 442
500	278	741	2 436
1000	563	1 386	4 784

TABLE II. LTE

File Size, kbytes	smUDP, ms	QUIC, ms	TCP, ms
5	304	594	447
100	408	966	1 310
250	516	1 370	3 395
500	530	2 063	7 182
1000	1 052	3 231	11 682

 ISBN: 978-1-61208-828-0

TABLE III. 3G

File Size, kbytes	smUDP, ms	QUIC, ms	TCP, ms
5	663	1 136	956
100	777	2 044	1 767
250	1 115	2 437	4 086
500	1 129	3 580	5 852
1000	2 248	5 383	12 439

TABLE IV. 2G

File Size, kbytes	smUDP, ms	QUIC, ms	TCP, ms
5	1 083	2 196	1 130
100	1 809	4 121	6 229
250	2 575	5 900	14 637
500	4 575	10 549	27 493
1000	8 403	17 379	59 152

TABLE V. RTT INFLUENCE

RTT, ms	smUDP, ms	QUIC, ms	TCP, ms
10	38	91	214
50	114	300	721
100	233	546	1 355
250	516	1 297	3 082
500	1 018	2 212	3 916
750	1 518	3 316	4 220
1000	1 816	4 505	5 411

TABLE VI. PACKET LOSS INFLUENCE

PL, %	smUDP, ms	QUIC, ms	TCP, ms
0.5	198	688	1 334
1	218	728	1 701
1.5	237	756	2 144
2	220	852	2 721
2.5	237	929	3 145

TABLE VII. BANDWIDTH INFLUENCE

Bandwidth, Mbit/s	smUDP, ms	QUIC, ms	TCP, ms
0.2	29 556	29 707	29 567
0.6	9 847	10 135	17 792
1	5 843	9 450	17 754
1.4	4 131	9 544	17 730
1.8	3 183	9 430	17 971
2.2	2 588	9 516	17 758

The obtained data on the stability of each data transfer protocol to network interference are shown in Figures 2 – 5, 7 – 9.

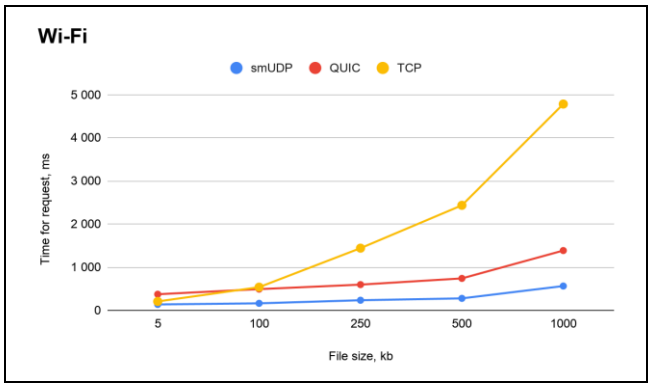

Figure 2. Wi-Fi

In Figures 2 through 5, we can see that the TCP protocol has worse behavior than other protocols. While for QUIC and smUDP, the increase in request time increases linearly with the increase in the size of the requested file, for TCP, there is an exponential increase.

TCP is designed in such a way that TCP generally uses a TCP 3-way handshake [9]: the sender sends a SYN packet, waits for a SYN-ACK packet from the recipient, then sends an ACK packet.

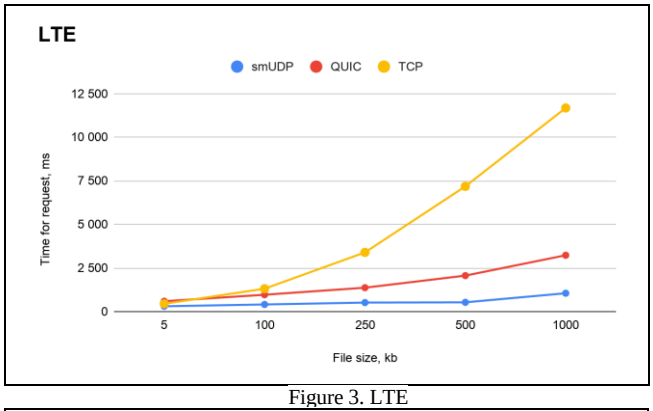

Figure 3. LTE

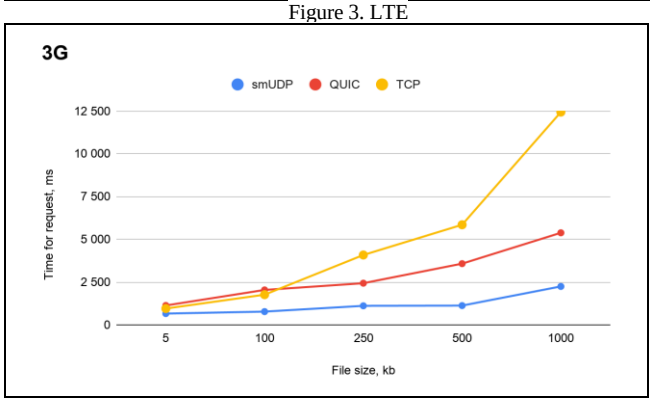

Figure 4. 3G

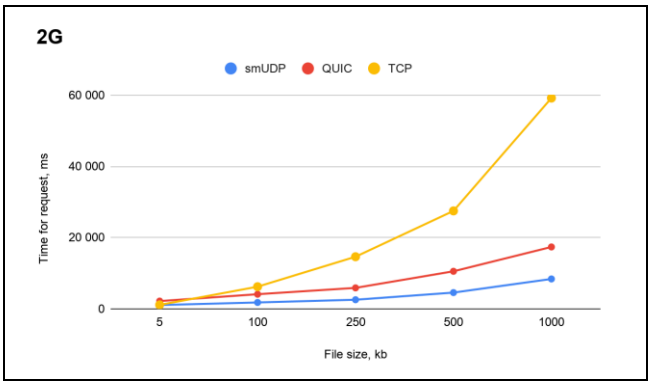

Figure 5. 2G

Additional second and third passes are spent on creating a TCP connection, while UDP and protocols based on it do not spend time on this and can send data in the first packet (see Figure 6). However, after the connection is established, the recipient continues to send a confirmation of receipt of each packet (ACK) to ensure reliable delivery.

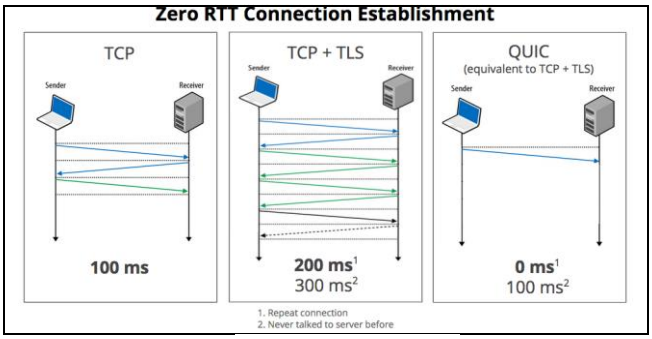

Figure 6. zeroRTT vs TCP

If a packet or ACK is lost, the sender makes a retransmission after a timeout (retransmission timeout - RTO). The RTO is calculated dynamically based on various factors, such as the expected RTT delay between the sender and receiver. At the same time, the RTT change is not expected to significantly affect the delivery speed - the growth is similar to that of UDP-based protocols, as shown in Figure 7.

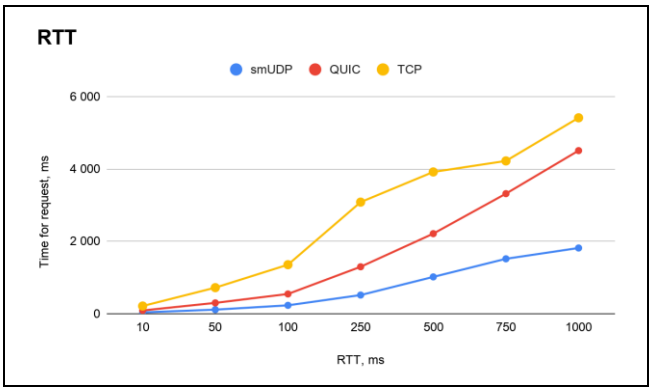

Figure 7. RTT impact comparison

However, due to the fact that some packets with ACK or the data itself may be lost due to network connection instability in TCP, the query execution time is greatly increased. This disadvantage can be clearly observed in Figure 8. In contrast to UDP-based protocols, with an increase in the percentage of lost packets, TCP also increases the time of data delivery. QUIC and smUDP demonstrate stable delivery speed, despite the presence of problems in the connection. This development is due to the fact that QUIC calls two Tail Loss Probes (TLP) before the RTO works – even when the losses are very noticeable. This is different from TCP implementations. TLP mainly forwards the last packet (or a new one, if there is one) to start fast replenishment. This is also due to the fact that TCP was originally developed as a protocol for wired network connections - which is more stable than wireless networks [10]. Wireless networks are designed differently. To deal with fluctuations in bandwidth and loss, wireless networks usually use large buffers for traffic spikes. TCP very often treats the queue as a loss due to the increased response timeout, which is why TCP is forced to retransmit packets, which leads to a full buffer and a longer query execution time.

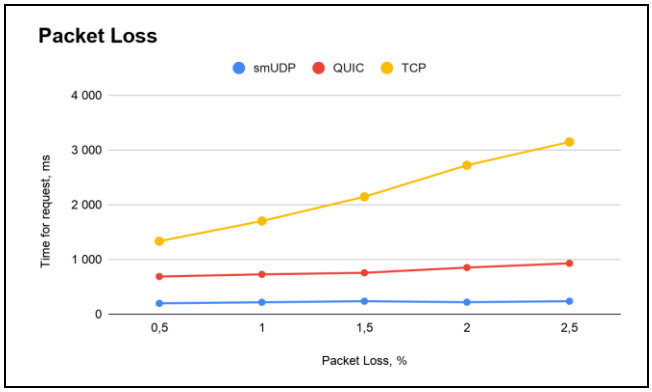

Figure 8. Packet Loss impact comparison

When studying the stability of protocols to change bandwidth, we can note that, in general, this parameter does not significantly affect the transfer speed. This is due to the fact that the TCP and QUIC protocols contain an implementation of Congestion Control that limits the channel load, as shown in Figure 9. This saves the network from being overloaded. This is because, if the network is overloaded, it is quite likely that data is sent, some packets do not reach the destination, then more data is sent, and all this data is lost again. Congestion Control is responsible for limiting the output of data in certain portions.

 ISBN: 978-1-61208-828-0

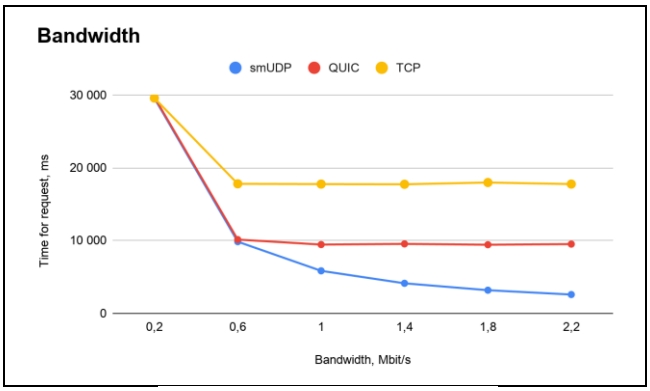

Figure 9. Bandwidth impact comparison

V. CONCLUSION

Based on the research in this paper, we can conclude that the TCP data transfer protocol is poorly optimized for wireless networks, which are currently very widely used and are rapidly spreading around the world, even in the most remote corners of it. Poor performance is associated with unstable wireless network connections. As a result, the data reaches the end customer over a longer period of time. However, the protocol provides guaranteed data delivery to the client.

At the same time, UDP-based protocols demonstrate good performance in fast data delivery to the client due to the fact that new solutions are implemented in new protocols separately by each protocol developer, and to use the protocol, it is enough to update the versions on the server and client. However, as for data integrity, this task falls on the shoulders of the one who will use this protocol for their own purposes.

It is also worth noting that there are already ready-made implementations of UDP-based protocols that are rapidly gaining popularity, such as QUIC. It is worth noting that QUIC is already used on 4.3% of all websites [11].

Thus, if the content on a service or resource is mostly consumed via wireless mobile networks, it is recommended to use a UDP-based protocol with its own implementation of the necessary mechanisms. However, if not enough resources are available to implement one's own protocol, one can use ready-made solutions. TCP can be used as a backup connection.

REFERENCES

[1] QUIC, [Online], Available from: https://www.chromium.org/quic [retrieved: August, 2020]

[2] Internet Stats & Facts, 2020, [Online], Available from: https://hostingfacts.com/internet-facts-stats/ [retrieved: August, 2020]

[3] AL-Dhief et al., "Performance Comparison between TCP and UDP Protocols in Different Simulation Scenarios.", International Journal of Engineering & Technology 7.4.36, 2018: pp. 172-176.

[4] I. Coonjah et al., "Experimental performance comparison between TCP vs UDP tunnel using OpenVPN.", International Conference on Computing, Communication and Security (ICCCS). IEEE, 2015: pp. 1-5

[5] M. P. Sarma, "Performance Measurement of TCP and UDP Using Different Queuing Algorithm in High Speed Local Area Network.", International Journal of Future Computer and Communication 2.6, 2013: pp. 682.

[6] S. A. Nor et al. "Simulated performance of TCP, SCTP, DCCP and UDP protocols over 4G network.", Procedia computer science, 111, 2017, pp. 2-7.

[7] NetPackets Simulator, [Online] Available from: https://github.com/dronnikovigor/NetPackets-Simulator [retrieved: August, 2020]

[8] A. Tobol, "UDP vs. TCP, or the Future of the network stack", Conference Saint HighLoad++, 2019, [Online] Available from: https://www.highload.ru/spb/2019/abstracts/4990 [retrieved: August, 2020]

[9] TCP 3-Way Handshake, [Online] Available from: https://www.inetdaemon.com/tutorials/internet/tcp/3-way_handshake.shtml [retrieved: August, 2020]

[10] Employing QUIC Protocol to Optimize Uber's App Performance, [Online] Available from: https://eng.uber.com/employing-quic-protocol/ [retrieved: August, 2020]

[11] Usage statistics of QUIC for websites, [Online] Available from: https://w3techs.com/technologies/details/ce-quic [retrieved: August, 2020]

 ISBN: 978-1-61208-828-0

Realization of RF and Microwave Energy Harvesting System Adapted to GSM 900 Network for Low Power Consumption Sensors Feeding

Chemseddine Benkalfate
Electrical and Electronics Engineering Department, ENSEA
Quartz laboratory
Cergy, France
e-mail: benkalfate.chemseddine@ensea.fr

Achour Ouslimani
Electrical and Electronics Engineering Department, ENSEA
Quartz laboratory
Cergy, France
e-mail: achour.ouslimani@ensea.fr

Abed-Elhak Kasbari
Electrical and Electronics Engineering Department, ENSEA
Quartz laboratory
Cergy, France
e-mail: abed-elhak.kasbari@ensea.fr

Mohammed Feham
Telecommunication Department, University of Tlemcen
STIC laboratory
Tlemcen, Algeria
e-mail: feham_m@yahoo.fr

***Abstract*— This paper presents a miniaturized Radio-Frequency (RF) and microwave energy harvesting system adapted to GSM-900 Network (Global System for Mobile Communication). Most researchers have worked in this domain by trying to harvest an enough DC output voltage to feed different electronic devices to ensure their energy autonomy. The matter with these systems lies in the antenna size. The proposed system is realized on Teflon hybrid technology. The size of the proposed multiband antenna is of 20x30x0.67 mm^3, and that of the rectifier matched to the antenna is of 10x15x0.67 mm^3. The measurement shows that the antenna is able to cover GSM900 (935 – 960) MHz, (1470 – 1550) MHz, GSM1900 (1935 – 1989) MHz and (3 – 3.2) GHz, bands. The output Direct Current (DC) harvested voltage measured is of 0.3 V for 2 kΩ resistance load. This result is sufficient for feeding low power consumption Wireless Sensor Networks (WSNs). In this paper, the selected temperature sensor operates for 0.2 V and 23 nW power supply. The equivalent resistor of this sensor is 2 kΩ. The DC output voltage can reach 0.8 V for open load.**

Keywords--RF Energy harvesting; Multi-bandes antenna; Miniaturized antenna; Impedance matching; Rectifier.

I. INTRODUCTION

The RF and micro-wave energy harvesting devices consist of 3 primary blocks, antenna, impedance matching and rectifier (see Figure 1). The antenna is a primordial device on these systems, which is a responsible of all electromagnetic waves catching from the environment with adapting frequencies and power levels. Antennas which allow to capture many waves at many frequency bandwidths improve widely the RF and microwave energy harvesting system performances. The proposed antenna is smallest (20x30x0.67 mm^3) compared to the GSM antennas (GSM-900, GSM-1800/1900) commonly used with keeping a high efficiency levels [7]. This answers to recommended miniaturization required for the harvesting systems [4][5]. The rectifier is matched to the antenna by using an impedance matching network, which is realized with Surface Mounted Devices (SMD) electronic elements (inductors and capacitors). The rectifier is based on Schottky diode (MBRS360T3G) and capacitor voltage doubler [5][8]. The dimension of the proposed RF and microwave energy harvesting circuit is of 10x15x0.67 mm^3. This miniaturized system could be used to power many applications (sensors, smart watches, etc.).

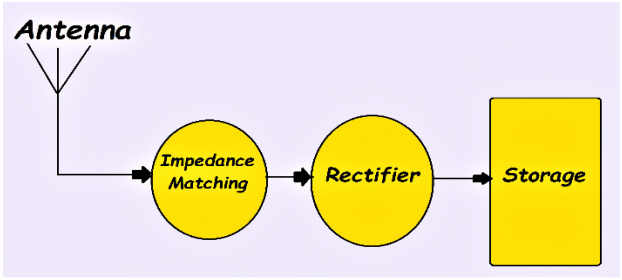

Figure 1. General RF energy harvesting system blocks [1].

II. ANTENNA SIMULATION CHARACTERISTICS

A. Antenna structure

Figure 2, depicts the proposed antenna structure.

 ISBN: 978-1-61208-828-0

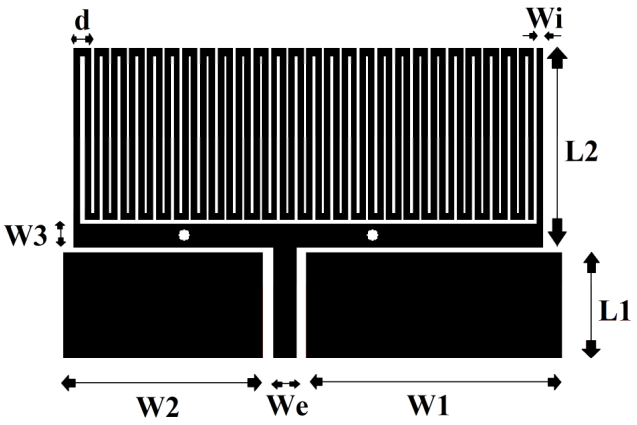

Figure 2. The proposed antenna structure .

The reported antenna in [10] is modified to cover multiband frequency by adding many meanders, which mean many bands. Each meander can be modeled electrically by inductors [3]. Table I presents the antenna dimensions in mm.

TABLE I. ANTENNA DIMENSIONS

L_1	L_2	W1	W2	W3	We	Wi	d
6	14	17	9	4	2	1.5	2

B. Antenna Response And Radiation Diagram

Figures 3 and 4 present respectively the return loss of this antenna and the radiation diagram getting by exploring the Computer Simulation Technology (CST) software.

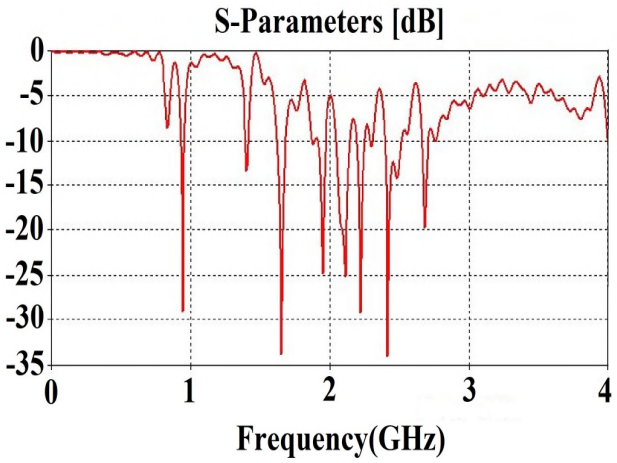

Figure 3. Simulated S_{11} antenna response.

we clearly see that this antenna is operational within the frequency bandwidths, (945 – 960) MHz with S11≤ -25 dB, (1780 – 1850) MHz with S11≤ -30dB, (1930 – 1980) MHz with S11≤ -25dB, (2450 – 2500) MHz with S11≤ -25dB and (2610 – 2680) MHz with S11≤ -20dB,

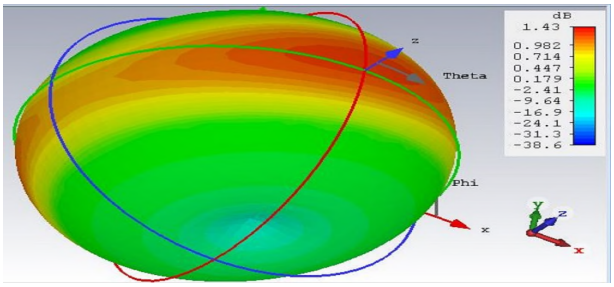

Figure 4. Radiation diagram at 948 MHz, 1.8 GHz, 1.96 GHz.

the radiation diagram of this antenna is omnidirectional, that is flawlessly tailored to the mobile communication GSM900, GSM1800 and GSM1900 (PCS network), the gain is around 1.43dB, 1.38 in linear scale.

C. Antenna Stability

The stability of this antenna is handled very cautiously by adjusting with precision its dimensions [9]-[11]. Figure 5 shows the smith-chart, in which the stability of this antenna appears when the graph stays inside the principal smith chart circle, as we can see, this antenna is within the stability restriction, because the S11 curve contacts the unit circle but it doesn't exceed it, in invers case we talk about the antenna instability. This analysis is imperative for such an antenna. Otherwise, the measured response might be definitely different from the simulations. The performance could then decrease drastically.

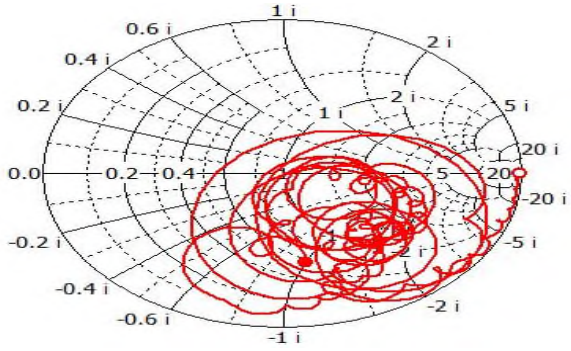

Figure 5. Smith chart representation.

D. Cosimulation Results

By using Advanced Design Systems (ADS) software (see Figure 6), the co-simulation response is depicted in the Figure 7.

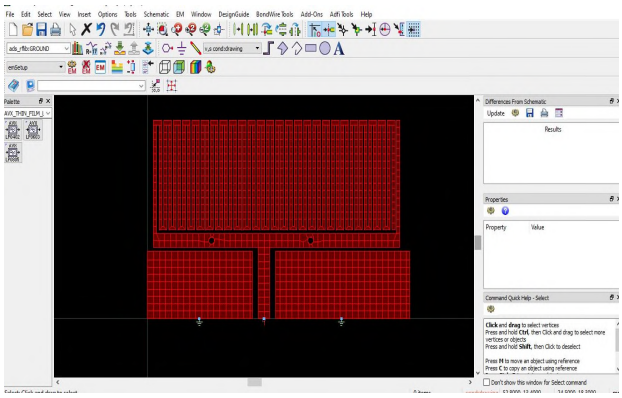

Figure 6. presented antenna model on ADS.

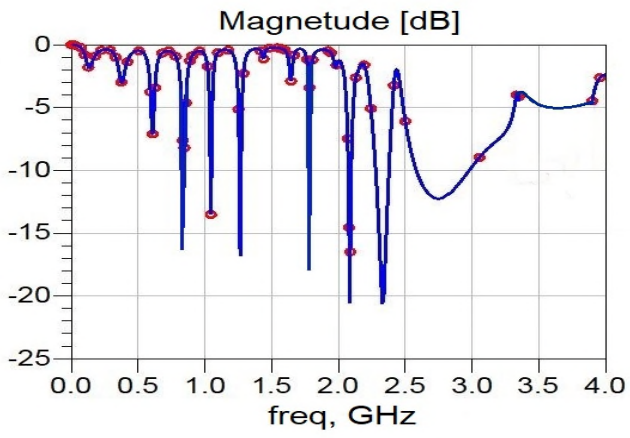

Figure 7. Proposed antenna co-simulation response.

In Figure 7, it is clear that the co-simulation response is in good agreement with that of the electromagnetic simulation obtained using CST software (see Figure 3).

E. Antenna Electrical Equivalent Circuit

As we noted in Section II-A, this antenna is formed from many LC resonators, theoretically [3], the meandered antennas models can be translated electrically to a superposition of many LC resonators as presented in the Figure 8. These resonator successions allow to have a multi-bands antenna, in level of sum resonators. The electromagnetic coupling phenomena are possible, due to the same resonance frequency of sum resonators.

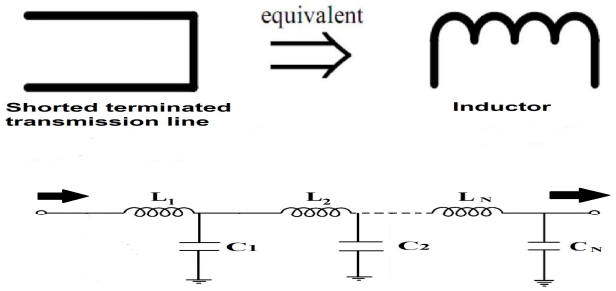

Figure 8. Equivalent electrical element.

We simulate the response of this antenna equivalent circuit on ADS. The proposed model is depicted in Figure 9, and its response in Figure 10.

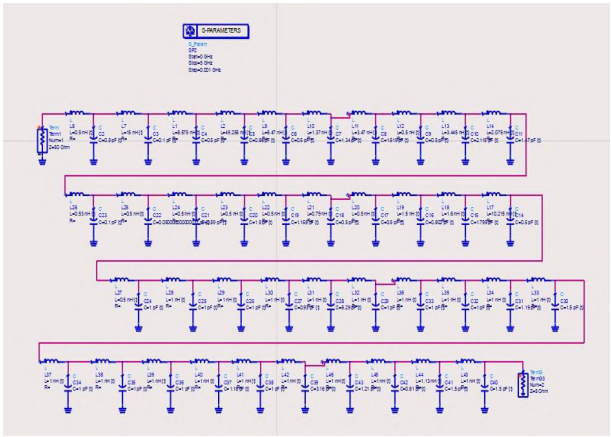

Figure 9. Equivalent electrical circuit on ADS software.

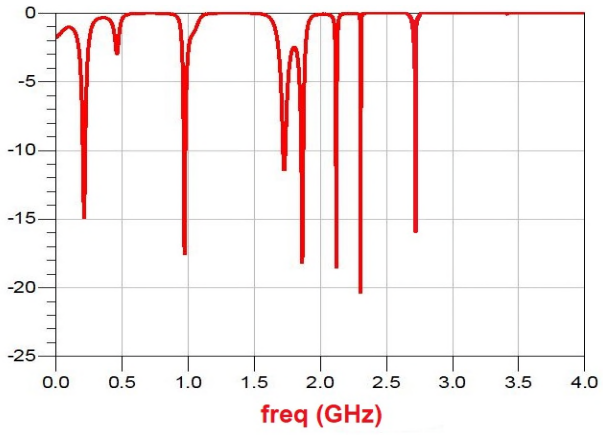

Figure 10. Antenna electrical equivalent circuit response.

 ISBN: 978-1-61208-828-0

We can clearly see in Figure 10, the electrical equivalent circuit response is too adapted to the simulation and co-simulation one, such as, for GSM900 band (950-960) MHz the S11 ⩽ -15 dB, GSM1900 (PSC) the S11 ⩽ -15 dB, UMTS2100 S11⩽-15 dB, Wi-Fi 2.45 GHz S11⩽-20 dB, LTE 2.6 GHz S11⩽-15 dB.

III. REALIZED ANTENNA AND MEASUREMENT

A. Realized Antenna Model

The proposed antenna structure represented in Figure 11, is printed on Teflon substrate (εr=2.1) with a dimension of 20 x 30 x 0.67 mm^3.

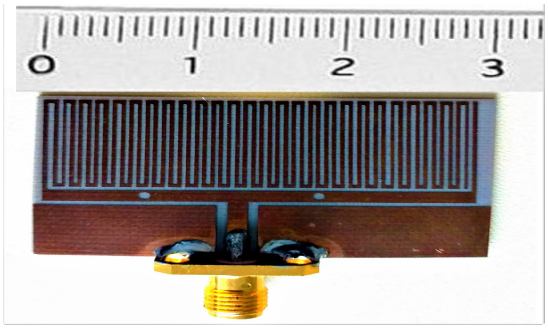

Figure 11. Realized antenna model.

B. Measured Response

Figure 12 shows the S_{11} parameter measured on vector network analyzer.

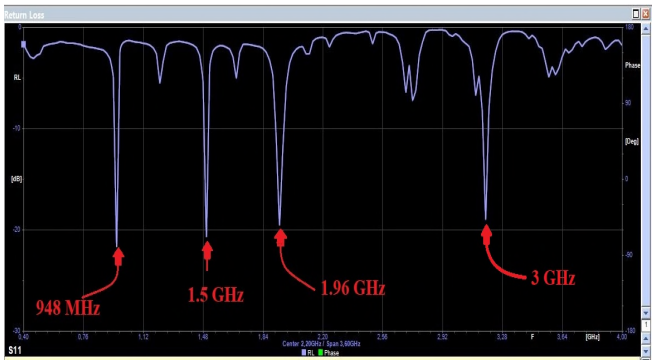

Figure 12. Measured antenna response.

In Figure 12, we see that this antenna is perfectly matched to GSM-900 and GSM-1900 bands. At the frequency 948 MHz the S_{11} is less than -20 dB and equal to -19 dB for 1.96 GHz frequency, there are two other resonance frequencies, at 1.5 GHz and 3 GHz with an S_{11} less than -18 dB.

IV. RECTIFIER AND IMPEDANCE MATCHING CIRCUITS

C. Proposed Rectifier

The rectification circuit has the function of transforming an alternating signal into another continuous. The proposed circuit is designed based on Schottky diodes (MBRS360T3G), and two capacitors connected in parallel which allows to double the output DC voltage. Figure 13 shows the proposed rectification circuit.

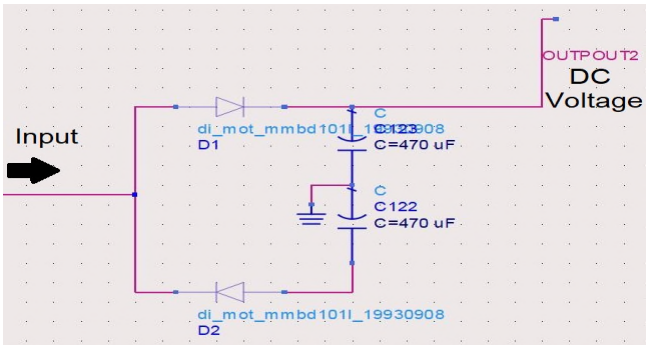

Figure 13. The proposed rectifier.

An impedance matching circuit is required to match this circuit to the antenna. The first step is to calculate the equivalent impedance of the rectifier, by using ADS software and streaming Smith chart. Figure 14 depicts the value of this impedance. At this level, we know both impedance va-

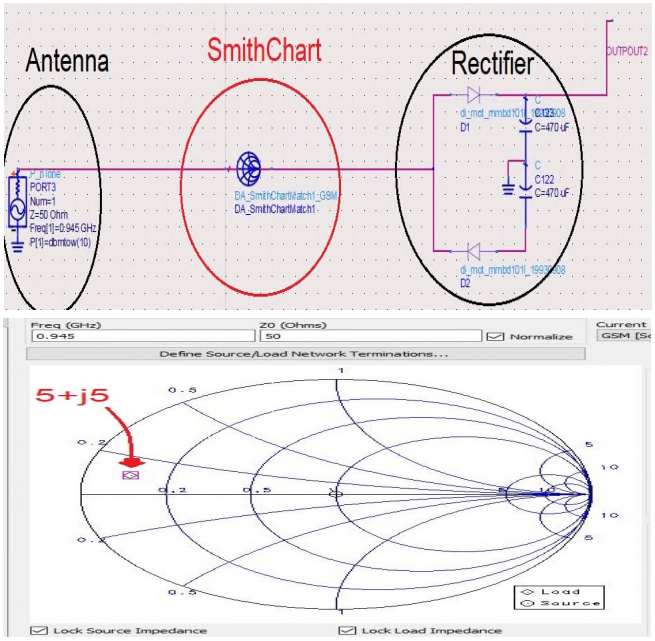

Figure 14. Smith Chart Presentation (Zeq = 5+j5).

lues, 50 Ohm for the antenna and 5+j5 Ohm for the rectifier. Now, we can design the impedance matching circuit between both sides (antenna and rectifier).

D. Proposed Impedance Matching

Figure 15 shows the proposed model designed on ADS software.

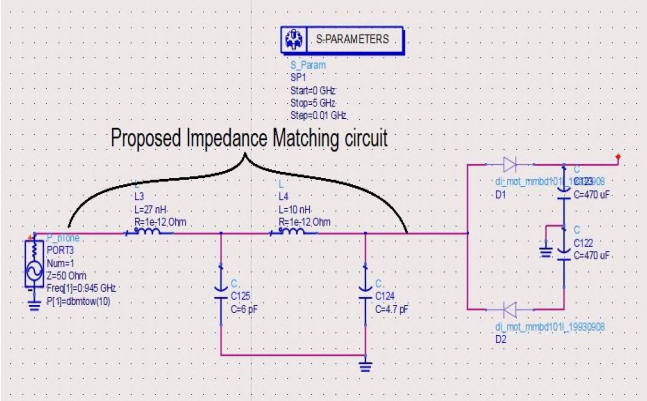

Figure 15. Proposed impedance matching circuit.

For adapting this circuit to GSM-900, we use Smith chart on ADS software, which is presented in Figure 16.

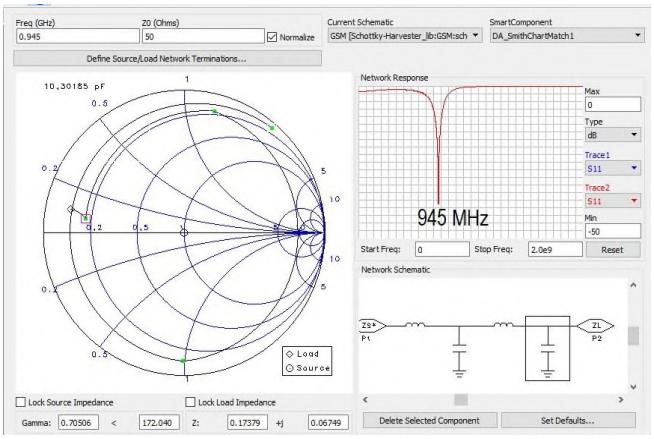

Figure 16. Impedance matching circuit S11.

We can clearly see that the proposed circuit is too adapted to GSM-900 at 945 MHz, the value of each elements is tuned by ADS, we can also calculate them by using the resonance formula.

E. Simulated Output DC Voltage

Figure 17 presents simulated output voltage for -40 dBm input power.

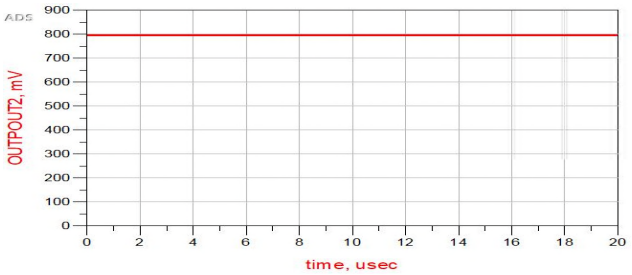

Figure 17. DC output voltage for -40 dBm input power

From this result, the harvested DC voltage is 0.8 V, simulated on ADS without termination load. This system is designed to feed low power consumption Wireless Sensor Networks (WSNs). The temperature sensor of [2] is operational for 0.2V and its equivalent resistance is 2 kΩ. Figures 18 and 19 show the proposed system with sensor load termination and its simulated DC output voltage, respectively.

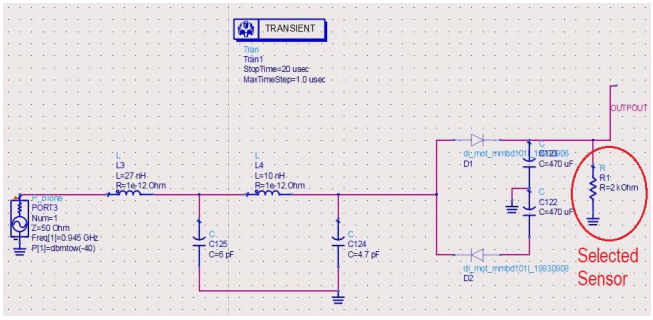

Figure 18. The proposed RF energy harvesting system with 2 kΩ load.

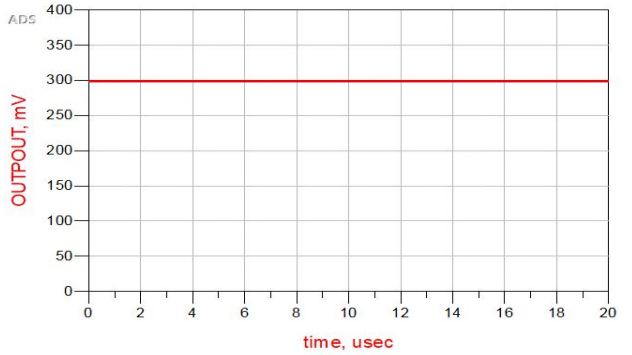

Figure 19. DC output voltage for -40 dBm input power and 2kΩ load.

 ISBN: 978-1-61208-828-0

The output DC voltage is 0.3V, which is enough for feeding the selected temperature sensor of [2].

V. SYSTEM REALISATION AND MEASUREMENT

A. Model Realization

Figure 20 presents the realized RF energy harvesting circuit (impedance matching + rectifier circuits).

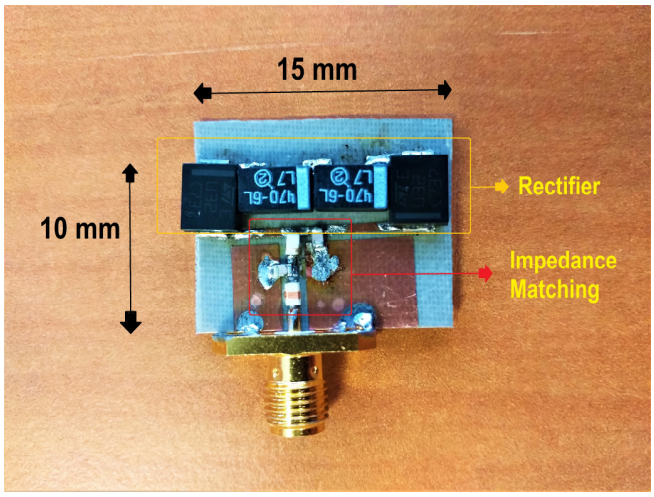

Figure 20. Proposed RF energy harvesting circuit (Impedance matching + Rectifier circuits).

B. S_{11} circuit Measurement

Figure 21 depicts the measured return loss.

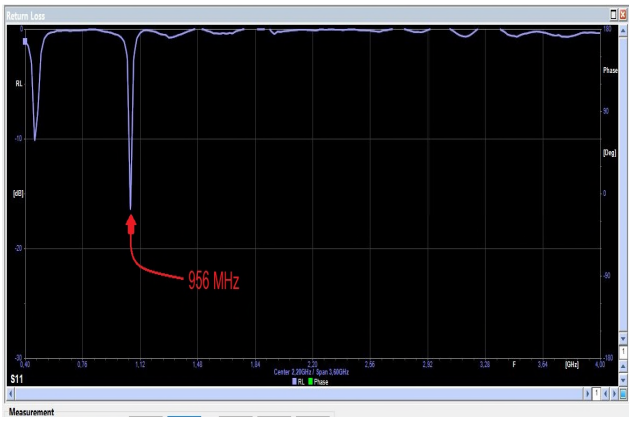

Figure 21. RF energy harvesting circuit return loss measurement.

As shown in Figure 21, the return loss is centered at 958 MHz, therefore, this circuit is adapted to GSM-900 downlink band.

C. Measured DC output voltage

Figure 22 shows the realized system (Antenna + RF energy circuit).

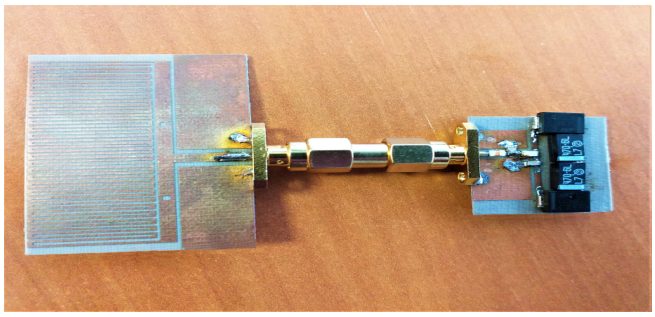

Figure 22. Realized proposed system.

The DC output voltage measurement has been achieved by using a Multimeter and an Oscilloscope. Figures 23 and 24 show the obtained results.

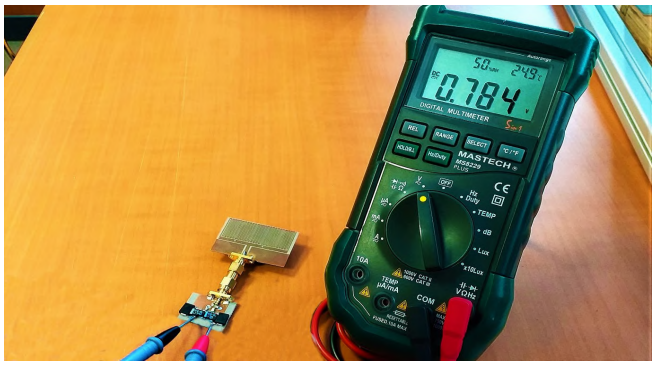

Figure 23. Measured output DC voltage using multimeter.

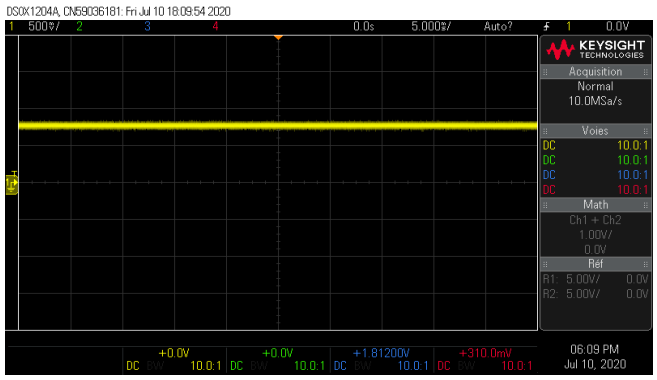

Figure 24. Measured output DC voltage using Oscilloscope with 500 mV per Division.

We can see that the measured output DC voltage is too near from that of the simulation one with 0.8 V, which

confirms that the simulation and measurement are in good agreement. This proposed system can perfectly feed the low power consumption temperature sensor in [2], which requires 0.2 V for working.

VI. CONCLUSION

In this work, we proved that is possible to feed low power consumption electronic devices (sensors, Radio-cognitive devices, smart watches, etc.) using RF and microwave energy harvesting systems, by exploring all mobile communication and wireless networks. A circuit adapted to GSM 900 network is proposed for feeding a low power consumption temperature sensor reported in [2], and by exploring more mobile communication networks more we increase the DC output voltage. The realized antenna and RF and microwave energy harvesting circuit (impedance matching + rectifier) are miniature with a dimension of 20x30x0.67 mm^3 and 10x15x0.67 mm^3, respectively. The harvested DC voltage from GSM-900 is 0.8 V for open load termination and 0.3 V for 2 kΩ resistance load, which is the sensor equivalent resistance.

REFERENCES

[1] C. Benkalfate, M. Feham, A. Ouslimani and A. Kasbari, "Investigation on the RF and Microwave Energy Harvesting from wireless and mobile communication networks," 2019 International Symposium on Networks, Computers and Communications (ISNCC), Istanbul, Turkey, 2019, pp. 1-6, doi: 10.1109/ISNCC.2019.8909092.

[2] A. Kamakshi; A. Shrivastava and B.H Calhoun. "A 0.2 V, 23 nW CMOS Temperature Sensor for Ultra-Low-Power IoT Applications". *J. Low Power Electron. Appl.* 2016, pp. 1-16, doi: 10.3390/jlpea6020010.

[3] A. Das, S. Dhar and B. Gupta, "Lumped circuit model analysis of meander line antennas," 2011 11th Mediterranean Microwave Symposium (MMS), Hammamet, 2011, pp. 21-24, doi: 10.1109/MMS.2011.6068520.

[4] N. Pournoori, M. W. A. Khan, L. Ukkonen and T. Björninen, "RF Energy Harvesting System Integrating a Passive UHF RFID Tag as a Charge Storage Indicator," 2018 IEEE International Symposium on Antennas and Propagation & USNC/URSI National Radio Science Meeting, Boston, MA, 2018, pp. 685-686, doi: 10.1109/APUSNCURSINRSM.2018.8608530.

[5] P. Sivagami, M. Pushpavalli, P. Abirami, S. Sindhuja and N. S. Reddy, "Implementation Of RF Energy Harvesting For Mobile Charging," 2018 IEEE International Conference on Computational Intelligence and Computing Research (ICCIC), Madurai, India, 2018, pp. 1-4, doi: 10.1109/ICCIC.2018.8782427.

[6] R. K. Sidhu, J. Singh Ubhi and A. Aggarwal, "A Survey Study of Different RF Energy Sources for RF Energy Harvesting," 2019 International Conference on Automation, Computational and Technology Management (ICACTM), London, United Kingdom, 2019, pp. 530-533, doi: 10.1109/ICACTM.2019.8776726.

[7] L. Lizzi, F. Ferrero, J. Ribero and R. Staraj, "Light and Low-Profile GSM Omnidirectional Antenna," in IEEE Antennas and Wireless Propagation Letters, vol. 11, pp. 1146-1149, 2012, doi: 10.1109/LAWP.2012.2219291.

[8] R. Suryadevara, T. Li, K. Modepalli and L. Parsa, "High-gain soft-switching DC-DC converter with voltage-doubler rectifier modules," 2017 IEEE Energy Conversion Congress and Exposition (ECCE), Cincinnati, OH, 2017, pp. 5692-5697, doi: 10.1109/ECCE.2017.8096946.

[9] V. Bande, P. T. R. Kumar and K. Krishnamoorthy, "Dual Band-Dual Sense Circularly Polarized Patch Antenna for Wi-Max Application," 2018 IEEE Indian Conference on Antennas and Propogation (InCAP), Hyderabad, India, 2018, pp. 1-4, doi: 10.1109/INCAP.2018.8770719.

[10] C. Huang, Y. Jiao, Z. Weng and X. Li, "A planar multiband antenna based on CRLH-TL ZOR for 4G compact mobile terminal applications," 2018 International Workshop on Antenna Technology (iWAT), Nanjing, 2018, pp. 1-3, doi: 10.1109/IWAT.2018.8379200.

[11] L. Shen, H. Wang, N. Hojjat, W. Lotz and H. Jamali, "Dual-Polarized Wideband Remote Electrical Tilt Multi-Beam Antennas," 2018 IEEE International Symposium on Antennas and Propagation & USNC/URSI National Radio Science Meeting, Boston, MA, 2018, pp. 2225-2226, doi: 10.1109/APUSNCURSINRSM.2018.8608298.

[12] C. Tienda, A. Katsounaros and S. Stirland, "Dual Reflectarray Ka-band Multibeam Antenna," 2019 13th European Conference on Antennas and Propagation (EuCAP), Krakow, Poland, 2019, pp. 1-4.

 ISBN: 978-1-61208-828-0

A New Paradigm for Spectrum Allocation in Millimeter-Wave Systems

Rony Kumer Saha
Radio and Spectrum Laboratory
KDDI Research, Inc.
2-1-15 Ohara, Fujimino-shi, Saitama 356-8502, Japan
Email: ro-saha@kddi-research.jp

Abstract—**The traditional static and dedicated allocation of a portion of the spectrum specified for a country suffers from low spectrum availability and utilization for a Mobile Network Operator (MNO). To overcome these constraints, in this paper, we present an idea of a new technique for the spectrum allocation called Countrywide Full Spectrum Allocation (CFSA) that considers a dynamic allocation of the countrywide full millimeter-wave spectrum to each MNO to operate its in-building small cells subject to the co-channel interference management for a certain renewed-term. We present CFSA comprehensively, highlighting its rationale, significance, major concern, possible solution, and performance evaluation with respect to the traditional static spectrum allocation technique.**

Keywords-millimeter-wave; small cell; mobile network operator; spectrum allocation; spectrum utilization; countrywide.

I. INTRODUCTION

A. Background

The radio spectrum in mobile communication systems is one of the most critical requirements. Over time, though the demand of mobile users in terms of data rate and volume increases due to the increased use of rich multimedia services, the available spectrum to serve user demands allocated to a Mobile Network Operator (MNO) has not been increased proportionately (Saha [1]). As this trend continues to grow, the gap between the required spectrum to serve user demands and the spectrum available for an MNO continues to increase accordingly. Another major reason for the scarcity of spectrum goes to how the spectrum specified for a country is allocated to its MNOs. More specifically, traditionally, a portion of the countrywide spectrum is allocated to each MNO exclusively in an equal amount (in most cases) and a static manner for the long term.

However, the number of users of one MNO differs from another and so does their required spectrum. This causes an MNO with more users to experience insufficiency of the spectrum, whereas the other, with fewer users, to waste part of its allocated spectrum. Moreover, irrespective of the number of users of each MNO, the user traffic demand of one MNO varies much from another in time and space. But, due to the static and dedicated use of spectrum by each MNO over a large coverage, a significant amount of its allocated spectrum may be either unused or underutilized (Hasan et al. [2]). Hence, such a static and dedicated allocation of a portion of the full spectrum specified for a country to each MNO is no longer considered sufficient to address its ever-increasing user demands (Saha [3]), as well as efficient to utilize the allocated spectrum, particularly in urban multistory buildings as most data is generated in such indoor environments.

B. Related Work

Numerous approaches, namely spectrum aggregation, trading, sharing, and reusing have been proposed in the existing literature to increase the amount, as well as the utilization of the spectrum. For example, Yuan et al. [4] have analyzed the key challenges of realizing carrier aggregation techniques, whereas Park et al. [5] have evaluated the performances of carrier aggregation schemes in Long-term Evolution-Advanced systems. Further, Xing et al. [6] have considered spectrum trading in the context of multiple sellers and multiple buyers, whereas Niyato et al. [7] have proposed a scheme for selling the spectra of multiple primary users to multiple secondary users.

For spectrum sharing, Saha [8] has proposed a technique to share both licensed and unlicensed spectra with small cells, whereas Attiah et al. [9] have studied spectrum sharing approaches in millimeter-wave systems. Likewise, Joshi et al. [10] have proposed an analytical model to reuse the microwave spectrum, whereas Saha [11] has proposed an analytical model to reuse the 28 GHz millimeter-wave spectrum in a building of Small Cell Base Stations (SBSs). However, the above approaches can be avoided if the countrywide full-spectrum is made available to each MNO, as opposed to just a portion of it in the traditional static spectrum allocation technique, to ensure large spectrum availability, as well as efficient utilization of the allocated spectrum, to serve a large volume of indoor data at high rates for the existing and upcoming mobile networks.

C. Organization

To address the above-mentioned issues, we propose a technique for allocating the countrywide full millimeter-wave spectrum in Section II. In Section III, major concerns (e.g., co-channel interference) and possible solutions of the proposed technique are discussed. We evaluate the performance of the proposed technique in Section IV and conclude the paper in Section V.

 ISBN: 978-1-61208-828-0

II. PROPOSED TECHNIQUE

The microwave spectrum, particularly below 3 GHz is almost occupied, and the millimeter-wave spectrum has been considered as a potential candidate for the Fifth-Generation (5G) and beyond mobile systems. Hence, to overcome these aforementioned constraints associated with the traditional static and dedicated spectrum allocation technique, in this paper, we present a new idea for the millimeter-wave spectrum allocation called countrywide full spectrum allocation (CFSA) stated as follows.

Each MNO of a country is allocated dynamically to the full millimeter-wave spectrum specified for the country to operate its in-building small cells subject to managing Co-Channel Interference (CCI) for a certain renewed-term t_r. The spectrum licensing fee for each MNO is updated in accordance with the number of its subscribers for each term. Hence, the proposed CFSA technique ensures the availability of a large amount of spectrum by allocating the countrywide full (instead of a portion) millimeter-wave spectrum, as well as an efficient spectrum utilization by allowing dynamic and flexible (instead of static and dedicated) access to each MNO. Moreover, as opposed to being bound to pay for the unused spectrum with few users, an MNO can pay only for the amount of spectrum that it uses to serve user demands at t_r, resulting in reducing the cost per unit capacity (i.e., bps).

Besides, to consider the dynamic number of users of MNOs, each SBS of all MNOs in an apartment of a building can keep sensing to detect the status of the shared full countrywide spectrum usage. Based on the CCI avoidance in time-domain, frequency-domain, or power-domain, each SBS updates the amount of time, spectrum, or transmission power, respectively. In this regard, depending on the maximum allowable control signaling overhead generated due to the coordination, SBSs either per apartment, per floor, or per building basis can form a cluster to coordinate with each other to update the CCI status locally in a distributed manner. Moreover, to detect the usage of the shared full spectrum, both reactive and proactive spectrum sensing approaches can be applied. In the reactive approach, an MNO performs the spectrum sensing mechanism to detect the usage on the shared spectrum, whereas in the reactive approach, based on the knowledge of the traffic model of User Equipments (UEs) of other MNOs $\boldsymbol{O}\backslash o$, the arrival of UEs can be predicted to update beforehand the usage of the shared countrywide full spectrum by an SBS of MNO o, where $\boldsymbol{O}$ denotes a set of MNOs in a country such that $o \in \boldsymbol{O}$.

III. MAJOR CONCERN AND POSSIBLE SOLUTION

A major concern of the proposed technique is that CCI may be generated when in-building small cells of more than one MNO attempt to access the same spectrum simultaneously. However, such CCI can be managed either in time, frequency, and power domains. In time-domain and frequency-domain, CCI can be avoided (Fig.1(b)) by allocating small cells of different MNOs in a different time interval (e.g., a transmission time interval of 1 ms) and frequency range (e.g., a resource block of 180 kHz) of the spectrum, respectively, using techniques such as time-domain and frequency-domain Enhanced Intercell Interference Coordination (eICIC) (Lopez-Perez et al. [12]; Saha and Aswakul [13]).

Recall that each MNO pays the spectrum licensing fee based on its number of subscribers for term t_r. So, the optimal value of time and frequency for an SBS of an MNO o to serve its user traffic can be derived as the ratio of the number of subscribers N_o of an MNO o to the sum of the total number of subscribers of MNOs $\boldsymbol{O}\backslash o$ (including those of MNO o) given that UEs corresponding to MNOs $\boldsymbol{O}\backslash o$ are present within the coverage of SBS of MNO o and each MNO has exactly one SBS in each apartment that can serve only one UE at a time (Fig.1(b)). For example, in time-domain eICIC, the optimal value of time in terms of the number of Transmission Time Intervals (TTIs) for an MNO o at any Almost Blank Subframe (ABS) Pattern Period (APP) of duration T_A in TTIs is given by,

$$T_o = \left\lceil \left(\left(N_o \Big/ \sum_{o=1}^{O} \left(1_{\varphi_o}(N_o) \times N_o \right) \right) \times T_A \right) \right\rceil \quad (1)$$

where $\varphi_o \in \{N_1, N_2, N_3, N_4\}$. $1(\cdot)$ is defined such that $1(\cdot) = 1$ if N_o exists in the set φ_o ; otherwise, $1(\cdot) = 0$. Similarly, following (1), we can find the amount of spectrum for MNO o in a TTI in frequency-domain eICIC.

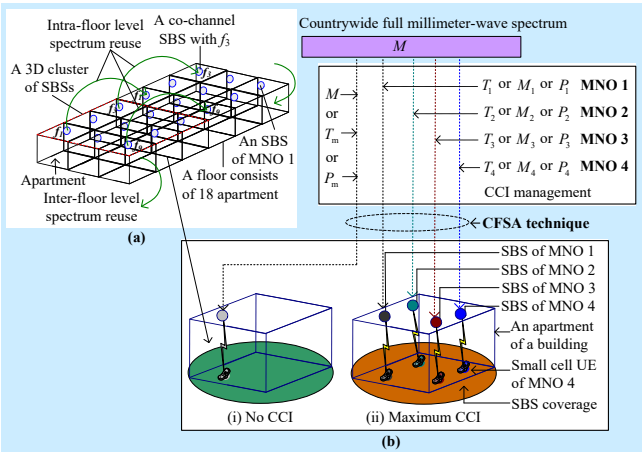

Figure 1. (a) A floor of a multistory building for 3D clustering of SBSs, (b) Illustration of the proposed CFSA technique. T_o , M_o , and P_o denote, respectively, operating time, spectrum, and power in time-domain, frequency-domain, and power-domain corresponding to MNOs $o \in \boldsymbol{O} = \{1,2,3,4\}$.

Further, in power-domain (Fig.1(b)), using cognitive radio access, such as interweave and underlay spectrum

access techniques, the transmission power of an SBS can be controlled to manage CCI. More specifically, using the interweave spectrum access, an SBS of an MNO o can be allowed to serve its user traffic at the maximum power as long as no UE of other MNOs $\boldsymbol{O}\backslash o$ exists in the same apartment. If otherwise, the SBS of MNO o stops serving its users immediately by switching its transmission power off. Likewise, using the underlay spectrum access, an SBS of an MNO o can transmit simultaneously on the countrywide full spectrum by reducing its transmission power to a predefined CCI threshold level if a UE of other MNOs $\boldsymbol{O}\backslash o$ exists in the same apartment as that of an SBS of MNO o. Hence, based on the presence of a UE of other MNOs $\boldsymbol{O}\backslash o$, using a hybrid interweave-underlay spectrum access, CCI can be managed.

Let $P_{\max}$ and P_{red} denote, respectively, the maximum transmission power and the reduced transmission power of an SBS of any MNO o when operating under the interweave and underlay access techniques such that $P_{\max} > P_{\text{red}}$. Then, the transmission power of an SBS of MNO o is given by

$$P_o = \begin{cases} P_{\max}, & \text{for interweave (if no UE of MNOs } \boldsymbol{O} \setminus o \text{ exists)} \\ P_{\text{red}}, & \text{for underlay (if a UE of MNOs } \boldsymbol{O} \setminus o \text{ exists)} \end{cases} \quad (2)$$

Note that, by exploiting the spatial domain, the countrywide full spectrum can be reused to in-building SBSs of an MNO o to increase the achievable capacity and spectrum utilization even further. For example, following Saha [14], by forming a 3-Dimensional (3D) cluster of SBSs in a building of an MNO o subject to satisfying a minimum CCI threshold both in the intra-floor, as well as inter-floor, levels, the same spectrum can be reused for each 3D cluster, as shown in Fig.1(a). Further, due to the high external wall penetration loss of a building for millimeter-wave signals, the countrywide full spectrum can be reused to SBSs of MNO o in adjacent buildings resulting in improving system-level capacity and spectrum utilization further. The detailed modeling of the 3D clustering of SBSs can be found in Saha [14].

IV. Performance Evaluation

We consider a simple example to evaluate the outperformance of CFSA, as follows. Assume that four MNOs are operating in a country such that $o \in \boldsymbol{O} = \{1,2,3,4\}$ with a subscriber base of 40%, 30%, 20%, and 10%, respectively, of the total number of subscribers countrywide at t_r. Let M=200 MHz denote the countrywide full millimeter-wave spectrum, which is allocated to each MNO based on its aforementioned subscriber base. Considering applying the frequency-domain CCI avoidance, the spectra allocated to MNOs 1, 2, 3, and 4 are given by 80 MHz, 60 MHz, 40 MHz, and 20 MHz, respectively. Assume that the millimeter-wave link quality of each UE is given by 3 bps/Hz.

Note that the number of Resource Blocks (RBs) corresponding to 80 MHz for MNO 1 is given by 400 where an RB is equal to 180 kHz. Consider that the total observation time T_m=8 TTIs where each TTI equals to 1 ms. Also, Shannon's capacity formula is given by $\sigma_{o=1} = W \log_2(1+\text{SINR})$ where W denotes bandwidth, SINR defines Signal-to-Interference-Plus-Noise Ratio, and $\log_2(1+\text{SINR})$ denotes link quality.

Now, using Shannon's capacity formula, the capacity and Spectral Efficiency (SE) of MNO 1 when UEs of all MNOs $\boldsymbol{O}\backslash o$=1 are present with a small cell in each apartment of MNO 1 in a building are given by 1.728 Gbps (i.e., $(400\,\text{RBs} \times 0.18\,\text{MHz/RB} \times 3\,\text{bps/Hz} \times 8\,\text{ms})$) and 3 bps/Hz (i.e., $(1.728\,\text{Gbps}/(400\,\text{RBs} \times 0.18\,\text{MHz/RB} \times 8\,\text{ms}))$), respectively. Following the same procedure, the capacity and SE of MNO 1 are given by 4.32 Gbps and 7.5 bps/Hz, respectively, when no UE of MNOs $\boldsymbol{O}\backslash o$=1 is present with a small cell in each apartment of MNO 1 (Fig.1(b)). However, when applying the Traditional Static Spectrum Allocation (TSSA) technique, by assuming that each MNO is allocated to an equal amount of 50 MHz spectrum, using the same procedure as above, the capacity and SE are given by 1.08 Gbps and 3 bps/Hz, respectively. These show an outperformance in capacity and SE of 60% and 0% for the maximum CCI, and 300% and 150% for no CCI of CFSA over TSSA. Hence, CFSA improves the capacity ranging from 60% to 300%, as well as the SE ranging from 0% to 150%, over TSSA.

Now, assume that due to a high floor penetration loss, a 3D cluster comprises 9 SBSs per floor each having 18 apartments of a 10-story building. If we consider reusing the countrywide full spectrum to each 3D cluster of SBSs of MNO 1, it can be reused 20 times to SBSs in the building. Since the capacity is directly proportional to the spectrum reuse factor, and the allocated spectrum to MNO 1 of 80 MHz does not change, the above capacity and SE improve by 20 times, irrespective of the level of CCI.

V. Conclusion and Future Work

In this paper, we have presented an idea of allocating a countrywide full millimeter-wave spectrum to each MNO to increase the spectrum availability and utilization. We have broadly detailed the proposed technique and shown its outperformance in terms of capacity and spectral efficiency over the traditional static spectrum allocation technique. The proposed idea needs extensive study for its concrete realization. In this regard, a good starting point is to justify the possible solutions discussed in this paper to address the major concern of the proposed idea. More specifically, it is necessary to elaborate and develop techniques to manage co-channel interference in time, frequency, and power domains when allocating the full millimeter-wave spectrum to each MNO in a country, which we consider carrying out as part of our future work.

 ISBN: 978-1-61208-828-0

REFERENCES

[1] R. K. Saha, "Spectrum Sharing in Satellite-Mobile Multisystem Using 3D In-Building Small Cells for High Spectral and Energy Efficiencies in 5G and Beyond Era," IEEE Access, vol. 7, pp. 43846-43868, Mar. 2019, doi: 10.1109/ACCESS.2019.2908203.

[2] M. R. Hassan, G. C. Karmakar, J. Kamruzzaman, and B. Srinivasan, "Exclusive Use Spectrum Access Trading Models in Cognitive Radio Networks: A Survey," IEEE Communications Surveys & Tutorials, vol. 19, pp. 2192-2231, Fourthquarter 2017, doi: 10.1109/COMST.2017.2725960.

[3] R. K. Saha, "On Exploiting Millimeter-Wave Spectrum Trading in Countrywide Mobile Network Operators for High Spectral and Energy Efficiencies in 5G/6G Era," Sensors, vol. 20, Art. No. 3495, 2020, doi.org/10.3390/s20123495.

[4] G. Yuan, X. Zhang, W. Wang, and Y. Yang, "Carrier Aggregation for LTE-Advanced Mobile Communication Systems," IEEE Communications Magazine, vol. 48, pp. 88-93, Feb. 2010, doi: 10.1109/MCOM.2010.5402669.

[5] C. M. Park, H. B. Jung, S. H. Kim, and D. K. Kim, "System level performance evaluation of various carrier aggregation scenarios in LTE-advanced," Proc. The 2013 15th International Conference on Advanced Communications Technology (ICACT), IEEE Press, Jan. 2013, pp. 814-817.

[6] Y. Xing, R. Chandramouli, and C. M. Cordeiro, "Price Dynamics in Competitive Agile Spectrum Access Markets," IEEE Journal on Selected Areas in Communications, vol. 25, pp. 613-621, Apr. 2007, doi: 10.1109/JSAC.2007.070411.

[7] D. Niyato, E. Hossain, and Z. Han, "Dynamics of Multiple-Seller and Multiple-Buyer Spectrum Trading in Cognitive Radio Networks: A Game Theoretic Modeling Approach," IEEE Transactions on Mobile Computing, vol. 8, pp. 1009-1022, Aug. 2009, doi: 10.1109/TMC.2008.157.

[8] R. K. Saha, "A Technique for Massive Spectrum Sharing with Ultra-Dense in-Building Small Cells in 5G Era," Proc. The 2019 IEEE 90th Vehicular Technology Conference (VTC2019-Fall), IEEE Press, Sept. 2019, pp. 1-7, doi: 10.1109/VTCFall.2019.8891437.

[9] M. L. Attiah et al., "A Survey of mmWave User Association Mechanisms and Spectrum Sharing Approaches: An Overview, Open Issues and Challenges, Future Research Trends," Wireless Networks, vol. 26, pp. 2487-2514, May 2020, doi.org/10.1007/s11276-019-01976-x.

[10] S. K. Joshi, K. B. S. Manosha, M. Codreanu, and M. Latva-aho, "Dynamic Inter-Operator Spectrum Sharing via Lyapunov Optimization," IEEE Transactions on Wireless Communications, vol. 16, pp. 6365-6381, Oct. 2017, doi: 10.1109/TWC.2017.2722999.

[11] R. K. Saha, "Modeling Interference to Reuse Millimeter-Wave Spectrum to In-Building Small Cells Toward 6G," (accepted) Proc. The 2020 IEEE 92nd Vehicular Technology Conference (VTC2020-Fall), IEEE Press, Oct. 2020, pp. 1-6.

[12] D. Lopez-Perez, I. Guvenc, G. de la Roche, M. Kountouris, T. Q. S. Quek, and J. Zhang, "Enhanced Intercell Interference Coordination Challenges in Heterogeneous Networks," IEEE Wireless Communications, vol. 18, pp. 22-30, Jun. 2011, doi: 10.1109/MWC.2011.5876497.

[13] R. K. Saha and C. Aswakul, "A Novel Frequency Reuse Technique for In-Building Small Cells in Dense Heterogeneous Networks," IEEJ Transactions on Electrical and Electronic Engineering, vol. 13, pp. 98-111, Jan. 2018, doi.org/10.1002/tee.22503.

[14] R. K. Saha, "3D Spatial Reuse of Multi-Millimeter-Wave Spectra by Ultra-Dense In-Building Small Cells for Spectral and Energy Efficiencies of Future 6G Mobile Networks," Energies, vol. 13, Art. No. 1748, 2020, doi.org/10.3390/en13071748.

 ISBN: 978-1-61208-828-0

Stabilizing Voronoi Diagrams for Sensor Networks with Hidden Links

Jorge A. Cobb

Department of Computer Science
The University of Texas at Dallas
Richardson, Texas 75080
Email: cobb@utdallas.edu

***Abstract*—We present an efficient and self-stabilizing protocol for computing the Voronoi region of a sensor node in a large wireless sensor network deployed in the two dimensional plane. This protocol surpasses the preceding ones in that it is fully distributed, is self-stabilizing, and in particular, it moves away from the unit-disk transmission model. That is, the topology induced by the wireless communication links is assumed to be arbitrary. This naturally incorporates the practical case of obstacles interfering in the communication of some pairs of sensor nodes that are close to each other. Due to being self-stabilizing, the protocol converges to a normal operating state regardless of the initial value of its variables. Because faults can be modeled as having variable values that do not properly reflect the state of the network, the protocol is resilient against all types of transient faults, provided the network does not become partitioned.**

Keywords–Stabilizing systems; Voronoi diagram; Delaunay triangulation; Sensor networks.

I. INTRODUCTION

Wireless sensor networks are characterized by having a limited number of resources. In particular, they operate on battery power, and have reduced processing and transmission capabilities. In order to preserve these critical resources, it is of paramount importance that every task performed by the sensors consumes the least amount of memory and energy [1].

Routing between nodes is a fundamental aspect of computer networks. Due to the limited resources in a wireless sensor network, it is desirable to use a routing protocol where the routing state stored at each node is independent of the network size; this is particularly important in a large-scale sensor network. One such approach is greedy routing [2]–[5]. Greedy routing is also known as geographic routing because, for a packet with destination d, a node u selects as the next hop to d a neighbor that minimizes the physical distance from u to d.

In general, greedy routing on an arbitrary graph may become trapped at a local minimum and not reach the destination. However, on a Delaunay triangulation, greedy routing is guaranteed to reach the destination. Hence, in the particular context of network routing, Delaunay triangulations, and their dual, the Voronoi diagram, are well suited for greedy routing [6].

In this paper, we develop a distributed protocol where each node can compute its Voronoi region, and thus, is able to support greedy routing. Given that the objective is to support greedy routing, the protocol does not require an additional routing mechanism that can be used to aid in communication between nodes. The only assumption is that each node is initially only aware of those nodes with whom it can communicate in a single transmission hop. This is an extension to our earlier work [7]. In [7], we assumed the unit-disk transmission model. That is, there is a transmission radius r such that, if any pair of nodes are within a distance of r of each other, then they can communicate directly. In this paper, we relax this model, and assume that the network topology induced by the transmission links is arbitrary. This naturally incorporates the practical case of obstacles interfering in the communication of some pairs of sensor nodes that are close to each other.

In addition to being distributed, our solution is *stabilizing* [8]–[11], i.e., starting from *any* state, a subsequent state is reached and maintained where the sensors become aware of their Voronoi region. A system that is stabilizing is resilient against transient faults, because the variables of the system can be corrupted in any way (that is, the system can be moved into an arbitrary configuration by a fault), and the system will naturally recover and progress towards a normal operating state. Thus, stabilizing systems are resilient against node failures, node additions, undetected corrupted messages, and improper initialization states.

Distributed protocols exist in the literature that allow each node to obtain its Voronoi region. However, they do not exhibit all our desired features. Algorithms, such as those in [12], are fully distributed, but they are not fault tolerant, and they assume an underlying routing protocol exists. Works designed for wireless greedy routing make no such assumption [13] [14], but they have limited fault-tolerance, and, in particular, are not stabilizing. Solutions that are distributed and stabilizing exist [15], but they also assume an underlying routing protocol, and are thus not suitable for greedy routing.

The paper is organized as follows. Section II presents a review of Voronoi diagrams, Delanuay triangulations, and also our network model. In Section III, we present the local information that each node maintains about its Voronoi region, and how this information can be used to forward messages between distant Voronoi neighbors. In Section IV, we describe the adaptations that have to be made in order to deal with our general communication model. Section V presents the different types of messages used in the protocol and how they are used to route between nodes. Our protocol notation is presented in Section VI. The techniques that make the protocol stabilizing are reviewed in Section VII, and the specification of the protocol itself is given in Section VIII. We argue the correctness of the protocol in Section IX. Concluding remarks and possible future work are given in Section X.

 ISBN: 978-1-61208-828-0

II. Voronoi Diagrams and Network Model

In this section, we review Voronoi diagrams and Delaunay triangulations. In addition, we present our network model and its relationship to Delaunay triangulations. This is similar to the review we presented in [7].

A. Voronoi Diagrams and Delaunay Triangulations

As shown in Figure 1(i), consider two points, a and x, in the two-dimensional Euclidean plane. The line segment from a to x is shown with dots, and the solid line corresponds to the perpendicular bisector of this line segment. Observe that any point below the bisector is closer to a than to x. Similarly, any point above the bisector will be closer to x than to a.

A *Voronoi Diagram* (VD) consists of a set of *generator points* $P = p_1, p_2, \ldots, p_n$ and a set of regions $R = R_1, R_2, \ldots, R_n$. Each R_i consists of all points on the plane that are closer to p_i than to any other generator point in P. In Figure 1(i), $P = \{a, x\}$, R_a are all points below the bisector, and R_x are points above the bisector.

Figure 1(ii) shows the region R_a after a few more generator points are added. Region R_a becomes the convex hull obtained from the intersection of all the bisectors with all other generator points. Finally, Figure 1(iii) shows the regions of all five generator points.

An equivalent structure to the VD is the *Delaunay Triangulation* (DT), shown in Figure 1(iv). Here, there is an edge between a pair of generator points p_i and p_j iff R_i and R_j share a face. E.g., point x has three edges: (x, y), (x, a), (x, w), because R_x shares a face with each of the regions R_a, R_y, and R_w. Thus, both the VD and the DT have the same information, but presented in different form.

B. Network Model and Connectivity

We consider a two-dimensional Euclidean space in which a total of n sensor nodes have been placed. In [7], sensors are assumed to have the same transmission radius, and hence, if the distance between any pair of sensors is less than this radius, then the pair is able to directly exchange data messages. In this paper, we relax this assumption. We assume that obstacles could exist between nodes, and thus, nodes may not be able to communicate directly even though they are within transmission range. We thus assume a very general and arbitrary topology, in which the fact that a pair of nodes u and v can communicate directly is independent of whether u can communicate directly with another node w. This will have significant impacts on the algorithm, as discussed in later sections.

Nodes u and v are joined by a *physical link*, $\langle u, v \rangle$, if they can directly exchange messages. The set of nodes with whom u has a physical link is denoted by $L_{phy}(u)$. We assume that the sensor network is connected. I.e., for every pair of nodes u and v, there is a path of nodes $w_1, w_2, \ldots, w_k$, such that $w_1 = u$, $w_k = v$, and for each i, $1 \leq i < k$, $w_{i+1} \in L_{phy}(w_i)$.

As discussed earlier, sensor nodes correspond to point generators, and each sensor node has the objective of identifying each of its neighbors in the DT (equivalently, the VD). I.e., each sensor node must learn the location of all other sensor nodes with whom it shares a DT edge. Throughout the paper, we use DT and VD interchangeably.

Let $V(u)$ be the set of neighbors of u in the DT. These are referred to as the *Voronoi neighbors* of u. For each v in $V(u)$, we refer to pair (u, v) as a *Voronoi edge*.

In Figure 1(iv), $V(x) = \{a, w, y\}$. Some of the nodes in $V(u)$ will be able to exchange messages directly with u, i.e., they are also contained in $L_{phy}(u)$. The nodes in $V(u) \cap L_{phy}(u)$ are said to be the *physical* Voronoi neighbors of u.

Note that it is possible for $w \in L_{phy}(u)$ but $w \notin V(u)$. This is because other nodes can be in between u and w, and thus, the Voronoi region of u does not overlap that of w. I.e., the fact that nodes can communicate directly does not imply that they are Voronoi neighbors, and vice versa.

Without obstacles in the network, such as the model we used in [7], between every pair of nodes there must exist a path such that each hop along the path consists of physical Voronoi neighbors. This allowed each node u to learn about its Voronoi neighbors by only exchanging messages with their physical Voronoi neighbors, i.e., nodes in $V(u) \cap L_{phy}(u)$. As we will show below, this is no longer the case if obstacles are present in the network.

III. Region Construction

We next describe the details of the information that a node maintains about its region, and how it provides assistance in building the regions of its neighbors.

A. Region Anatomy

Figure 2 depicts the region of u, consisting of eight Voronoi neighbors. Of these, neighbors i, m, and o are physical, i.e., they are contained in $L_{phy}(u)$. The set of physical Voronoi neighbors of a node u will be denoted by $core(u)$. The figure consists of only the region of u; the whole network is not shown.

Node u is aware of its core neighbors because it can communicate directly with them. On the other hand, consider node n. It must be that either o, m, or perhaps both, are able to communicate with n (recall that the network is connected), and inform u about n. Node u will remember which node informed it of the Voronoi edge (u, v). We will refer to this node as the *origin* of the edge.

In addition, each node keeps track of the number of transmission hops necessary to cross the link; this is known as the *label* of the link. E.g., if the origin of (u, n) is m, then $label(u, n) = label(m, n) + 1$. Both o and m report to u the expected number of hops to cross edge (u, v) through them. Node u chooses as origin the neighbor providing the least number of hops (a final tie-breaker is made using the node identifier). In the figure, o is the origin of (u, n), as indicated by the small arrow.

Consider now core nodes i and m, and the nodes in between them, j, k, and l. Node i is the origin of edge (u, j), and j is the origin of (u, k). We denote by *segment* the sequence of nodes starting at a core node where each node is the origin of the previous edge. The clockwise segment starting at i is (i, j, k). The counter-clockwise segment starting at m is (m, l), while the counter-clockwise segment starting at i is simply i itself.

Consider next nodes k and l. They are not aware of each other, and thus they do not report each other to u. In this case,

 ISBN: 978-1-61208-828-0

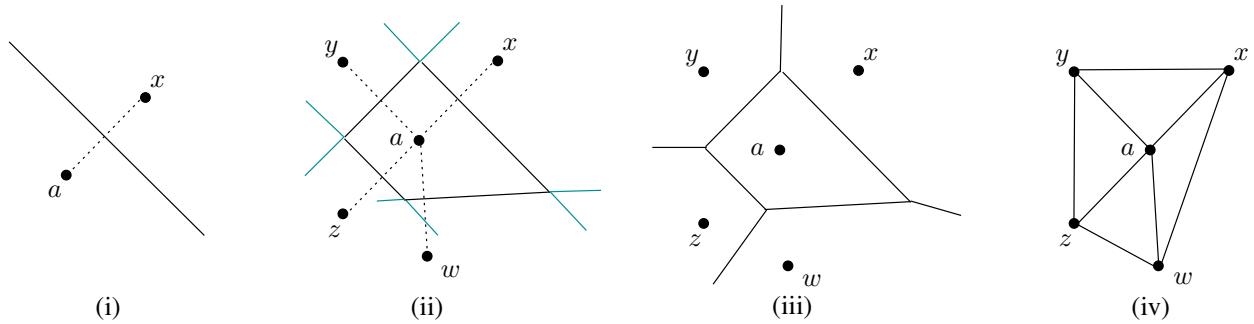

Figure 1. Voronoi diagram.

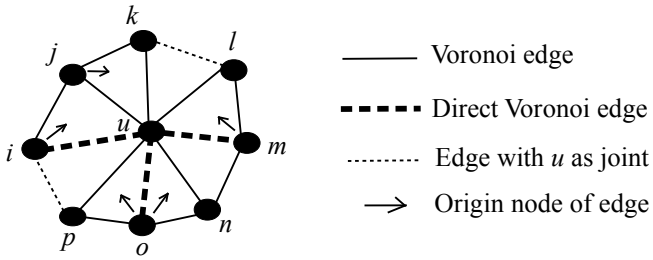

Figure 2. Segment construction.

u must introduce them to each other, and u becomes the origin of edge (k, l). Similarly, it introduces i and p to each other, and becomes the origin of edge (i, p).

We next describe the notion of a segment more formally [7]. For terseness, we use the terms *right* and *left* instead of clockwise and counter-clockwise, respectively. Additionally, we use *dir* to represent either *right* or *left*, and ¬*dir* to represent the opposite direction of *dir*.

Let v be any Voronoi neighbor of u. Let *next*$(u, v,$ *dir*$)$ be the next node along direction *dir* on region $R(u)$. For example, in Figure 2, *next*$(u, i,$ *right*$) = j$, and *next*$(u, m,$ *left*$) = l$. Also, for any pair of neighbors v and w of u, let *bet*$(u, v, w,$ *dir*$)$ denote the sequence of nodes found in $R(u)$ along direction *dir* starting from v and ending in w.

Let *segment*$(u, v,$ *dir*$)$ be the longest sequence of nodes, $w_0, w_1, \ldots, w_j$, along the periphery of $R(u)$, starting from core node v, $v \in$ *core*(u), such that:

- $w_0 = v$,
- for each i, $0 \leq i < j$, $w_{i+1} =$ *next*$(u, w_i,$ *dir*$)$, and
- for each i, $0 \leq i < j$, *origin*$(u, w_{i+1}) = w_i$.

In addition, node w_j is denoted by *last*$(u, v,$ *dir*$)$.

B. Forwarding of Control Messages

In [7], we adopted the following general strategy. There is a single type of control message, namely *edge*, whose purpose is to inform a node that it has a Voronoi neighbor. Consider node u: it has to inform k and l of each other. To send an *edge* message to k, the destination field in the message is set to k, the direction is set to *right*, and the message is given to i. The message will then traverse *the entire segment* (reaching i, j, and k).

The reason the whole segment is traversed is the way in which nodes forward messages that are not addressed to them: the message is forwarded to the adjacent core node. For example, assume node u receives an *edge* message from m and the destination is not u. If the direction is *right*, it forwards the message to i, and if the direction is *left*, it forwards the message to o.

As another example, assume node l wants to send an *edge* message to k to inform it of a potential neighbor. Because u is the origin of (k, l), the message will arrive to u (via m). Node u is oblivious to the source, and it simply forwards it to the adjacent core node, i.e., i, and the message traverses the segment and arrives at k. Even further, the message may not even originate at l, it may simply need to traverse edge (l, k), and the source is not in the region of u. Nonetheless, since the message is received from m, it is forwarded to i, and the message arrives at k, as desired.

C. Obstacle Pitfalls

As discussed in Section II-B, we assume that, due to obstacles, the physical links form an arbitrary graph. Consider Figure 3(a), where the physical links are shown as dashed lines. Without obstacles, there would be a physical link between every pair of nodes. However, due to obstacles, the physical links $\langle t, v\rangle$, $\langle t, w\rangle$, and $\langle v, w\rangle$ are not present.

In Figure 3(b), the Voronoi edges computed are shown as solid lines. Node u is aware of its neighbors v and w, and thus it considers them part of its region, and sends an *edge* message to each of them, which makes them aware of each other. However, since t is not in the region of u, u ignores t. Thus, node t is not aware of v and w, and it thus cannot compute its own region. We address a mechanism to correct this below.

IV. Extended Links

In order to fix the problem described above, node t must be made aware that, if it were not for the obstacles, it would actually have a physical link with v and w. We can accomplish this by node u *extending* the link $\langle u, t\rangle$ to v and w. That is, to make v and w aware that they should have a link with t.

To become aware of this need, node u notices that its physical link $\langle u, t\rangle$ intersects its Voronoi edge (v, w). Thus, u notifies both v and t that they have an *extended link* between them. This link is shown as a gray dotted line in Figure 3 (c). Thus, v and t consider this link as an ordinary physical link, and add it to their set L of links. The extended link $\langle t, v\rangle$ is

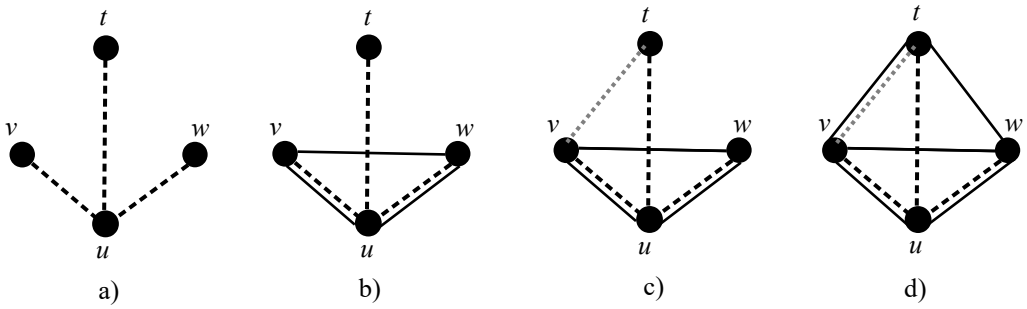

Figure 3. Extended links.

treated in the algorithm like any other link, e.g., it could be part of the core of t and the core of v. The difference only lies in that for t to send a message to v (and viceversa) the message has to be sent through u.

Once v and t are aware of each other, they add link $\langle t, v\rangle$ to their region. Node v then becomes the origin of edge (t, w), and it sends an *edge* message to both t and w making them aware of edge (t, w). The final results is shown in Figure 3(d).

Note that u does not need to extend the link $\langle u, t\rangle$ to w. Although possible, it is not necessary, since v will become the origin of the edge and join t with w. Thus, u will extend the link towards the neighbor that is closest of the two.

The extension of a link can become more complex, requiring the same link to be extended *multiple times*. This is illustrated in Figure 4. Part (a) of the figure indicates the physical links as dashed lines, and the solid lines correspond to the desired Voronoi edges. Without extending physical links, the Voronoi edges found are in part (b) of the figure. Part (c) shows the extension of edge $\langle p, t\rangle$ into edge $\langle q, t\rangle$. Node t disregards this edge since it is not part of its region (the Voronoi face with q is blocked by the faces of nodes s and u). Node q, however, will try to join t and r. This may be accepted by r, but t will reject it since edge (t, r) is not part of its region. The nodes will not learn the correct edges shown in part (a).

Note, however, that the extended link $\langle q, t\rangle$ crosses the Voronoi edge (s, u) of the region of t. Thus, t could extend it even further, by notifying s that it should have an extended link $\langle s, q\rangle$, as shown in part (d). Node s thus adds this link to its region, and joins q and u. This makes node q desist in attempting to join t with r, and instead joins u and r, yielding the correct result.

V. Message Types and Routing

We discussed above the need for extended links. In this section, we discuss the method for creating them and for sending messages across them. Our objective is to modify the method we presented in [7] the least possible, and still account for extended links. For example, consider again Figure 2, and assume node u receives a message from core node m, which is not destined for u. Thus, u forwards it to i. This should remain in effect even if the link $\langle i, u\rangle$ is an extended link, as opposed to a physical link. Thus, note that the core of a node may now consist of a mixture of physical links plus extended links.

Before discussing creating an extended link, we recall that in [7] we had only one message type, *edge*, to inform two nodes that there should be joined by a Voronoi edge. For example, in Figure 2, node u would send the following message to node k via link $\langle i, u\rangle$.

$$(ttl, \textit{edge}, dir, dst, src, nbr, lbl)$$

where dir = *right*, $dst = k$, $src = u$, $nbr = l$, and $lbl = \textit{label}(u, k) + \textit{label}(u, l)$. Also, the time to live, ttl, is the number of physical links traversed by the message. It is initially equal to one, and is incremented by one per physical link traversed. The message is discarded if it reaches an upper bound discussed in Section VII-A.

A. Creating an Extended Link

Consider now creating an extending a link, such as Figure 3(c), where node u wants to extend its physical link $\langle u, t\rangle$ to create the link $\langle v, t\rangle$. To do so, it sends a *link* message to both v and t, as follows:

$$(ttl, \textit{link}, dir, dst, src, nbr, lbl).$$

For v, $dst = v$, $src = u$, $nbr = t$, and $lbl = \textit{label}(u, v) + \textit{label}(u, t)$. Similarly for t, we have $dst = t$ and $nbr = v$.

In general, one of the endpoints (i.e., v) is a Voronoi neighbor, and the other (i.e., t) is a physical link. To send the message to the Voronoi neighbor, we simply send it as before, by sending it to the core neighbor of the segment containing the destination, and the message will traverse the whole segment until it is removed at the destination. In the case of v, v itself is the core node, and the message arrives in just one hop. For t, it is a physical link, so the message is sent directly.

A more interesting scenario occurs Figure 4(d), where node t is extending its link, $\langle t, q\rangle$ to create the link $\langle s, q\rangle$. In this case, neighbor s is a Voronoi neighbor, as expected, but node q is not a physical link, it is an *extended* link. Thus, the *link* message has to be routed in a manner that is different from routing around a segment of the region of node t. This is because extended links bypass Voronoi edges, in particular, link $\langle t, q\rangle$ crosses over Voronoi edges (s, u), (q, u), and (q, r). We discuss this next.

B. Transferring Messages Across an Extended Link

As mentioned at the beginning of the section, we need a general mechanism by which *any* message can be *tunneled* across an extended link. To send an arbitrary message over the extended link $\langle t, q\rangle$, node t must remember the *source* of

 ISBN: 978-1-61208-828-0

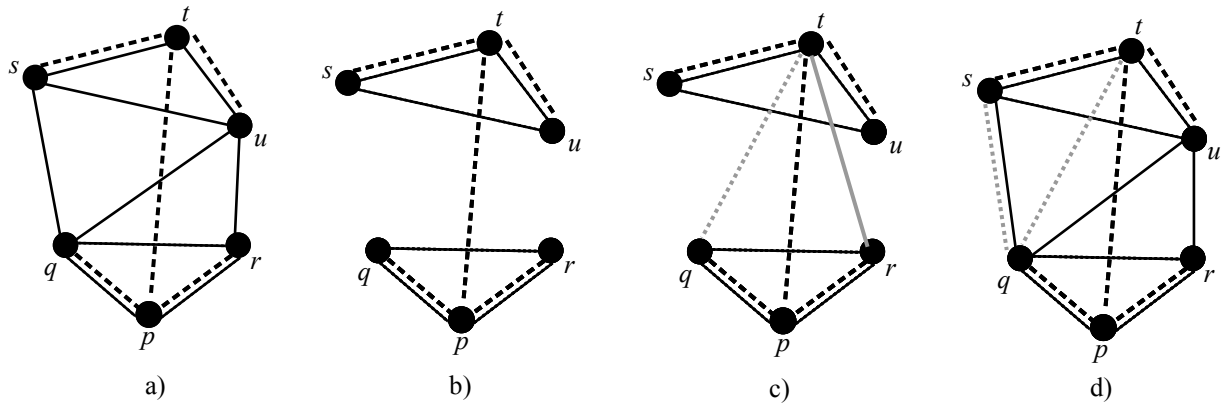

Figure 4. Link extended multiple times.

the link, in this case node p, and send the message to it. Node p cannot handle this message in the normal way, since the message is not being routed along Voronoi edges. We thus need a new message type to indicate to p that the message is being *thrown* across network, and that p should then find a way to forward it to the other end point q.

We introduce two additional message types, *throw* and *catch*, to tunnel the message across the extended link. For the specific case above, t sends the following message to p:

$$(ttl, \textit{throw}, dir, dst, src, nbr, (msg)),$$

where $dst = p$ (p should process and not just forward this message), $src = t$, and $nbr = q$. Node p then retrieves the encapsulated message msg, notices that it should be sent to q, and sends the following message to q:

$$(ttl, \textit{catch}, dir, dst, src, (msg))$$

where $dst = q$, and $src = t$, which allows q to learn that msg originated at t.

Note that, given that q is a Voronoi neighbor of p, p will use normal Voronoi routing to route the *catch* message. I.e., it will find the core node of the segment containing q, and forward the catch message to this node.

C. Generalized Send Operation

Sending a message across a link can become more complex, and it requires an iterative approach as follows. Consider Figure 4(d) again, and assume node q needs to route a message msg to node s along the extended link. To do so, it has to encapsulate msg in a *throw* message and send it to the source of the link, i.e., t. To send the message to t it has to encapsulate it in another *throw* message and send it to the source of that link, i.e., p. In the figure, p is a physical neighbor, so the message could be sent directly. However, it is easy to extend the network so that p is a Voronoi neighbor of q, but not a physical neighbor. This would then require q to find the core node of the segment of p, and then send the message to this core neighbor, etc..

VI. Protocol Notation

Before presenting the protocol in detail, we overview our notation. The notation used originates from [10] [11], and is typical for specifying stabilizing systems. The behavior of each node is specified by a set of inputs, a set of variables, a set of parameters, and a set of actions.

The inputs declared in a node can be read, but not written, by the actions of that node. The variables declared in a node can be read and written by the actions of that node. For simplicity, a shared memory model is used, i.e., each node u is able to read the variables of nodes in $L_{phys}(u)$. To maintain a low atomicity, and thus a possible transition to a message-passing model, each action is able to read the variables of a *single* neighbor.

Every action in a node u is of the form:

$$<\text{guard}> \rightarrow <\text{statement}>.$$

The <guard> is a boolean expression over the inputs, variables, and parameters of the node, and also over the variables declared in a single node in $L_{phy}(u)$. The <statement> is a sequence of assignment, conditional, and iteration statements that change some of the variables of the node.

The parameters declared in a node are used to write a set of actions as one action, with one action for each possible value of the parameters. For example, if the following parameter definition is given,

par g : 1 .. 2

then the following action

$x = g \quad \rightarrow \quad x := x + g$

is a shorthand notation for the following two actions.

$$\begin{array}{lll} x = 1 & \rightarrow & x := x + 1 \\ x = 2 & \rightarrow & x := x + 2 \end{array}$$

An execution step consists in evaluating the guards of all the actions of all nodes, choosing an action whose guard evaluates to true, and executing the statement of this action. An execution consists of a sequence of execution steps, which either never ends, or ends in a state where the guards of all the actions evaluate to false. All executions are assumed to be weakly fair, that is, an action whose guard is continuously true must be eventually executed.

In order to simplify the presentation and proofs, we assume a *shared memory model with low atomicity*. In particular, a

 ISBN: 978-1-61208-828-0

node is able to read the variables of its neighbors. However, in any action, it is only allowed to read the variables of a single neighbor. This will allow for an easy transformation into the message passing model.

To distinguish between variables of different nodes, the variable name is prefixed with the node name. For example, variable $u.v$ corresponds to variable v in node u. If no prefix is given, then the variable corresponds to the node whose code is being presented.

The main inputs and variables of each node are as follows. Each node has a unique identifier from the set **ID**. Each node u receives as input the set L_{phys} consisting of the identifiers of all neighbors with whom it shares a physical link.

In order to represent the exchange of messages, each node has the following array.

$$send \quad : \quad \textbf{array}[L_{phy}] \textbf{ of set of } (\textbf{ID}, message) \qquad (*)$$

Element $send[v]$ contains the set of messages that node u wishes v to read. The purpose of the identifier attached to the message will be made clear in the next section. Each node u also has a variable, $rcvd$, as follows.

$$rcvd \quad : \quad \textbf{set of } message$$

To read the messages of a neighbor v, node u copies $v.send[u]$ into $u.rcvd$ (discarding the identifiers coupled with each message).

VII. Stabilization

We next describe the changes that are necessary to strengthen our protocol and achieve stabilization. We begin with a formal definition of stabilization.

A *predicate* P of a network is a boolean expression over the variables in all nodes of the network. A network is called *P-stabilizing* iff every computation has a suffix where P is true at every state of the suffix [9] [11].

Stabilization is a strong form of fault-tolerance. Normal behavior of the system is defined by predicate P. If a fault causes the system to a reach an abnormal state, i.e., a state where P is false, then the system will converge to a normal state where P is true, and remain in the set of normal states as long as the execution remains fault-free.

In a stabilizing system, we assume each node can be in an arbitrary initial state, where its variables can have corrupt and misleading information. To ensure stabilization, the system must eliminate information which is not consistent with the current network state. Below, we describe how to eliminate non-existent nodes, stale edges, and stale messages.

A. Eliminating Ghost Nodes

Due to faults, information about nodes that have died may still exist in the data structures of a node, or perhaps a fault introduced information about non-existent nodes. We discuss below how this extraneous information is eliminated, provided nodes are aware of the number of nodes, N, that are in the system.

Obtaining N can be easily achieved by running a self-stabilizing leader election protocol, such as the one in [16], which builds a spanning tree in the network without knowledge of the network size. A simple diffusing computation allows the root to compute the number of nodes in the network, and report this value to all other nodes. This can be accomplished by periodically exchanging a constant-sized packet over each physical link.

Armed with the knowledge of N, no node will forward a message whose ttl is greater than N. Thus, any message in the network with a non-existing source will be removed from the network within N execution rounds.

Consider again Figure 2. Assume u receives an *edge* message from j joining k and u. If node j does not exist, as mentioned above, due to the ttl, messages from j will disappear and never be reintroduced. On the other hand, if j does exist, does k exist? Note that k may not be a physical neighbor of j, and hence, does not have immediate access to it. Nonetheless, the label assigned to (k, u) by j will be less than the label of (j, k), and as we approach closer to node k (by following the origin node of edge (j, k), which is not drawn in the figure), the labels continue to decrease. Since the smallest possible label is one, which is the case of a physical link, node k must exist.

B. Eliminating Stale Edges, Links, and Messages

Voronoi edges and extended links are created at a node after receiving a message of the appropriate type. If these messages cease to exist, then the corresponding edge/link is stale, and should be removed. Thus, we maintain the following array:

$$inc \quad : \quad \textbf{array}[L_{ext} \bigcup V_{join}] \textbf{ element of } \ L_{phy}$$

Entry $u.inc[v]$ stores the incoming physical link over which the message that created the edge/link (u, v) was received. Whenever u copies into $u.rcvd$ the messages from $v.send[u]$, all edges and links in $inc[v]$ are marked as stale. If an edge or link is not refreshed by any of the messages in $u.rcvd$, then it is discarded.

Similarly, as mentioned in Section III-B, node u forwards messages that are not destined for it, and places them in the appropriate entry in array $send$. Note that, as indicated in (*), each message is associated with an ID. This is the ID of the physical link over which the message was received. Thus, to prevent stale messages, whenever node u copies into $u.rcvd$ the messages from $v.send[u]$, it removes all messages in array $send$ whose ID is v.

VIII. Protocol Specification

We next present the specification of our protocol for an arbitrary node u. As discussed before, its inputs consists of the total number of nodes in the system, N, and the set of physical links, L_{phy}. It also contains several parameters to expand an action into multiple actions.

In terms of variables, L_{ext} contains the set of extended links. At all times, $L_{ext} \cap L_{phy} = \emptyset$. For conciseness, we define $L = L_{ext} \bigcup L_{phy}$. In addition, V contains the Voronoi neighbors found thus far.

We reuse the definitions related to a region $R(u)$, such as *segment*, *last*, and *next*, but instead based on the neighbors V found so far by node u, rather than the actual region $R(u)$ defined by the network topology.

Also, since node u is understood, we omit it from some definitions. E.g., $core$ is the set of core nodes of u, which we

define as $core = V \cap L$, and ($last(v, dir)$ is the last node of the segment of u starting at core node v in the direction *dir*. Finally, we define $V_{join} = V - core$.

The node contains three arrays not yet discussed. The first is *origin*, in which the origin of each link in L_{ext} and each edge V_{join} is stored. As discussed in Section VII, stale edges are marked in array *stale*. Finally, array *label* stores the label of each edge in V that is not a direct edge. By definition, $label[v] = 1$ for all v, $v \in L_{phy}$.

The complete specification is below, followed by a description of each action.

node u
inp
N : **integer** {number of nodes}
L_{phys} : **set of ID** {physical links}
param
t, t', i : **ID** {any node}
dir : **element of** *left . . right* {direction}
var
L_{ext} : **set of ID** {extended links}
V : **set of ID** {Voronoi neighbors}
inc : **array** $[L_{ext} \cup V_{join}]$ **element of** L_{phy}
{incoming physical link announcing the link/edge}
$origin$: **array** $[L_{ext} \cup V_{join}]$ **element of** V
{Voronoi neighbor announcing the link/edge}
$stale$: **array** $[L_{ext} \cup V_{join}]$ **of boolean**
{stale links/edges}
$label$: **array** $[L_{ext} \cup V_{join}]$ **of** $2 \; . \; . \; N$
{hops needed to traverse edge/link}
$rcvd$: **set of** *message*
$send$: **array** $[L_{phy}]$ **of set of**
(**element of** $L_{phy} \cup u$, *message*)
begin
{extend a link}
$t \in L \wedge t \notin V \wedge$ *outside*$(t, V) \quad \rightarrow$
(q, r) := *closest*(t, V);
dir := *direction*$(core(q), q)$;
msg := $(1,$ *link*$, dir, q, u, t,$
max$($*label*$[q],$ *label*$[r]) +$ *label*$[t])$;
sendmsg$(u, core(q), msg)$

{join an edge}
$t \in$ *core* $\wedge \; t' =$ *next-core*$(t, dir) \quad \rightarrow$
x := *last*(t, dir);
y := *last*$(t', \neg dir)$;
msg := $(1,$ *edge*$, dir, x, u,$ *label*$[x] +$ *label*$[y])$;
sendmsg(u, t, msg);
msg := $(1,$ *edge*$, \neg dir, y, u,$ *label*$[x] +$ *label*$[y])$;
sendmsg(u, t', msg)

{receive a message}
$i \in L_{phy} \quad \rightarrow$
$rcvd$:= $i.send[u]$;
clear$(send, i)$;
for each $v \in (L_{ext} \cup V_{join})$ **do**
if $inc[v] = i$ **then**
$stale[v]$:= *true*;
for each $msg \in rcvd$ **do**
process-msg(msg);
for each $v \in (L_{ext} \cup V_{join})$ **do**
if $stale[v]$ **then**
$V := V - \{v\}$;
$L_{ext} := L_{ext} - \{v\}$;
clean(V);
end

In the first action, a link to a node t is extended via a Voronoi neighbor q. Node t should be outside of the region defined by V. If so, the Voronoi edge in V, namely (q, r), crossed by t, such that t is closer to q than r, is found, and a *link* message is sent to the core node of the segment containing q. Note that the label in the message is *max*$($*label*$[q],$ *label*$[r]) +$ *label*$[t]$ rather than simply *label*$[q] +$ *label*$[t]$. The reason for this will be made clear in Section IX.

In the second action, the nodes at the end of two segments are joined together by sending an *edge* message to them. The core nodes are t and t', without any core nodes between them. An *edge* message is sent to the two endpoints of the corresponding segments to indicate to them that they are potential neighbors. Function *next-core* is defined as follows:

next-core$(v,$ *dir*$) = w \; \Leftrightarrow$
$\langle \forall x : (x \in$ *bet*$(v, w,$ *dir*$) \wedge x \notin \{v, w\}) \Rightarrow x \notin$ *core*$\rangle$

Also, the *sendmsg* routine, as described in Section V-C, is as follows.

sendmsg(in, out, msg)
$h := msg.ttl + 1$;
if $h > N$ **then** *return*;
if $out \in L_{phys}$ **then**
$send[out] := send[out] \cup (in, msg)$
if $out \in L_{ext}$ **then**
$or := origin[out]$;
out' := *core*(or);
dir := *direction*(out', or);
msg' := $(h,$ *throw*$, dir, or, u, out', msg)$;
$send(in, out', msg')$

In the third action, a message is received from a physical link, by copying the appropriate contents of the $send$ array of physical neighbor i. Then, the $send$ array is cleared of all earlier messages that were received from neighbor i, and every edge and link whose message that created them was received along link i are marked stale. If these edges and links are refreshed by messages from i, then their staleness is removed at the end of the action. In addition, routine *clean*(V) removes from V edges that are inconsistent with each other. It's objective is to remove all nodes in V that violate the following *clean* consistency requirement between successive nodes of a segment:

$\langle \forall x, dir, v, w,$
$(x \in core \wedge w \in$ *segment*$(x, dir) \wedge v \in$ *segment*$(x, dir) \wedge$
$v \neq w \wedge w =$ *next*$(v, dir))$
$\Rightarrow$
$(label[w] > label[v] \wedge origin[w] = v)$
$\rangle$

That is, every neighbor should have as origin the previous neighbor on its segment, and furthermore, its label should be also greater than that of the previous neighbor. Routine $clean(V)$ is as follows.

```
clean(V)
    V := convex-hull(V ∪ L_phy);
    clean := core;
    for each i ∈ L_phy do
      label[i] := 1;
    for each i ∈ core do
      for dir ∈ {left, right}
        v := i;
        while (next(v, dir) ≠ nil, ∧
               origin(next(v, dir)) = v ∧
               label(v) < label(next(v, dir))) do
            clean := clean ∪ {v};
    V := clean
```

Each received message is processed according to its message type. The code for routine *process-msg* is as follows.

```
process-msg(msg)
    if msg.dst ≠ u ∧ i ∈ V ∧ msg.ttl < N then
        dir := msg.dir;
        sendmsg(i, next-core(i, dir)), dir);
    if msg.dst = u ∧ msg.ttl < N
        if msg.type = edge then
            process-edge-msg;
        if msg.type = link then
            process-link-msg;
        if msg.type = throw then
            process-throw-msg;
        if msg.type = catch then
            process-catch-msg
```

We next discuss the processing of each message type. The processing of an *edge* message is as follows.

```
process-edge-msg
    nbr := msg.nbr;
    src := msg.src;
    l := msg.lbl;
    if src ∈ V ∧ nbr ∉ L_phy ∧
      nbr ∈ convex-hull(V ∪ {nbr}) ∧
      (nbr ∉ V ∨ l < label[nbr] ∨
      (l = label[nbr] ∧ src < origin[nbr])) then
        V := V ∪ nbr;
        origin[nbr] := src;
        inc[nbr] := i;
        label[nbr] := l;
        stale[nbr] := false
```

An edge is added to V under certain conditions. First, the origin of the edge, i.e., the source of the message, must already be in V. Next, it should not be a physical neighbor because these neighbors are always present and considered for V. Also, the node will only be added to V if it takes part in the convex-hull, i.e., the region, of the node. Finally, either the node is a new addition to V, or it provides a better label than before (ties broken in favor of smaller origin ID).

The processing of a *link* message is as follows.

```
process-link-msg
    ngh := msg.ngh;
    src := msg.src;
    or := origin[ngh];
    if src ∈ V ∧
      (ngh ∉ L_ext ∨ label[src] < label[or] ∨
      (label[or] = label[src] ∧ src < or)
    then
        L_ext = L_ext ∪ {ngh};
        origin[ngh] := src;
        inc[ngh] := i;
        stale[ngh] := false
```

In order to add a node as an extended link, the origin of the link (i.e., the source of the message), must already be a Voronoi neighbor. Also, either it is a new extended link, or the origin of the link has a better label than the origin of the current extended link. If so, the node is added to the extended link set and the book-keeping arrays are updated accordingly.

The processing of a *throw* message is as follows.

```
process-throw-msg
    m'.type := catch;
    m'.ttl := msg.ttl;
    m'.msg := decap(msg);
    dst := msg.ngh;
    src := msg.src;
    if dst ∈ V_join ∧ src ∈ L_ext then
        msg.dir := direction(core(dst), dst);
        sendmsg(i, core(dst), m')
    if dst ∈ L_ext ∧ src ∈ V_join then
        dir := nil;
        sendmsg(i, dst, m')
```

The original message is retrieved from decapsulation of the catch message. If the destination of the message, i.e., the origin of the extended link, is a Voronoi neighbor, then the core node associated with this Voronoi neighbor is found, and the message is sent to it. On the other hand, if the destination of the message is the endpoint of an extended link, then the message is sent directly over the link.

The processing of a *catch* message is as follows. The original message is simply retrieved from the *catch* message, and then processed like a normal message.

```
process-catch-msg
    msg' := decap(msg);
    msg'.ttl := msg.ttl;
    process-msg(msg')
```

IX. CORRECTNESS

We show that regardless of the initial state of the system, $R(u) = V$ will hold permanently for every u.

We define an *execution round* to be a subsequence of an execution in which every action of every node has either been executed or its guard is not enabled. A round captures the notion of taking enough execution steps guaranteeing that every node makes progress.

Note that after executing the third action to receive messages, the clean requirement on V is satisfied due to the *clean*(V) routine. We thus assume that this always holds in between action executions.

A. Eliminating Non-Existing Nodes

If there is a message msg in a send queue that is paired with a neighbor v in L_{phys}, then, the next time node u reads messages from v, msg is removed from the send queue. I.e., after each execution round, all messages disappear unless being received again from the corresponding neighbor.

Consider first all messages whose src value is a non-existent node. No new messages with a non-existing node as a src field can be created, because the value of src is set to the node creating the message, i.e., a valid live node. Any of these messages with $ttl = N - x$ will disappear within x execution rounds, because in a round all existing messages are deleted, and the forwarded messages have their ttl increased by one, and are discarded when it reaches N.

We next argue that all messages with a non-existent ngh disappear. We do so in conjunction with showing that these nodes disappear from $V_{join} \cup L_{ext}$. We do a combined induction over the label values and the ttl.

Consider first messages with $lbl = 1$. No new message can be created with this label since new messages have a label equal to the sum of two other labels, all of which are at least 1 (i.e., L_{phy} neighbors). Thus, by induction on the ttl, these messages will disappear. Note that $label[v]$ is defined to be at least 2, and thus any non-existent neighbor in $V_{join} \cup L_{ext}$ must have a label of at least 2.

Consider next that all messages with a non-existent ngh have a label of at least x, permanently, and all nodes in $V_{join} \cup L_{ext}$ have a label at least x, permanently. Similarly, any new message with label x is obtained by adding the labels of two nodes. Since non-existing nodes have a label of at least x, no such message can be created. Hence, by a simple induction on the ttl, all messages with non-existent ngh and a label of x will disappear permanently. Also, in the next execution round, edges and links in $V_{join} \cup L_{ext}$ with a non-existent ngh and a label of x will be marked as stale and not be refreshed, and thus removed. Hence, all messages with a non-existent ngh will have a label of at least $x + 1$, permanently, and all nodes in $V_{join} \cup L_{ext}$ will have a label at least $x + 1$, permanently. The desired result follows by induction.

B. Constructing $R(u)$

Due to lack of space, we present an overview of the proof. We begin by observing that if a node v is in $R(u)$, and if it is also in V, then $v \in$ *convex-hull*(V). That is, no existing node can block v. Since non-existing nodes have been shown to disappear, v cannot be blocked by any other node. Thus, the only reason v could be removed from V is if v does not satisfy the clean condition that is required of V. We will show by induction that this is not the case.

Also, similar to the first argument in Section IX-A, an induction argument can show that if a message is not recreated at its source node, then, due to the ttl, all copies of the message will be removed from the network. This observation will be used throughout.

We define the notion of the *DTlabel* of an edge (u, v) in the DT of the network in a similar way as was done in [7]. Our induction will be over the *DTlabel*. The *DTlabel* of edge (u, v) is the smallest positive integer such that:

(i) If (u, v) is a direct physical link between u and v, then *DTlabel*$(u, v) = 1$.

(ii) If (u, v) is not a physical or an extended link, then note that (u, v) can be involved it at most two triangles in the DT. Let those triangles be (x, u, v) and (y, u, v), i.e., either x or y is the origin of edge (u, v) ($x = y$ in the case of only one triangle). Then, *DTlabel*$(u, v) =$ *min*(*label*(x, u) + *label*(x, v), *label*(y, u) + *label*(y, v)).

(iii) If (u, v) is an extended link formed by extending another link (p, v) that crosses an edge (u, w) in $R(p)$, then *DTlabel*(u, v) = *max*(*label*(p, u), *label*(p, w)) + *label*(p, v).

The reason for (iii) above being *max*(*label*(p, u), *label*(p, w)) rather than simply *label*(p, u) is that our induction will be based on *DTlabel*, and *both* edges/links (p, u) and (p, w) must exist and be stable before the link (u, v) can be created (or considered stable).

We require one additional finding. By following the routing along Voronoi edges as described in Section III-B, if u sends a message to a neighbor v, $v \in V$, then the message will only traverse along edges that have a *DTlabel* value smaller than that of (u, v), as shown earlier in [7].

We need to show by induction that, for all h, $1 \leq h \leq N$,

(i) For every message of type *edge* or *link* with label h, the message will arrive at its destination and always be available at the destination.

(ii) For every message of type *catch* or *throw* that encapsulates a message with label h or less, the message will arrive at its destination.

(iii) For every node u and every v, $v \in u.V$, if $u.label[v] \leq h$, then *DTlabel*$(u, v) = u.label[v]$, and $v \in R(u)$.

(iv) For every node u and every v, $v \in R(u)$, if $DTlabel(u, v) \leq h$, then $u.label[v] =$ *DTlabel*(u, v), and $v \in V$.

(v) For each extended link (u, v), if *DTlabel*$(u, v) \leq h$, then $v \in u.L_{ext}$, $u.label[v] =$ *DTlabel*(u, v), and $u.origin[v] =$ *origin*(u, v).

(vi) For every node u and every node v, $v \in u.L_{ext}$, if $u.label[v] \leq h$, then *DTlabel*$(u, v) = u.label[v]$ and $u.origin[v] =$ *origin*(u, v).

Consider first $h = 1$. Extended links and non-direct Voronoi edges have a $DTlabel$ greater than one. Only direct physical links can have a label of one, which is hard-coded in the protocol. Also, routine $clean(V)$ ensures that the physical links in $R(u)$ are included in V. The origin value of a physical link is *nil* since it does not depend on other links. Furthermore, any message created has as label the sum of two other labels, and thus, its label is at least two. Any existing messages that have a label of one will not be recreated by their sources, and thus, by the ttl, they will be permanently removed.

Assume the induction hypothesis is correct for all labels at most h. We now consider labels at most $h + 1$. Consider first a message with label $h + 1$ whose (src, dst, nbr) do not correspond to a triangle in the DT. In order for a message of label $h+1$ to be recreated, both edges (src, dst) and (src, nbr) must have a label at node src of at most h. But, by the induction hypothesis, these would correspond to real edges in the DT, and hence, this message cannot be recreated. By the ttl, the message will disappear permanently from the network.

Consider now a Voronoi edge (u, v) in the DT with *DTlabel*$(u, v) = h + 1$ and origin x. This implies

DTlabel$(x, u) \leq h$ and *DTlabel*$(x, v) \leq h$. By the induction hypothesis, u and v are in $x.V$ with the correct label and origin, and also in $R(x)$. Thus, no node can be in between u and v in $x.V$, and in consequence, x will send an *edge* message of label $h + 1$ to both u and v. From the induction hypothesis, these messages will be delivered to u and v. Since edge (u, v) belongs to both $R(u)$ and $R(v)$, no node can block the edge from being added to $u.V$ and $v.V$, as desired.

The argument that extended links will be created from *link* messages follows a similar argument. Likewise, if a *throw* or *catch* message contains a message with label $h + 1$, it implies that both the link and the edge that join the extended link have labels at most h, and thus, the contained message will be delivered correctly.

X. Conclusion and Future Work

We presented an efficient and self-stabilizing protocol for computing the Voronoi region of a sensor node in a large wireless sensor network. In particular, it departs from the unit-circle communication model. Because faults can be modeled as making arbitrary changes to the network state, any self-stabilizing protocol is resilient against all type of transient faults, provided the network does not become partitioned. There is no assumption of having an underlying routing protocol to aid in routing control messages. Thus, the protocol can successfully communicate with any Voronoi neighbor without any additional aid, and can be used as the foundation for a geographic routing protocol.

If nodes are distributed in the plane according to a Poisson process with constant intensity, then each node in the DT of these nodes has on average six neighbors [17]. In general, a node u receives messages from a source s to destination d if s and d are Voronoi neighbors and their Voronoi path crosses u. Given the small number of surrounding neighbors, if the deployment area is regular, as opposed to a long linear shape, then we expect the number of such pairs to be small, even of constant size. Thus, the overhead in most networks will be small, even smaller than $O(N)$. In our future work, we will perform simulations over randomly generated networks to measure the worst and average node overhead over various topologies and node densities.

References

[1] J. Yick, B. Mukherjee, and D. Ghosal, "Wireless sensor network survey," Computer Networks, vol. 52, no. 12, 2008, pp. 2292 – 2330.

[2] P. Bose, P. Morin, I. Stojmenović, and J. Urrutia, "Routing with guaranteed delivery in ad hoc wireless networks," Wireless Networks, vol. 7, no. 6, Nov 2001, pp. 609–616.

[3] B. Karp and H. T. Kung, "Gpsr: Greedy perimeter stateless routing for wireless networks," in Proc. of the 6th Annual International Conference on Mobile Computing and Networking, ser. MobiCom '00. New York, NY, USA: ACM, 2000, pp. 243–254.

[4] S. S. Lam and C. Qian, "Geographic routing in d-dimensional spaces with guaranteed delivery and low stretch," SIGMETRICS Perform. Eval. Rev., vol. 39, no. 1, Jun. 2011, pp. 217–228.

[5] B. Leong, B. Liskov, and R. Morris, "Geographic routing without planarization," in Proc. of the 3rd Conf. on Networked Systems Design & Implementation, ser. NSDI'06. Berkeley, CA, USA: USENIX Association, 2006, pp. 25–25.

[6] P. Bose and P. Morin, "Online routing in triangulations," in Proc. of the 10th International Symposium on Algorithms and Computation, ser. ISAAC '99. London, UK: Springer-Verlag, 1999, pp. 113–122.

[7] J. A. Cobb, "Stabilizing voronoi diagrams for sensor networks," in Proc. of The 14th Int. Conf. on Systems and Networks Communications, Valencia, Spain, 2019, pp. 7 – 13.

[8] M. Schneider, "Self-stabilization," ACM Computing Surveys, vol. 25, no. 1, Mar. 1993, pp. 45–67.

[9] E. W. Dijkstra, "Self-stabilizing systems in spite of distributed control," Commun. ACM, vol. 17, no. 11, 1974, pp. 643–644.

[10] S. Dolev., Self-Stabilization. Cambridge, MA: MIT Press, 2000.

[11] M. G. Gouda, "The triumph and tribulation of system stabilization," in Proc. of the 9th International Workshop on Distributed Algorithms (WDAG). London, UK: Springer-Verlag, 1995, pp. 1–18.

[12] Y. Nnez-Rodrguez, H. Xiao, K. Islam, and W. Alsalih, "A distributed algorithm for computing voronoi diagram in the unit disk graph model," in Proc. of the 20th Canadian Conference in Computational Geometry, Quebec, Canada, 2008, pp. 199–202.

[13] D. Y. Lee and S. S. Lam, "Protocol design for dynamic delaunay triangulation," in 27th International Conference on Distributed Computing Systems (ICDCS '07), June 2007, pp. 26–26.

[14] ——, "Efficient and accurate protocols for distributed delaunay triangulation under churn," in 2008 IEEE International Conference on Network Protocols, Oct 2008, pp. 124–136.

[15] R. Jacob, S. Ritscher, C. Scheideler, and S. Schmid, "A self-stabilizing and local delaunay graph construction," in Algorithms and Computation, Y. Dong, D.-Z. Du, and O. Ibarra, Eds. Berlin, Heidelberg: Springer Berlin Heidelberg, 2009, pp. 771–780.

[16] J. A. Cobb, "Preserving routes during fast convergence," in Proc. of the 13th IEEE International Workshop on Assurance in Distributed Systems and Networks (ADSN), Madrid, Spain, June 2014, pp. 125–132.

[17] R. A. Dwyer, "Higher-dimensional voronoi diagrams in linear expected time," Discrete & Computational Geometry, vol. 6, no. 3, Sep 1991, pp. 343–367.

 ISBN: 978-1-61208-828-0

On Evaluating Spectrum Allocation Techniques in Millimeter-Wave Systems Using Indoor Smalls for 5G/6G

Rony Kumer Saha
Radio and Spectrum Laboratory
KDDI Research, Inc.
2-1-15 Ohara, Fujimino-shi, Saitama 356-8502, Japan
Email: ro-saha@kddi-research.jp

***Abstract*— In this paper, we present three spectrum allocation techniques, namely Static and Equal Spectrum Allocation (SESA), Flexible and Unequal Spectrum Allocation (FUSA), and Countrywide Full Spectrum Allocation (CFSA), and evaluate their performances for the 28 GHz millimeter-wave spectrum using in-building small cells. We discuss each technique broadly by identifying major concerns, presenting possible solutions, as well as evaluating performances relative to each other in terms of Spectral Efficiency (SE), Energy Efficiency (EE), and Cost Efficiency (CE). It is found that FUSA improves SE by 22.8%, EE by 18.56%, and CE by 18.56%, whereas CFSA improves SE by 164.27%, EE by 74.77%, and CE by 59.64% in comparison with that of SESA. As CFSA outperforms SESA and FUSA, CFSA can be considered as a potential spectrum allocation technique for the existing and next-generation mobile networks to allow a large spectrum availability, as well as efficient spectrum utilization, for an operator to serve high indoor data rates and capacity demands.**

Keywords-28 GHz; spectrum allocation; millimeter-wave; small cell; spectrum utilization; technique.

I. INTRODUCTION

Spectrum allocation techniques have a significant impact on the efficient utilization of the radio spectrum in mobile communication systems [1]. Traditionally, each Mobile Network Operator (MNO) in a country is allocated statically and exclusively to an equal amount of the licensed spectrum (termed as Static and Equal Spectrum Allocation (SESA)) for a long term, irrespective of the demand of its users. Since the demand for user traffic of different MNOs in a country varies with time and locations, the requirements of the spectra of MNOs also vary accordingly. Due to this phenomenon, a great portion of the allocated spectrum to an MNO may be either unused or underutilized [2]-[3], while another MNO at the same time and location may suffer from an insufficient amount of spectrum. This, in turn, results in low spectrum utilization and Quality-of-Service (QoS), which raises concerns over how to allocate the spectrum among MNOs such that the required user demand can be served while ensuring an efficient countrywide spectrum utilization.

One way to address this concern is to allocate spectrum to each MNO based on the actual requirement to serve its user traffic [4]. In this regard, a simple, yet effective, measure to define the actual requirement for an MNO is to allocate spectrum flexibly in accordance with its number of subscribers. Since the number of subscribers of an MNO is usually different from that of other MNOs, such a flexible and on-demand spectrum allocation technique allocates an unequal amount of spectrum to MNOs (termed as Flexible and Unequal Spectrum Allocation (FUSA)), unlike SESA. Also, to address frequent variations in the statistics of subscribers of MNOs, in FUSA, the allocation of spectrum to each MNO needs to be updated in the short term, unlike SESA.

Another key technique to address an efficient spectrum utilization and the required QoS is to allow access to the countrywide full spectrum to each MNO subject to managing Co-Channel Interference (CCI) from one MNO to another (termed as Countrywide Full Spectrum Allocation (CFSA)). In this regard, since different MNOs have a different number of subscribers, an MNO can pay the spectrum licensing fee for a short term based on its number of subscribers with respect to the total number of subscribers countrywide to ensure fairness. Note that CFSA takes advantage of allocating a large amount of spectrum to each MNO to address the required QoS, as well as the dynamic allocation of the spectrum to each MNO corresponding to serving its user demand to address an efficient countrywide spectrum utilization. Figure 1 shows an illustration of allocating the countrywide spectrum to MNOs using SUSA, FUSA, and CFSA techniques.

Since existing and next-generation mobile networks will be spectrum hungry to serve a high data rate and a large volume of traffic, particularly in urban multistory buildings, ensuring high spectrum bandwidth is one of the major concerns to MNOs. To address the high bandwidth availability for an MNO indoors, the Millimeter-Wave (mmWave) spectrum is considered as an effective solution. In this regard, the 28 GHz band has been considered as a potential mmWave band due to its favorable indoor characteristics to address a high data rate and capacity demand within a short distance. Hence, in this paper, we intend to evaluate the SESA, FUSA, and CFSA techniques indoors for 28 GHz spectrum in terms of Spectral Efficiency (SE), Energy Efficiency (EE), and Cost Efficiency (CE).

II. MATHEMATICAL ANALYSIS

Let O denote the maximum number of MNOs in a country such that $o \in \boldsymbol{O} = \{1,2,...,O\}$. Let M_{C} and N_{C} denote the countrywide 28 GHz mmWave spectrum and the total number of users of all MNOs in a country,

 ISBN: 978-1-61208-828-0

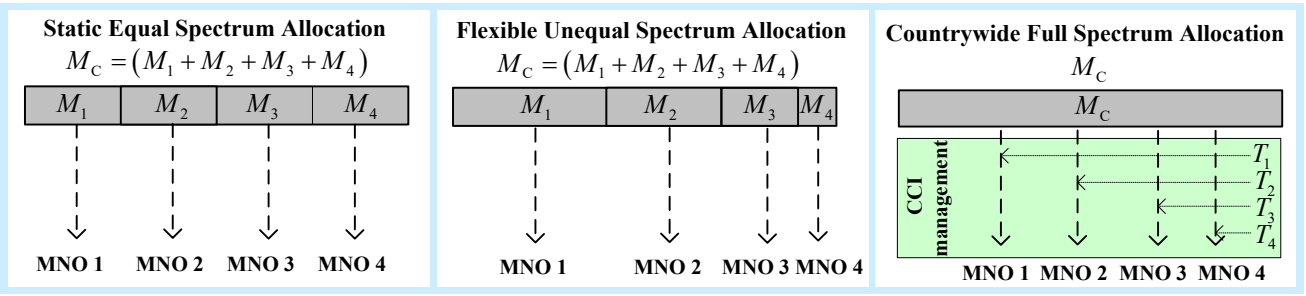

Figure 1. An illustration of SESA, FUSA, and CFSA techniques at any term t_r.

respectively. M_C is expressed in terms of the number of Resource Blocks (RBs) where an RB is equal to 180 kHz such that $\sum_{o=1}^{O} M_{o,t_r} \le M_C$, as well as $\sum_{o}^{O} N_{o,t_r} \le N_C$, at any license renewed term t_r. Now, based on the aforementioned criterion for each technique, the amount of allocated spectrum to an MNO o in SESA at any term t_r can be given by $M_{o,t_r} = M : o \in \boldsymbol{O}$, where M is the same for all MNOs. Likewise, the amount of allocated spectrum to an MNO o in FUSA at term t_r can be given by $M_{o,t_r} = \left(N_{o,t_r} \times M_C\right) / N_C : o \in \boldsymbol{O}$, as shown in Figure 1.

However, in CFSA, the amount of spectrum allowed to be accessed by each MNO at term t_r is given by $M_{o,t_r} = M_C : t \in \boldsymbol{T}^{\mathrm{nA}}_{o,t_r} \wedge o \in \boldsymbol{O}$ where $\boldsymbol{T}^{\mathrm{nA}}_{o,t_r}$ denotes a set of Transmission Time Intervals (TTIs) t during which an MNO o can get access to M_C in an observation period $\boldsymbol{T}$ with the maximum time of Q (in time step each lasting 1 ms) such that $t \in \boldsymbol{T}$. Since each MNO is allocated to the same spectrum, CCI can occur in CFSA. We consider the time-domain CCI management as an example. Hence, to avoid CCI in time-domain, we consider time orthogonality in allocating the full spectrum to small cell User Equipments (UEs) of all MNOs such that in any TTI t Small cell UEs (SUs) of only one MNO in a building can be scheduled using techniques, such as the Almost Blank Subframe (ABS) based Enhanced Intercell Interference Coordination (eICIC) [5]-[6].

Assume that the number of TTIs per ABS Pattern Period (APP) t_{APP} allocated to any UE of an MNO o is the number of non-ABSs allocated to the corresponding MNO o over t_{APP} in any building, which is defined as follows. The number of non-ABSs per APP allocated to any UE of an MNO o in a building is defined in accordance with the ratio of the number of subscribers N_{o,t_r} of the MNO o at any renewed term t_r to the sum of the number of subscribers of MNOs $\boldsymbol{O} \backslash o$ (plus N_{o,t_r} of MNO o) so that at least an SU corresponding to the MNO $\boldsymbol{O} \backslash o$ is present within the same building in any TTI t of the previous APP $\left(t_{\mathrm{APP}} - 1\right)$.

Let $\boldsymbol{T}^{\mathrm{A}}_{o,t_r}$ and $\boldsymbol{T}^{\mathrm{nA}}_{o,t_r}$ denote, respectively, a set of all ABSs and a set of all non-ABSs at term t_r for an MNO $o \in \boldsymbol{O}$ at all APPs in $\boldsymbol{T}$, such that $T^{\mathrm{A}}_{o,t_r} \in \boldsymbol{T}^{\mathrm{A}}_{o,t_r}$, $T^{\mathrm{nA}}_{o,t_r} \in \boldsymbol{T}^{\mathrm{nA}}_{o,t_r}$, and $\boldsymbol{T} = \boldsymbol{T}^{\mathrm{A}}_{o,t_r} + \boldsymbol{T}^{\mathrm{nA}}_{o,t_r}$. Hence, the number of non-ABSs (i.e., operating time) T^{nA}_{o,t_r} of small cells of MNO o at term t_r to use the full countrywide spectrum using CFSA for O=4 at any t_{APP} [7] is given by

$$T^{\mathrm{nA}}_{o,t_r} = \left\lceil \left(\left(N_{o,t_r} \Big/ \sum_{o=1}^{O} \left(1_{\nu_o}\left(N_{o,t_r}\right) N_{o,t_r} \right) \right) \times T_{\mathrm{APP}} \right) \right\rceil \quad (1)$$

where $\nu_o \in \left\{ N_{1,t_r}, N_{2,t_r} N_{3,t_r}, N_{4,t_r} \right\}$. $1(\cdot)$ is defined such that $1(\cdot) = 1$ if N_{o,t_r} exists in the set ν_o; otherwise, $1(\cdot) = 0$. T_{APP} denotes the duration of an APP in TTIs.

III. Problem Formulation

Let S_F denote the maximum number of small cells in a building such that $s \in \{1,2,...,S_F\}$. Let S_M denote the number of macrocells, and let S_P denote the number of picocells per macrocell of each MNO. Let P_M, P_P, and P_S denote, respectively, the transmission power of a macrocell, a picocell, and a small cell of an MNO o. Using Shannon's capacity formula, a link throughput at RB=i in TTI=t for an MNO o at term t_r in bps per Hz is given by [8]

$$\sigma^{t_r}_{t,i,o}\left(\rho^{t_r}_{t,i,o}\right) = \begin{cases} 0, & \rho^{t_r}_{t,i,o} < -10\,\mathrm{dB} \\ \beta \log_2\left(1 + 10^{\left(\rho^{t_r}_{t,i,o}(\mathrm{dB})/10\right)}\right), & -10\,\mathrm{dB} \le \rho^{t_r}_{t,i,o} \le 22\,\mathrm{dB} \\ 4.4, & \rho^{t_r}_{t,i,o} > 22\,\mathrm{dB} \end{cases} \quad (2)$$

where β denotes the implementation loss factor.

Let $M_{\mathrm{MBS},o}$ denote the spectrum in RBs of a macrocell for an MNO o. Then, the total capacity of all macrocell UEs for an MNO o at t_r can be expressed as

$$\sigma^{t_r}_{\mathrm{MBS},o} = \sum_{t=1}^{Q} \sum_{i=1}^{M_{\mathrm{MBS},o}} \sigma^{t_r}_{t,i,o}\left(\rho^{t_r}_{t,i,o}\right) \quad (3)$$

 ISBN: 978-1-61208-828-0

where σ and ρ are responses over $M_{\mathrm{MBS},o}$ RBs of all macro UEs in $t \in \boldsymbol{T}$ for an MNO o at t_{r}.

If all Small cell Base Stations (SBSs) in a multistory building serve simultaneously in t, the aggregate capacity served by all SBSs in a building of an MNO o at term t_{r} is given by

$$\sigma_{S_{\mathrm{F}},o}^{t_{\mathrm{r}}} = \sum_{s=1}^{S_{\mathrm{F}}} \sum_{t} \sum_{i=1}^{M_{o,t_{\mathrm{r}}}} \sigma_{t,i,o}^{t_{\mathrm{r}}} \left(\rho_{t,i,o}^{t_{\mathrm{r}}} \right) \quad (4)$$

Let us define Cost Efficiency (CE) as the cost required per unit achievable average capacity (i.e., per bps). Let ε_{C} denote the cost of M_{C} such that an MNO o pays $\varepsilon_{o,t_{\mathrm{r}}}$ for its licensed spectrum $M_{o,t_{\mathrm{r}}}$ at t_{r}. The system-level average aggregate capacity, SE, EE, and CE for all MNOs O countrywide at t_{r} for all techniques are given, respectively, by

$$\sigma_{\mathrm{cap},O}^{\mathrm{sys},t_{\mathrm{r}}} = \sum_{o=1}^{O} \left(\sigma_{\mathrm{MBS},o}^{t_{\mathrm{r}}} + \sigma_{S_{\mathrm{F}},o}^{t_{\mathrm{r}}} \right) \quad (5)$$

Since $\sigma_{S_{\mathrm{F}},o}^{t_{\mathrm{r}}} >> \sigma_{\mathrm{MBS},o}^{t_{\mathrm{r}}}$, $\sigma_{\mathrm{cap},O}^{\mathrm{sys},t_{\mathrm{r}}} \cong \sum_{o=1}^{O} \sigma_{S_{\mathrm{F}},o}^{t_{\mathrm{r}}}$

$$\sigma_{\mathrm{SE},O}^{\mathrm{sys},t_{\mathrm{r}}} = \sigma_{\mathrm{cap},O}^{\mathrm{sys},t_{\mathrm{r}}} \Big/ \left(\sum_{o=1}^{O} \left(M_{\mathrm{MBS},o} + M_{o,t_{\mathrm{r}}} \right) \times Q \right) \quad (6)$$

$$\sigma_{\mathrm{EE},O}^{\mathrm{sys},t_{\mathrm{r}}} = \left(O\left(S_{\mathrm{F}} P_{\mathrm{S}} + S_{\mathrm{P}} P_{\mathrm{P}} + S_{\mathrm{M}} P_{\mathrm{M}} \right) \right) \Big/ \left(\sigma_{\mathrm{cap},O}^{\mathrm{sys},t_{\mathrm{r}}} / Q \right) \quad (7)$$

$$\varsigma_{\mathrm{CE},O}^{\mathrm{sys},t_{\mathrm{r}}} = \varepsilon_{\mathrm{C}} \Big/ \sigma_{\mathrm{cap},O}^{\mathrm{sys},t_{\mathrm{r}}} \quad (8)$$

where $t \in \begin{Bmatrix} \boldsymbol{T}, & \text{for SESA} \\ \boldsymbol{T}, & \text{for FUSA} \\ \boldsymbol{T}_{\boldsymbol{o},\boldsymbol{t_{\mathrm{r}}}}^{\mathbf{nA}}, & \text{for CFSA} \end{Bmatrix}$ and

$$M_{o,t_{\mathrm{r}}} = \begin{Bmatrix} M, & \text{for SESA} \\ \left(N_{o,t_{\mathrm{r}}} M_{\mathrm{C}} \right) / N_{\mathrm{C}}, & \text{for FUSA} \\ M_{\mathrm{C}}, & \text{for CFSA} \end{Bmatrix}.$$

IV. Performance Evaluation

A. Performance Result

Table I shows selected assumptions and parameters used for the performance evaluation. Detailed assumptions and parameters can be found in [7]. Figure 2 shows the outperformance of FUSA and CFSA techniques with respect to the traditional SESA in terms of countrywide SE, EE, and CE. It can be seen that FUSA improves SE by 22.8%, EE by 18.56%, and CE by 18.56%, whereas CFSA improves SE by 164.27%, EE by 74.77%, and CE by 59.64% in comparison with that of SESA. Hence, due to allowing dynamic access to the countrywide full mmWave spectrum to each MNO to utilize the full spectrum efficiently, CFSA provides the best SE, EE, and CE performances of all techniques.

TABLE I. Default Parameters and Assumptions

Parameters and assumptions	Value
Countrywide 28 GHz spectrum, MNOs, and subscribers	200 MHz; 4; N_{C}
Number of subscribers for MNOs 1, 2, 3, and 4	20%, 30%, 20% and 10% of N_{C}
E-UTRA simulation case[1]	3GPP case 3
Small cell model[2]	A building with square-grid apartments
Number of small cells	48
Observation time	8 ms

Taken [1]from [9] and [2]from [10].

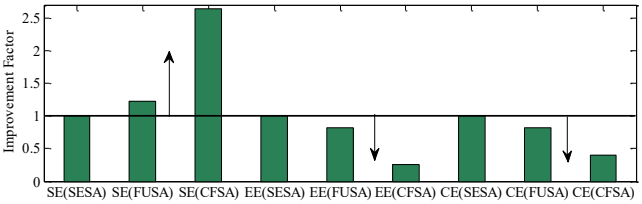

Figure 2. Performances of FUSA and CFSA with respect to SESA.

B. Issues with CFSA Implementation

Though CFSA provides the best performances of all techniques, a number of issues regarding, for example, its implementation, need to be addressed, as indicated below.

1) CCI management system: A key issue with CFSA is the co-channel interference generated when UEs of more than one MNO intend to access the countrywide spectrum. Though CCI can be managed, it requires additional management mechanisms either in time, frequency, or power domain, which, in turn, cause additional complexity and cost. For example, depending on the spectrum sensing techniques, such as either proactive or reactive, as well as management approaches, e.g. either centralized or distributed, the control signaling overhead may vary. More specifically, in the centralized management, though the global optimization of network performance can be obtained, it suffers from a large control signaling overhead in the network. In contrast, in the distributed management, the control signaling overhead is reduced by allowing the local network performance optimization.

2) Countrywide spectrum manager: Since all MNOs access the same countrywide spectrum, a common spectrum manager may be necessary to communicate and coordinate a timely and fair allocation of the spectrum to each MNO. In this regard, the deployment of the spectrum manager, the degree of information to be shared by each MNO with the spectrum manager, and tight coordination to allocate the spectrum among MNOs timely and fairly are a few challenges that need to be addressed for the spectrum manager.

3) Spectrum licensing fees: Distributing the licensing fee among MNOs in a country and the duration of the spectrum license renewed term t_{r} need a common mutual understanding among MNOs in a country, which sometimes may not be possible due to the competitive nature of MNOs in the market. In such a case, the central administration by

 ISBN: 978-1-61208-828-0

the spectrum regulatory bodies may be required to sort out the issues among MNOs countrywide [11].

V. CONCLUSION

In this paper, we have presented three spectrum allocation techniques, namely SESA, FUSA, and CFSA, and shown that CFSA outperforms SESA and FUSA techniques in SE, EE, and CE such that CFSA can be considered as a potential spectrum allocation technique for Fifth Generation (5G)/Sixth Generation (6G) mobile networks.

REFERENCES

[1] S. J. Kim, E. C. Kim, S. Park, and J. Y. Kim, "Dynamic Spectrum Allocation with Variable Bandwidth for Cognitive Radio Systems," Proc. The 2009 9th International Symposium on Communications and Information Technology, IEEE Press, Sept. 2009, pp. 106-109, doi: 10.1109/ISCIT.2009.5341278.

[2] M. R. Hassan, G. C. Karmakar, J. Kamruzzaman, and B. Srinivasan, "Exclusive Use Spectrum Access Trading Models in Cognitive Radio Networks: A Survey," IEEE Communications Surveys & Tutorials, vol. 19, Fourthquarter 2017, pp. 2192-2231, doi: 10.1109/COMST.2017.2725960.

[3] I. F. Akyildiz, W.-Y. Lee, M. C. Vuran, and S. Mohanty, "NeXt Generation/Dynamic Spectrum Access/Cognitive Radio Wireless Networks: A Survey," Computer Networks, vol. 50, Sep. 2006, pp. 2127-2159, doi: 10.1016/j.comnet.2006.05.001.

[4] R. K. Saha, "On Exploiting Millimeter-Wave Spectrum Trading in Countrywide Mobile Network Operators for High Spectral and Energy Efficiencies in 5G/6G Era," Sensors, vol. 20, 2020, Art. No. 3495, doi: 10.3390/s20123495.

[5] D. Lopez-Perez, I. Guvenc, G. de la Roche, M. Kountouris, T. Q. S. Quek, and J. Zhang, "Enhanced Intercell Interference Coordination Challenges in Heterogeneous Networks," IEEE Wireless Communications, vol. 18, pp. 22-30, Jun. 2011, doi: 10.1109/MWC.2011.5876497.

[6] R. K. Saha, "A Hybrid System and Technique for Sharing Multiple Spectrums of Satellite Plus Mobile Systems with Indoor Small Cells in 5G and Beyond Era," IEEE Access, vol. 7, pp. 77569-77596, 2019, doi: 10.1109/ACCESS.2019.2921723.

[7] R. K. Saha, "A Countrywide Licensed Full Spectrum Allocation Method for Millimeter-Wave Mobile Systems for 6G," (accepted) Proc. The 2020 IEEE 92nd Vehicular Technology Conference (VTC2020-Fall) Workshops, IEEE Press, Oct. 2020, pp. 1-7.

[8] R. K. Saha, S. Nanba, and K. Nishimura, "A Technique for Cloud Based Clustering and Spatial Resource Reuse and Scheduling of 3D In-Building Small Cells Using CoMP for High Capacity CRAN," IEEE Access, vol. 6, pp. 71602-71621, Nov. 2018, doi: 10.1109/ACCESS.2018.2879835.

[9] Evolved Universal Terrestrial Radio Access (E-UTRA); Radio Frequency (RF) System Scenarios. document 3GPP TR 36.942, V.1.2.0, 3rd Generation Partnership Project, Jul. 2007. Available online: https://portal.3gpp.org/ desktopmodules /Specifications/Specification Details.aspx?specificationId=2592 [retrieved: February, 2020]

[10] R. K. Saha and C. Aswakul, "A Novel Frequency Reuse Technique for In-Building Small Cells in Dense Heterogeneous Networks," IEEJ Transactions on Electrical and Electronic Engineering, vol. 13, pp. 98-111, Jan. 2018, doi.org/10.1002/tee.22503.

[11] A. M. Foster, "Spectrum Sharing," Proc. The 8th Global Symposium for Regulators, International Telecommunication Union, Mar. 2008, pp. 1-35.

 ISBN: 978-1-61208-828-0

A Massive Millimeter-Wave Spectrum Allocation and Exploitation Technique Toward 6G Mobile Networks

Rony Kumer Saha
Radio and Spectrum Laboratory
KDDI Research, Inc.
2-1-15 Ohara, Fujimino-shi, Saitama, Japan
Email: ro-saha@kddi-research.jp

***Abstract*—In this paper, we propose a Countrywide Millimeter-Wave (mmWave) Spectrum Allocation and Reuse (CoMSAR) technique to allocate and reuse spatially the countrywide massive 28 GHz mmWave spectrum to each Mobile Network Operator (MNO) to operate its small cells per floor in a multistory building. A frequency-domain interference management scheme is developed, and the optimal amount of spectrum for each MNO is deduced to avoid Co-Channel Interference (CCI) at the presence of User Equipments (UEs) of multiple MNOs on each floor. We derive average capacity, Spectral Efficiency (SE), Energy Efficiency (EE), and Cost Efficiency (CE) for CoMSAR. Extensive numerical and simulation results and analyses are carried out for an example scenario of a country consisting of four MNOs, i.e., MNO 1, MNO 2, MNO 3, and MNO 4 with a subscriber base of, respectively, 40%, 30%, 20%, and 10% of the total countrywide subscribers. It is shown for MNO 1 that the proposed technique can improve average capacity, SE, EE, and CE by 300%, 165%, 75%, and 60%, respectively, with no CCI, whereas 60%, 6%, 37%, and 0.4%, respectively, with the maximum CCI. Further, we show that CoMSAR can satisfy the SE and EE requirements for sixth-generation (6G) mobile systems by reusing the countrywide 28 GHz mmWave spectrum to small cells of MNO 1 of about 60% less number of floors with no CCI, whereas 3.3% less number of floors with the maximum CCI, in a building.**

***Keywords*—6G; 28 GHz; countrywide; millimeter-wave; mobile network; spectrum allocation; spectrum exploitation; technique.**

I. INTRODUCTION

The high capacity and data rates requirements for the existing mobile networks impose a demand for the massive radio spectrum availability on a Mobile Network Operator (MNO). Though these requirements have been increased over time, the availability of the spectrum for an MNO has not increased correspondingly, resulting in the scarcity of the radio spectrum. In this regard, spectrum allocation and spectrum exploitation can play a vital role in addressing the spectrum scarcity for an MNO in a country. By carefully allocating the spectrum specified for a country among its MNOs, the available amount of spectrum for an MNO can be extended considerably. Furthermore, by exploiting the available spectrum for an MNO in space, for example, the utilization of the spectrum can be increased. Accordingly, the spatial reuse of the spectrum to small cells, particularly in a 3-Dimensional (3D) space, e.g. a multistory building, is considered as an effective approach to increase the utilization of the available spectrum.

Numerous research works have already addressed the issues of spectrum allocation [1]-[3], as well as spectrum exploitation [4]-[6]. For example, Yan et al. [1] have proposed methods for the dynamic spectrum allocation in cognitive radio systems. Kim et al. [2] have introduced the functionalities required for entities related to the spectrum allocation to propose a spectrum allocation algorithm in multiple network operators' scenario. Moreover, Kim et al. [3] have introduced and formulated the problem of the optimum spectrum allocation in cognitive radios. Besides, regarding the spectrum exploitation by means of reusing the available spectrum, Saha and Aswakul [4] have proposed an analytical model to reuse the spectrum in a 3D building of small cells. Likewise, Saquib et al. [5] have investigated a number of Fractional Frequency Reuse (FFR) schemes. Moreover, Saha [6] has proposed a technique to reuse the same spectrum by small cells deployed in a building by forming 3D clusters of small cells.

However, unlike the traditional static licensed spectrum allocation that considers allocating a certain portion of the countrywide spectrum to an MNO, the whole countrywide Millimeter-Wave (mmWave) spectrum can be allocated to each MNO to increase its spectrum. Besides, due to the high floor penetration loss, the same countrywide mmWave spectrum for each MNO can be exploited spatially in the inter-floor level to reuse it more than once by small cells within a building. Hence, a technique that can employ both the spectrum allocation and spectrum exploitation means to the mmWave spectrum using in-building small cells to allocate the countrywide mmWave spectrum to each MNO, which is exploited further to be spatially reused by small cells in a building is considered promising to achieve high Spectral Efficiency (SE) and Energy Efficiency (EE) requirements for the next generation mobile networks.

Numerous studies have already attempted to achieve the expected SE and EE requirements for the Sixth-Generation (6G) mobile networks by employing the mmWave spectrum allocation and exploitation. For example, by exploiting the power-domain, Saha [7] has proposed a hybrid interweave–underlay spectrum access and reuse technique to address the dynamic spectrum access and reuse of the countrywide 28 GHz mmWave spectrum to in-building small cells of each MNO in a country to achieve the required SE and EE of 6G. Unlike the countrywide mmWave spectrum, by exploiting the secondary spectrum trading, Saha [8] has proposed a dynamic exclusive-use spectrum access method to share partly and exclusively the licensed mmWave spectrum of one MNO to another in a country to address the SE and EE requirements for 6G. Further, Saha [9] has presented a technique for the 3D spatial reuse of

 ISBN: 978-1-61208-828-0

28 and 60 GHz mmWave spectra allocated to an MNO to its in-building small cells to achieve the expected SE and EE requirements for 6G networks.

Unlike these existing literature works, in this paper, by exploiting the frequency-domain, we propose A Countrywide MmWave Spectrum Allocation and Reuse (CoMSAR) technique that considers allocating and then reusing the massive 28 GHz mmWave spectrum specified countrywide to each MNO of a country to operate its small cells deployed on each floor in a multistory building to achieve the expected SE and EE requirements for 6G mobile networks. In addressing the proposed technique, we first present the system architecture and the proposed technique, as well as develop a frequency-domain Co-Channel Interference (CCI) avoidance scheme, in Section II. In Section III, we derive average capacity, SE, EE, and CE metrics for the proposed technique. In Section IV, extensive numerical and simulation results and analyses for an example scenario of a country consisting of four MNOs is carried out under two extreme CCI scenarios, including no CCI and the maximum CCI, for an MNO to show that the proposed technique can achieve the SE and EE requirements for 6G mobile systems. We conclude the paper in Section V. A list of acronyms/abbreviations is shown in Table I and a list of selected notations is given in Table II.

II. System Architecture and Proposed Technique

A. System Architecture

Figure 1 shows the system architecture consisting of four MNOs, defined as MNO 1, MNO 2, MNO 3, and MNO 4, operating in a country. We assume that all MNOs have similar system architectural features including three types of Base Stations (BSs), namely macrocell BSs (MBSs), Picocell BSs (PBSs), and Small Cell BSs (SBSs). Hence, for simplicity in evaluating the performances, the detailed architecture of only one MNO, i.e., MNO 1, is shown in Figures 1(a) and 1(b). SBSs are deployed only within 3-dimensional multistory buildings each serving one User Equipment (UE) at a time (Figure 1(d)). Both SBSs and PBSs are located within the coverage of an MBS. All macrocell UEs per MBS are served either by the MBS itself or any PBSs. Due to the favorable characteristics, MBSs and PBSs operate at a low-frequency band, i.e., 2 GHz, whereas all in-building SBSs operate at the 28 GHz mmWave band (Figure 1(a)).

We consider that each MNO is given access to the countrywide 28 GHz mmWave spectrum to extend its spectrum at all times by enforcing the frequency-domain CCI management, as shown in Figure 1(d). Given that CCI for an MNO o increases with an increase in the number of UEs of other MNOs $\boldsymbol{O}\backslash o$ (Figure 1(c) for MNO 1), Figure 1(d) shows two extreme CCI scenarios for small cells of MNO 1 on a floor based on the presence of UEs of other MNOs $\boldsymbol{O}\backslash o$ within the same floor of a building. For simplicity, CCI scenarios are shown for a single small cell in an apartment on a floor. Besides, the penetration loss of a typical reinforced concrete floor in the 28 GHz mmWave spectrum is about 55 dB for the first floor [10]-[12]. Hence, by exploiting the high floor penetration loss of 28 GHz mmWave spectrum, on top of the spectrum extension by allocating the countrywide massive 28 GHz spectrum to each MNO, we consider the spectrum exploitation by reusing the same countrywide spectrum to SBSs of each MNO on each floor of a building to increase spectral utilization (Figures 1(b) and 1(d)). We propose a technique for the spectrum allocation and the spectrum exploitation of the countrywide 28 GHz spectrum to each MNO in what follows.

B. Proposed Technique

We propose a countrywide mmWave spectrum allocation and reuse (CoMSAR) technique to extend the available spectrum for an MNO and to increase its utilization as follows. *Each MNO of a country is assigned with the massive 28 GHz mmWave spectrum specified countrywide, which is reused further, to operate its small cells deployed on each floor in a building at the cost of paying the spectrum licensing fee subject to avoiding CCI. The amount of the spectrum licensing fee for an MNO is updated corresponding to the change in its number of subscribers at each license renew term* t_{rnw}.

In this regard, for the 28 GHz mmWave spectrum allocation, each MNO is allocated to the countrywide 28 GHz mmWave spectrum by the National Regulatory Agency (NRA) or any third-party for a term t_{rnw}. For the 28 GHz mmWave spectrum reuse, each MNO can exploit the high floor penetration loss of a multistory building at mmWave such that the allocated countrywide full 28 GHz mmWave spectrum can be reused to its SBSs deployed on each floor (Figure 1(b)) due to the insignificant or no CCI generated between SBSs on adjacent floors. This results in reusing the allocated countrywide spectrum to an MNO more than once to its SBSs within a multistory building and, hence, in improving the countrywide 28 GHz mmWave spectrum utilization.

Each MNO pays the licensing fee to the NRA, which is defined by the administration based on the ratio of its actual number of subscribers to the sum of the total number of subscribers of all MNOs countrywide at t_{rnw}. Hence, the proposed technique can help overcome the lack of a sufficient amount of spectrum of an MNO to serve the necessary demand of its users, as well as address the issue of the under-utilized or unused spectrum of other MNOs, which in turn improve the overall countrywide spectrum utilization. Moreover, an MNO pays the licensing fee only for the amount of spectrum that it uses at any term t_{rnw} (i.e., in accordance with its number of users).

C. Interference Management

Since all MNOs consider operating in-building small cells at the same countrywide 28 GHz mmWave spectrum, CCI occurs when small cell UEs of more than one MNO on the same floor in a building are scheduled to the same frequency simultaneously. Such CCI can be avoided by allocating UEs orthogonally in the frequency-domain [13]. More specifically, UEs of MNOs located on the same floor in a building are allocated orthogonally to different parts of the countrywide 28 GHz mmWave spectrum, as shown in Figure 2. Hence, UEs of not more than one MNO can be allocated to the same frequency in any Transmission Time Interval (TTI). The existence of an

 ISBN: 978-1-61208-828-0

TABLE I. LIST OF ACRONYMS/ABBREVIATIONS

Acronym/ Abbreviation	Definition
3D	3-Dimensional
6G	Sixth-Generation
BS	Base Station
CCI	Co-Channel Interference
CE	Cost Efficiency
CoMSAR	Countrywide Millimeter-wave Spectrum Allocation and Reuse
EE	Energy Efficiency
FFR	Fractional Frequency Reuse
ISD	Inter-Site Distance
LoS	Line-of-Sight
mmWave	Millimeter-Wave
MNO	Mobile Network Operator
Non-LOS	NLOS
NRA	National Regulatory Agency
PBS	Picocell Base Station
RB	Resource Block
SBS	Small Cell Base Station
SE	Spectral Efficiency
SLSA	Static Licensed Spectrum Allocation
TTI	Transmission Time Interval
UE	User Equipment

TABLE II. LIST OF SELECTED NOTATIONS

Notation	Description
t	Index of a TTI
T	Simulation run time with the maximum time of Q
O	Number of MNOs of a country
o	Index of an MNO
M	Amount of mmWave spectrum per MNO in SLSA
l	Index of a building
L	Number of buildings per macrocell
i	Index of an RB
P_{MC} , P_{PC} , and P_{SC}	The transmission power of a macrocell, a picocell, and a small cell, respectively, of an MNO o
ω_{FL}	Number of floors in a building
ω_{fl}	Index of a floor in a building
$M_{\mathrm{C,max}}$	Countrywide mmWave spectrum in RBs
t_{mw}	Licensed renew term
$S_{\mathrm{F},o}$	Number of SBSs in any building l for an MNO o
ε_{C}	Cost of the countrywide 28 GHz mmWave spectrum $M_{\mathrm{C,max}}$
ε_o	Spectrum licensing fee paid by an MNO o
$N_{o,t_{\mathrm{mw}}}$	Number of subscribers of an MNO o at term t_{mw}
$N_{\mathrm{C,max},t_{\mathrm{mw}}}$	Number of subscribers of a country at term t_{mw}
$M_{o,t_{\mathrm{mw},l}}^{l,\omega_{fl}}$	The optimal amount of licensed spectrum in RBs for an MNO o on any floor ω_{fl} in a building l in TTI t at term t_{mw}
$\sigma_{t,i,o}^{t_{\mathrm{mw}}}(\cdot)$	A link throughput at RB=i in TTI=t for an MNO o at t_{mw} in bps per Hz
$\rho_{t,i,o}^{t_{\mathrm{mw}}}(\cdot)$	A link SINR at RB=i in TTI=t for an MNO o at t_{mw} in dB
$M_{\mathrm{MBS},o}$	Spectrum in RBs of a macrocell for an MNO o
$\sigma_{\mathrm{FD,cap},O}^{\mathrm{sys},t_{\mathrm{mw}}}(\cdot)$, $\sigma_{\mathrm{FD,SE},O}^{\mathrm{sys},t_{\mathrm{mw}}}(\cdot)$, $\sigma_{\mathrm{FD,EE},O}^{\mathrm{sys},t_{\mathrm{mw}}}(\cdot)$, and $\varsigma_{\mathrm{FD,CE},O}^{\mathrm{sys},t_{\mathrm{mw}}}$	System-level average capacity, SE, EE, and CE, respectively, for all MNOs O countrywide at t_{mw} for l=L when employing the proposed technique
$\sigma_{\mathrm{SLSA,cap},O}^{\mathrm{sys},t_{\mathrm{mw}}}(\cdot)$, $\sigma_{\mathrm{SLSA,SE},O}^{\mathrm{sys},t_{\mathrm{mw}}}(\cdot)$, $\sigma_{\mathrm{SLSA,EE},O}^{\mathrm{sys},t_{\mathrm{mw}}}(\cdot)$, and $\varsigma_{\mathrm{SLSA,CE},O}^{\mathrm{sys},t_{\mathrm{mw}}}$	System-level average capacity, SE, EE, and CE, respectively, for all MNOs O countrywide at t_{mw} for l=L when employing SLSA
$\varsigma_{\mathrm{cap},O,\mathrm{IF}}^{\mathrm{sys},t_{\mathrm{mw}}}$, $\varsigma_{\mathrm{SE},O,\mathrm{IF}}^{\mathrm{sys},t_{\mathrm{mw}}}$, $\varsigma_{\mathrm{EE},O,\mathrm{IF}}^{\mathrm{sys},t_{\mathrm{mw}}}$, and $\varsigma_{\mathrm{CE},O,\mathrm{IF}}^{\mathrm{sys},t_{\mathrm{mw}}}$	Improvement factors in average capacity, SE, EE, and CE, respectively, due to applying the proposed technique

 ISBN: 978-1-61208-828-0

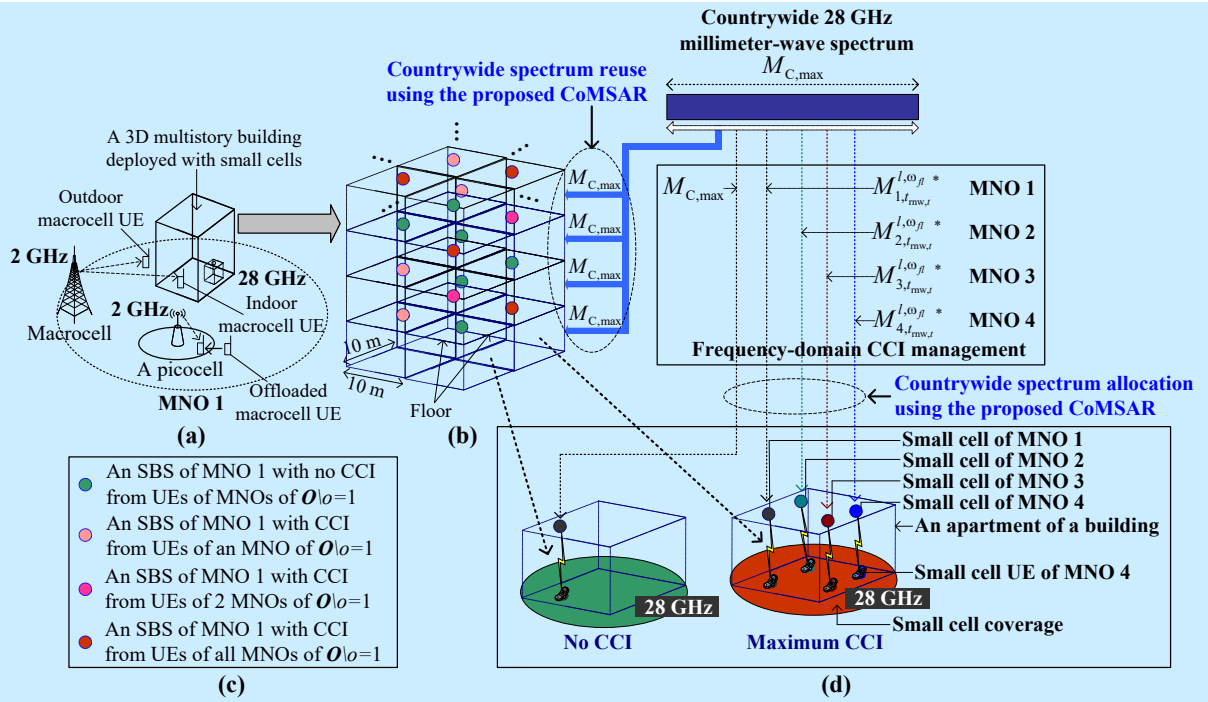

Figure 1. A system architecture consisting of four MNOs countrywide.

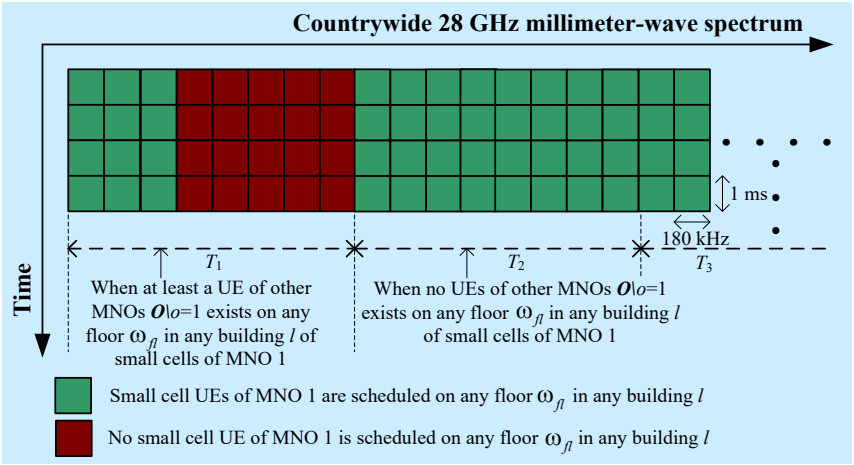

Figure 2. The frequency-domain CCI avoidance technique for UEs of MNO 1 on any floor ω_{fl} in a building l.

T_1, T_2, and T_3 define arbitrary and equal observation time intervals within $|\boldsymbol{T}| = Q$.

interfering UE can be detected either by the small cell or the small cell UE itself using any conventional spectrum sensing techniques.

D. Optimal Amount of Spectrum per MNO

Let O denote the maximum number of MNOs of a country such that $o \in \boldsymbol{O} = \{1,2,...,O\}$. Let $s_{x,o} \in \boldsymbol{S_{x,o}} = \{0,1,2,...,S_{\mathrm{F},o}\}$ denote the number of small cells of an MNO o deployed on a number of floors $\omega_{fl} \in \boldsymbol{\omega_{FL}} = \{1,2,...,\omega_{\mathrm{FL}}\}$ in any building $l \in \boldsymbol{L} = \{1,2,3,...,L\}$. Let $u_{x,o} \in \boldsymbol{U_{x,o}} = \{0,1,2,3,...,U_{\mathrm{F},o}\}$ denote the number of UEs of an MNO o corresponding to $s_{x,o} \in \boldsymbol{S_{x,o}}$ in any $l \in \boldsymbol{L}$. Denote $M_{\mathrm{C,max}}$ as the countrywide total amount of mmWave spectrum defined in terms of the number of Resource Blocks (RBs) where a RB is equal to 180 kHz.

Let $N_{o,t_{\mathrm{mw}}}$ denote the total number of subscribers of an MNO o such that $\sum_o^O N_{o,t_{\mathrm{mw}}} \le N_{\mathrm{C,max},t_{\mathrm{mw}}}$ where $N_{\mathrm{C,max},t_{\mathrm{mw}}}$ denotes the maximum number of subscribers of a country at term t_{mw}. Assume that each small cell $s_{x,o}$ of an MNO o can serve the maximum of one UE $u_{x,o}$ at a time. Also, UEs of not

 ISBN: 978-1-61208-828-0

more than one MNO o on the same floor ω_{fl} can be served at the same RBs in any TTI in a building l. The amount of spectrum allocated to UEs $u_{x,o}$ of an MNO o on a floor ω_{fl} in a building l at term t_{rnw} in TTI t is defined as follows.

The amount of spectrum allocated to UEs $u_{x,o}$ of an MNO o on any floor ω_{fl} in a building l at term t_{rnw} is defined in accordance with the ratio of the number of subscribers $N_{o,t_{\text{rnw}}}^{l,\omega_{fl}}$ of the MNO o to the sum of the total number of subscribers $N_{t_{\text{rnw}},t}^{l,\omega_{fl}}$ of all MNOs O=4 corresponding to the same floor ω_{fl} in the building l in any TTI t at term t_{rnw}. Note that the radio spectrum is not free of cost. Hence, licensing more spectrum causes an increase in the cost of an MNO. Moreover, as the total amount of the spectrum specified for a country is fixed, licensing more spectrum by one MNO causes the scarcity of the required spectrum by another MNO in a country, resulting in degrading the quality-of-service (QoS). This problem can be addressed if each MNO takes the license of the amount of the spectrum as low as possible corresponding to its actual number of subscribers so that the issue of the under-utilized or unused spectrum by one MNO, as well as the lack of a sufficient amount of spectrum for another MNO to serve its necessary user demand can be addressed. Since each MNO favors to minimizing the cost of licensing spectrum while ensuring to serve its user demands adequately to retain QoS, we consider a minimization problem for allocating the countrywide mmWave spectrum to each MNO to increase the overall countrywide mmWave spectrum utilization. Hence, the optimal amount of licensed spectrum $M_{o,t_{\text{mw},t}}^{l,\omega_{fl}}$ in RBs for an MNO $o \in \boldsymbol{O}$ on any floor ω_{fl} in a building l in TTI t at a renewal term t_{rnw} can be found by solving the following problem.

$$\begin{aligned} \min_{o\in\boldsymbol{O}} \quad & M_{o,t_{\text{mw},t}}^{l,\omega_{fl}} \\ \text{subject to} \quad & \text{(a) } N_{o,t_{\text{rnw}}}^{l,\omega_{fl}} \Big/ N_{t_{\text{rnw}},t}^{l,\omega_{fl}} = M_{o,t_{\text{mw},t}}^{l,\omega_{fl}} \Big/ M_{\text{C,max}} \qquad (1) \\ & \text{(b) } \forall o \forall t_{\text{rnw}} \forall l \forall \omega_{fl} \sum_{o}^{O} N_{o,t_{\text{rnw}}}^{l,\omega_{fl}} N_{o,t_{\text{mw}}} \le N_{\text{C, max},t_{\text{rnw}}}^{l,\omega_{fl}} \end{aligned}$$

The solution to the above optimization problem can be expressed as follows and is given in Proof 1.

$$M_{o,t_{\text{mw},t}}^{l,\omega_{fl}\ *} = \left\lceil \left(\left(N_{o,t_{\text{rnw}}}^{l,\omega_{fl}} \Big/ \sum_{o=1}^{O} \left(1_{\nu_o} \left(N_{o,t_{\text{rnw}}}^{l,\omega_{fl}} \right) \times N_{o,t_{\text{rnw}}}^{l,\omega_{fl}} \right) \right) \times M_{\text{C,max}} \right) \right\rceil \qquad (2)$$

Proof 1: The solution to the optimization problem in (1) can be found as follows. In general, the number of subscribers of all MNOs is not the same at any t_{rnw}. Hence, assume that $N_{1,t_{\text{rnw}}} > N_{2,t_{\text{rnw}}} > \ldots > N_{O,t_{\text{rnw}}}$ at t_{rnw} such that the constraint 1(b) is satisfied. Since a UE of any MNO $\boldsymbol{O}\backslash o$ in any TTI may not exist on any floor ω_{fl} in a building l of small cells of an MNO o, $N_{t_{\text{rnw}},t}^{l,\omega_{fl}}$ can be expressed for O=4 as

$$N_{t_{\text{rnw}},t}^{l,\omega_{fl}} = \sum_{o=1}^{O} \left(1_{\nu_o} \left(N_{o,t_{\text{rnw}}}^{l,\omega_{fl}} \right) \times N_{o,t_{\text{rnw}}}^{l,\omega_{fl}} \right) \qquad (3)$$

where $\nu_o \in \left\{ N_{1,t_{\text{rnw}}}^{l,\omega_{fl}}, N_{2,t_{\text{rnw}}}^{l,\omega_{fl}}, N_{3,t_{\text{rnw}}}^{l,\omega_{fl}}, N_{4,t_{\text{rnw}}}^{l,\omega_{fl}} \right\}$. $1(\cdot)$ defines that $1(\cdot) = 1$ if $N_{o,t_{\text{rnw}}}^{l,\omega_{fl}}$ exists in the set ν_o; otherwise, $1(\cdot) = 0$.

Since the number of RBs is strictly an integer, using (3), and the constraint 1(a), the optimal value of $M_{o,t_{\text{mw},t}}^{l,\omega_{fl}}$ is given by

$$M_{o,t_{\text{mw},t}}^{l,\omega_{fl}\ *} = \left(N_{o,t_{\text{rnw}}}^{l,\omega_{fl}} \Big/ N_{t_{\text{rnw}},t}^{l,\omega_{fl}} \right) \times M_{\text{C,max}}$$

$$M_{o,t_{\text{mw},t}}^{l,\omega_{fl}\ *} = \left\lceil \left(\left(N_{o,t_{\text{rnw}}}^{l,\omega_{fl}} \Big/ \sum_{o=1}^{O} \left(1_{\nu_o} \left(N_{o,t_{\text{rnw}}}^{l,\omega_{fl}} \right) \times N_{o,t_{\text{rnw}}}^{l,\omega_{fl}} \right) \right) \times M_{\text{C,max}} \right) \right\rceil \quad \blacksquare$$

Note that if a UE of any MNO $\boldsymbol{O}\backslash o$ in any TTI t on any floor ω_{fl} in a building l does not exist, then $N_{t_{\text{rnw}},t}^{l,\omega_{fl}} = N_{o,t_{\text{rnw}}}^{l,\omega_{fl}}$ in (3), which results in $M_{o,t_{\text{mw},t}}^{l,\omega_{fl}\ *} = M_{\text{C,max}}$. This implies that the whole countrywide 28 GHz mmWave spectrum can be allocated in all TTIs t to UEs $u_{x,o} \in \boldsymbol{U_{x,o}}$ of small cells $s_{x,o} \in \boldsymbol{S_{x,o}}$ of an MNO o on any floor ω_{fl} in a building l. The same process described above is applicable for all MNOs $o \in \boldsymbol{O}$ at each renewal term t_{rnw} to update $M_{o,t_{\text{mw},t}}^{l,\omega_{fl}\ *}$ in any TTI t to avoid CCI. Hence, using (2), the countrywide 28 GHz spectrum can be reused to small cells of each MNO o on any floor ω_{fl} in a building l at the cost of paying the licensing fee based on $N_{o,t_{\text{rnw}}}^{l,\omega_{fl}}$ of the corresponding MNO o at t_{rnw} with respect to that of other MNOs $\boldsymbol{O}\backslash o$ to improve countrywide 28 GHz mmWave spectrum utilization. Further, the higher the number of subscribers $N_{o,t_{\text{rnw}}}^{l,\omega_{fl}}$ of an MNO o on any floor ω_{fl} in a building l in any TTI t at term t_{rnw}, the greater the amount of mmWave spectrum $M_{o,t_{\text{mw},t}}^{l,\omega_{fl}}$ allocated to MNO o corresponding to the same floor in the building l in TTI t at term t_{rnw}.

III. Mathematical Analysis

Let $S_{\text{M},o}$ denote the number of macrocells, and $S_{\text{P},o}$ denotes the number of picocells per macrocell of an MNO o. Also, let $\boldsymbol{T}$ denote the simulation run time with the maximum time of Q (in time step each lasting 1 ms) such that $\boldsymbol{T}$= {1, 2, 3,…,Q}. Let P_{MC}, P_{PC}, and P_{SC} denote, respectively, the transmission power of a macrocell, a picocell, and a small cell of an MNO o. Using Shannon's capacity formula, a link throughput at RB=i in TTI=t for an MNO o at t_{rnw} in bps per Hz is given by [14][15]

$$\sigma_{t,i,o}^{t_{\text{mw}}} \left(\rho_{t,i,o}^{t_{\text{mw}}} \right) = \begin{cases} 0, & \rho_{t,i,o}^{t_{\text{mw}}} < -10\,\text{dB} \\ \beta \log_2 \left(1 + 10^{\left(\rho_{t,i,o}^{t_{\text{mw}}}(\text{dB})/10 \right)} \right), & -10\,\text{dB} \le \rho_{t,i,o}^{t_{\text{mw}}} \le 22\,\text{dB} \\ 4.4, & \rho_{t,i,o}^{t_{\text{mw}}} > 22\,\text{dB} \end{cases} \qquad (4)$$

where β denotes the implementation loss factor.

Let $M_{\mathrm{MBS},o}$ denote the spectrum in RBs of a macrocell for an MNO *o*. Then, the total capacity of all macrocell UEs for an MNO *o* at t_{rnw} can be expressed as

$$\sigma_{\mathrm{MBS},o}^{t_{\mathrm{rnw}}} = \sum_{t=1}^{Q} \sum_{i=1}^{M_{\mathrm{MBS},o}} \sigma_{t,i,o}^{t_{\mathrm{rnw}}} \left(\rho_{t,i,o}^{t_{\mathrm{rnw}}} \right) \tag{5}$$

where σ and ρ are responses over $M_{\mathrm{MBS},o}$ RBs of all macro UEs in $t \in \boldsymbol{T}$ for an MNO *o* at t_{rnw}. If all SBSs $s_{\omega_{fl},o}$ on any floor ω_{fl} in a building *l* of an MNO *o* serves simultaneously in all TTI $t \in \boldsymbol{T}$, then, the aggregate capacity served by an SBS, all SBSs per floor ω_{fl}, as well as all SBSs in a building *l,* of an MNO *o* at a renewal term t_{rnw} are given respectively by

$$\sigma_{\mathrm{FD},o,l,s_{x,o}}^{t_{\mathrm{rnw}},\omega_{fl}} = \sum_{t \in \boldsymbol{T}} \sum_{i=1}^{M_{o,t_{\mathrm{rnw}},t}^{l,\omega_{fl}}{}^{*}} \sigma_{t,i,o}^{t_{\mathrm{rnw}}} \left(\rho_{t,i,o}^{t_{\mathrm{rnw}}} \right) \tag{6}$$

$$\sigma_{\mathrm{FD},o,l,s_{\omega_{fl},o}}^{t_{\mathrm{rnw}},\omega_{fl}} = \sum_{s_{x,o}=1}^{S_{\omega_{fl},o}} \sigma_{\mathrm{FD},o,l,s_{x,o}}^{t_{\mathrm{rnw}},\omega_{fl}} \tag{7}$$

$$\sigma_{\mathrm{FD},o,l,s_{\omega_{fl},o}}^{t_{\mathrm{rnw}},\omega_{\mathrm{FL}}} = \sum_{\omega_{fl}=1}^{\omega_{\mathrm{FL}}} \sigma_{\mathrm{FD},o,l,s_{\omega_{fl},o}}^{t_{\mathrm{rnw}},\omega_{fl}} \tag{8}$$

Due to a short distance between a small cell UE and its SBS and a low transmission power of an SBS, we assume similar indoor signal propagation characteristics for all *L* buildings per macrocell for an MNO *o* at t_{rnw}. Then, by linear approximation, the system-level average aggregate capacity, SE, and EE for all MNOs O countrywide at t_{rnw} for *l*=*L* can be given by

$$\sigma_{\mathrm{FD,cap},O}^{\mathrm{sys},t_{\mathrm{rnw}}}(L) = \sum_{o=1}^{O} \left(\sigma_{\mathrm{MBS},o}^{t_{\mathrm{rnw}}} + \left(L \times \sigma_{\mathrm{FD},o,l,s_{\omega_{fl},o}}^{t_{\mathrm{rnw}},\omega_{\mathrm{FL}}} \right) \right) \tag{9}$$

Since $\left(L \times \sigma_{\mathrm{FD},o,l,s_{\omega_{fl},o}}^{t_{\mathrm{rnw}},\omega_{\mathrm{FL}}} \right) >> \sigma_{\mathrm{MBS},o}^{t_{\mathrm{rnw}}}$, roughly, (9) can be given by

$$\sigma_{\mathrm{FD,cap},O}^{\mathrm{sys},t_{\mathrm{rnw}}}(L) \cong \sum_{o=1}^{O} \left(L \times \sigma_{\mathrm{FD},o,l,s_{\omega_{fl},o}}^{t_{\mathrm{rnw}},\omega_{\mathrm{FL}}} \right) \tag{10}$$

$$\sigma_{\mathrm{FD,SE},O}^{\mathrm{sys},t_{\mathrm{rnw}}}(L) = \sigma_{\mathrm{FD,cap},O}^{\mathrm{sys},t_{\mathrm{rnw}}}(L) \Big/ \left(\left(M_{\mathrm{C,max}} + \sum_{o=1}^{O} M_{\mathrm{MBS},o} \right) \times Q \right) \tag{11}$$

$$\sigma_{\mathrm{FD,EE},O}^{\mathrm{sys},t_{\mathrm{rnw}}}(L) = \left(\sum_{o=1}^{O} \left(\begin{array}{l} \left(L \times S_{\mathrm{F},o} \times P_{\mathrm{SC}} \right) \\ + \left(S_{\mathrm{P},o} \times P_{\mathrm{PC}} \right) + \left(S_{\mathrm{M},o} \times P_{\mathrm{MC}} \right) \end{array} \right) \right) \Big/ \left(\sigma_{\mathrm{FD,cap},O}^{\mathrm{sys},t_{\mathrm{rnw}}}(L) / Q \right) \tag{12}$$

where $S_{\mathrm{F},o} = \sum_{\omega_{fl}=1}^{\omega_{\mathrm{FL}}} s_{\omega_{fl},o}$ denotes the total number of SBSs in any building *l* for an MNO *o*.

However, in a traditional Static Licensed Spectrum Allocation (SLSA) technique, a fair allocation of the licensed mmWave spectrum to each MNO in a country is assumed, i.e., each MNO is given license exclusively for an equal amount of the mmWave spectrum of *M* RBs such that for *O*=4, $M_{\mathrm{C,max}} = 4M$. Now, using (8)-(12), the system-level average capacity, SE, and EE for all MNOs O countrywide at t_{rnw} for *l*=*L* can be given by

$$\sigma_{\mathrm{SLSA,cap},O}^{\mathrm{sys},t_{\mathrm{rnw}}}(L) = \sum_{o=1}^{O} \left(\sigma_{\mathrm{MBS},o}^{t_{\mathrm{rnw}}} + \left(L \times \sum_{\omega_{fl}=1}^{\omega_{\mathrm{FL}}} \sum_{s_{x,o}=1}^{S_{\omega_{fl},o}} \sum_{t \in \boldsymbol{T}} \sum_{i=1}^{M} \sigma_{s_{x,o},t,i,o}^{t_{\mathrm{rnw}},\omega_{fl}} \left(\rho_{s_{x,o},t,i,o}^{t_{\mathrm{rnw}},\omega_{fl}} \right) \right) \right) \tag{13}$$

$$\sigma_{\mathrm{SLSA,cap},O}^{\mathrm{sys},t_{\mathrm{rnw}}}(L) \cong \sum_{o=1}^{O} \left(L \times \sum_{\omega_{fl}=1}^{\omega_{\mathrm{FL}}} \sum_{s_{x,o}=1}^{S_{\omega_{fl},o}} \sum_{t \in \boldsymbol{T}} \sum_{i=1}^{M} \sigma_{s_{x,o},t,i,o}^{t_{\mathrm{rnw}},\omega_{fl}} \left(\rho_{s_{x,o},t,i,o}^{t_{\mathrm{rnw}},\omega_{fl}} \right) \right) \tag{14}$$

$$\sigma_{\mathrm{SLSA,SE},O}^{\mathrm{sys},t_{\mathrm{rnw}}}(L) = \sigma_{\mathrm{SLSA,cap},O}^{\mathrm{sys},t_{\mathrm{rnw}}}(L) \Big/ \left(\left(M_{\mathrm{C,max}} + \sum_{o=1}^{O} M_{\mathrm{MBS},o} \right) \times Q \right) \tag{15}$$

$$\sigma_{\mathrm{SLSA,EE},O}^{\mathrm{sys},t_{\mathrm{rnw}}}(L) = \left(\sum_{o=1}^{O} \left(\begin{array}{l} \left(L \times S_{\mathrm{F},o} \times P_{\mathrm{SC}} \right) + \\ \left(S_{\mathrm{P},o} \times P_{\mathrm{PC}} \right) + \left(S_{\mathrm{M},o} \times P_{\mathrm{MC}} \right) \end{array} \right) \right) \Big/ \left(\sigma_{\mathrm{SLSA,cap},O}^{\mathrm{sys},t_{\mathrm{rnw}}}(L) / Q \right) \tag{16}$$

Now, let ε_{C} denote the cost of the countrywide 28 GHz mmWave spectrum $M_{\mathrm{C,max}}$. Recall that an MNO *o* pays the spectrum licensing fee based on its number of subscribers $N_{o,t_{\mathrm{rnw}}}$ at t_{rnw} with respect to that of all MNOs $N_{\mathrm{C,max},t_{\mathrm{rnw}}}$. Assume that an MNO *o* pays the spectrum licensing fee of ε_o corresponding to $N_{o,t_{\mathrm{rnw}}}$ at t_{rnw} such that ε_o can be given by

$$\varepsilon_o = \left(N_{o,t_{\mathrm{rnw}}} / N_{\mathrm{C,max},t_{\mathrm{rnw}}} \right) \times \varepsilon_{\mathrm{C}} \tag{17}$$

Now, define Cost Efficiency (CE) as the cost required per unit achievable average capacity (i.e., per bps) such that the CE at term t_{rnw} can be expressed as follows for both techniques.

$$\varsigma_{\mathrm{FD,CE},O}^{\mathrm{sys},t_{\mathrm{rnw}}} = \varepsilon_{\mathrm{C}} \Big/ \sigma_{\mathrm{FD,cap},O}^{\mathrm{sys},t_{\mathrm{rnw}}}(L) \tag{18}$$

$$\varsigma_{\mathrm{SLSA,CE},O}^{\mathrm{sys},t_{\mathrm{rnw}}} = \varepsilon_{\mathrm{C}} \Big/ \sigma_{\mathrm{SLSA,cap},O}^{\mathrm{sys},t_{\mathrm{rnw}}}(L) \tag{19}$$

Hence, the factor representing an improvement in average capacity, SE, EE, and CE due to applying the proposed technique can be expressed respectively as follows.

$$\varsigma_{\mathrm{cap},O,\mathrm{IF}}^{\mathrm{sys},t_{\mathrm{rnw}}} = \sigma_{\mathrm{FD,cap},O}^{\mathrm{sys},t_{\mathrm{rnw}}}(L) \Big/ \sigma_{\mathrm{SLSA,cap},O}^{\mathrm{sys},t_{\mathrm{rnw}}}(L) \tag{20}$$

$$\varsigma_{\mathrm{SE},O,\mathrm{IF}}^{\mathrm{sys},t_{\mathrm{rnw}}} = \sigma_{\mathrm{FD,SE},O}^{\mathrm{sys},t_{\mathrm{rnw}}}(L) \Big/ \sigma_{\mathrm{SLSA,SE},O}^{\mathrm{sys},t_{\mathrm{rnw}}}(L) \tag{21}$$

$$\varsigma_{\mathrm{EE},O,\mathrm{IF}}^{\mathrm{sys},t_{\mathrm{rnw}}} = \sigma_{\mathrm{FD,EE},O}^{\mathrm{sys},t_{\mathrm{rnw}}}(L) \Big/ \sigma_{\mathrm{SLSA,EE},O}^{\mathrm{sys},t_{\mathrm{rnw}}}(L) \tag{22}$$

$$\varsigma_{\mathrm{CE},O,\mathrm{IF}}^{\mathrm{sys},t_{\mathrm{rnw}}} = \varsigma_{\mathrm{FD,CE},O}^{\mathrm{sys},t_{\mathrm{rnw}}} \Big/ \varsigma_{\mathrm{SLSA,CE},O}^{\mathrm{sys},t_{\mathrm{rnw}}} \tag{23}$$

IV. Performance Evaluation

A. Performance Result and Analysis

Table III shows the default simulation parameters and assumptions used for evaluating the performances of the proposed technique. We generate performance results by

simulating all assumptions and parameters given in Table III by a simulator that is built by using the default instruction sets of the computational tool MATLAB R2012b version running on a personal computer. Further, the algorithm used to generate the performance results is given in Algorithm 1. The performance of the proposed technique is evaluated with regard to the traditional SLSA technique. We assume that MNO 1, MNO 2, MNO 3, and MNO 4 have the number of subscribers of 40%, 30%, 20%, and 10%, respectively, of the total number of

TABLE III. DEFAULT PARAMETERS AND ASSUMPTIONS

Parameters and Assumptions		Value
28 GHz spectrum countrywide		200 MHz
Number of MNOs and subscribers		4 and $N_{\mathrm{C,max}}$
Number of subscribers for MNOs 1, 2, 3, and 4, respectively		40%, 30%, 20%, and 10% of $N_{\mathrm{C,max}}$
For each MNO		
E-UTRA simulation case[1,6]		3GPP case 3
Cellular layout[2,6], Inter-Site Distance (ISD)[1,2,6], transmit direction		Hexagonal grid, dense urban, 3 sectors per macrocell site, 1732 m, downlink
Carrier frequency[2,5,6]		2 GHz Non-line-of-Sight (NLOS) for macrocells and picocells, 28 GHz Line-of-Sight (LOS) for all small cells
Number of cells		1 macrocell, 2 picocells, 280 small cells per building
Total BS transmit power[1] (dBm)		46 for macrocell[1,4], 37 for picocells[1], 19 for small cells[1,3,4]
Co-channel small-scale fading model[1,3,5]		Frequency selective Rayleigh for 2 GHz, none for 28 GHz
Path loss	MBS and a UE[1] Outdoor macrocell UE	PL(dB)=15.3 + 37.6 $\log_{10}R$, R is in m
	MBS and a UE[1] Indoor macrocell UE	PL(dB)=15.3 + 37.6 $\log_{10}R$ + L_{ow}, R is in m
	PBS and a UE[1]	PL(dB)=140.7+36.7 $\log_{10}R$, R is in km
	SBS and a UE[1,2,5]	$PL(\mathrm{dB}) = 61.38 + 17.97\log_{10}(d)$, d is in m
Lognormal shadowing standard deviation (dB)		8 for MBS[2], 10 for PBS[1], and 9.9 for SBS[2,5]
Antenna configuration		Single-input single-output for all BSs and UEs
Antenna pattern (horizontal)		Directional (120^0) for MBS[1], omnidirectional for PBS[1] and SBS[1]
Antenna gain plus connector loss (dBi)		14 for MBS[2], 5 for PBS[1], 5 for SBS[1,3]
UE antenna gain[2,3]		0 dBi (for 2 GHz), 5 dBi (for 28 GHz, Biconical horn)
UE noise figure[2,3] and UE speed[1]		9 dB (for 2 GHz) and 10 dB (for 28 GHz), 3 km/hr
Picocell coverage, number of macrocell UEs, and macrocell UEs offloaded to all picocells[1]		40 m (radius), 30, 2/15
Indoor macrocell UEs[1]		35%
3D multistory building and SBS models (square-grid apartments): number of buildings, number of floors per building, number of apartments per floor, number of SBSs per apartment, number of SBSs per building, area of an apartment, materials used		L, 35, 8, 1, 280, 10×10 m^2, reinforced concrete
Scheduler and traffic model[2]		Proportional Fair and full buffer
Type of SBSs		Closed Subscriber Group femtocell BSs
Channel State Information		Ideal
TTI[1] and scheduler time constant (t_c)		1 ms and 100 ms
Total simulation run time		8 ms

taken [1]from [16], [2]from [17], [3]from [18], [4]from [19], from [5][20], from [6][21].

Algorithm 1. Proposed CoMSAR technique

01: **Input:** O=4, Q, t_{rnw}, $N_{\mathrm{C,max},t_{\mathrm{rnw}}}$ M, $N_{o,t_{\mathrm{rnw}}}$, $M_{\mathrm{C,max}}$
02: $s_{x,o} \in \boldsymbol{S}_{x,o} = \{0,1,2,...,S_{\mathrm{F},o}\}$, P_{MC}, P_{PC}, P_{SC}
03: **For** $L = \{1,2,3,...,\}$
04: **For** t={1, 2, 3,…,Q}
05: **For** $o \in \boldsymbol{O} = \{1,2,...,O\}$
06: **Find** $M_{o,t_{\mathrm{rnw},t}}^{l,\omega_{jl}\,*}$ using (2)
07: **Estimate** Capacity, $\sigma_{\mathrm{FD,cap},O}^{\mathrm{sys},t_{\mathrm{rnw}}}(L)$ using (9)
08: and $\sigma_{\mathrm{SLSA,cap},O}^{\mathrm{sys},t_{\mathrm{rnw}}}(L)$ using (14)
09: **Estimate** SE $\sigma_{\mathrm{FD,SE},O}^{\mathrm{sys},t_{\mathrm{rnw}}}(L)$ using (11)
10: and $\sigma_{\mathrm{SLSA,SE},O}^{\mathrm{sys},t_{\mathrm{rnw}}}(L)$ using (15)
11: **Estimate** EE $\sigma_{\mathrm{FD,EE},O}^{\mathrm{sys},t_{\mathrm{rnw}}}(L)$ using (12)
12: and $\sigma_{\mathrm{SLSA,EE},O}^{\mathrm{sys},t_{\mathrm{rnw}}}(L)$ using (16)
13: **Estimate** CE $\varsigma_{\mathrm{FD,CE},O}^{\mathrm{sys},t_{\mathrm{rnw}}}$ using (18)
14: and $\varsigma_{\mathrm{SLSA,CE},O}^{\mathrm{sys},t_{\mathrm{rnw}}}$ using (19)
15: **End**
16: **End**
17: **End**
18: **Find** Improvement factors using (20)-(23):
19: $\varsigma_{\mathrm{cap},O,\mathrm{IF}}^{\mathrm{sys},t_{\mathrm{rnw}}}$, $\varsigma_{\mathrm{SE},O,\mathrm{IF}}^{\mathrm{sys},t_{\mathrm{rnw}}}$, $\varsigma_{\mathrm{EE},O,\mathrm{IF}}^{\mathrm{sys},t_{\mathrm{rnw}}}$, $\varsigma_{\mathrm{CE},O,\mathrm{IF}}^{\mathrm{sys},t_{\mathrm{rnw}}}$
20: **Output:** Display for MNO o=1 the followings:
21: $\varsigma_{\mathrm{cap},O,\mathrm{IF}}^{\mathrm{sys},t_{\mathrm{rnw}}}$ $\varsigma_{\mathrm{SE},O,\mathrm{IF}}^{\mathrm{sys},t_{\mathrm{rnw}}}$ $\varsigma_{\mathrm{EE},O,\mathrm{IF}}^{\mathrm{sys},t_{\mathrm{rnw}}}$, $\varsigma_{\mathrm{CE},O,\mathrm{IF}}^{\mathrm{sys},t_{\mathrm{rnw}}}$
22: **Plot:** For no and maximum CCI for MNO o=1:
23: $\sigma_{\mathrm{FD,SE},O}^{\mathrm{sys},t_{\mathrm{rnw}}}(L)$, $\sigma_{\mathrm{SLSA,SE},O}^{\mathrm{sys},t_{\mathrm{rnw}}}(L)$, $\sigma_{\mathrm{FD,EE},O}^{\mathrm{sys},t_{\mathrm{rnw}}}(L)$, $\sigma_{\mathrm{SLSA,EE},O}^{\mathrm{sys},t_{\mathrm{rnw}}}(L)$

subscribers countrywide $N_{\mathrm{C,max},t_{\mathrm{rnw}}}$ at any term t_{rnw} (Table III). Using (20)-(23), the performance of the proposed technique is evaluated for MNO 1 under two extreme scenarios, including when no CCI occurs due to the absence of UEs of all other MNOs $\boldsymbol{O}\backslash o$=1, and when the maximum CCI occurs due to the presence of at least a UE of each MNO of $\boldsymbol{O}\backslash o$=1 on a floor in a building. With no CCI, the whole countrywide mmWave spectrum, whereas with the maximum CCI, only 40% of the countrywide spectrum, can be allocated to SBSs of MNO 1 in all TTIs. Since the achievable capacity depends directly on the amount of spectrum, the maximum average capacity, SE, EE, and CE for MNO 1 can be achieved with no CCI, as shown in Figure 3(a), in contrast to that with the maximum CCI, shown in Figure 3(b). Specifically, with regard to the traditional SLSA, the proposed technique improves the average capacity, SE, EE, and CE by 300%, 165%, 75%, and 60%, respectively with no CCI, whereas only 60%, 6%, 37%, and 0.4%, respectively with the maximum CCI.

Moreover, Figure 3 shows that the proposed technique with no CCI provides 2.5 times higher average capacity, SE, EE, and CE performances than that with the maximum CCI. Hence, CCI plays a vital role in the overall performances of an MNO

 ISBN: 978-1-61208-828-0

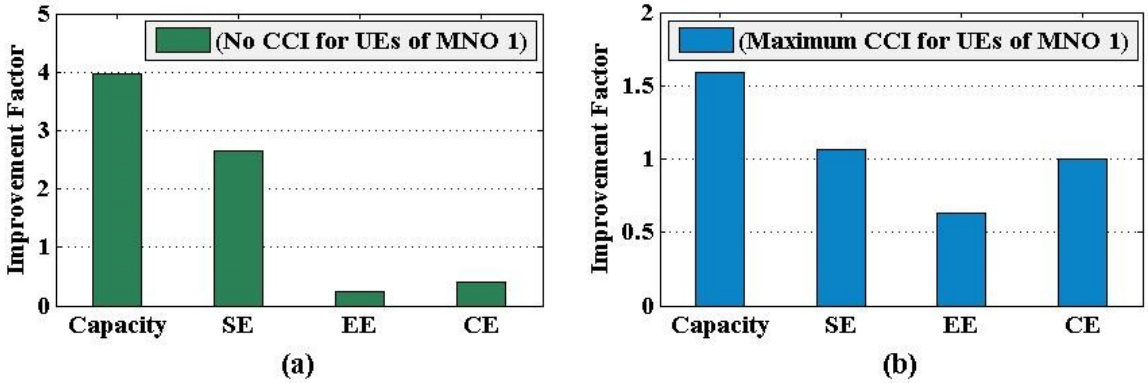

Figure 3. Performance improvement of the proposed CoMSAR technique for MNO 1 in terms of average capacity, SE, EE, and CE (a) with no CCI and (b) with the maximum CCI for UEs of MNO 1 on a single floor in a building.

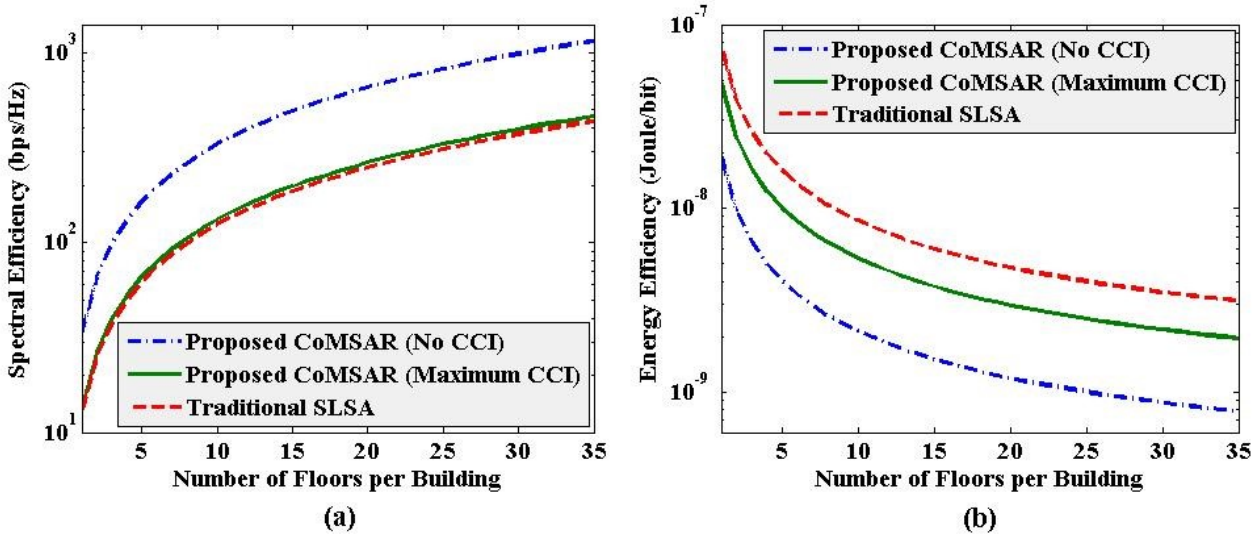

Figure 4. (a) SE and (b) EE performances of CoMSAR with respect to SLSA for a multistory building with $\omega_{FL} = 35$.

when allocated to the countrywide spectrum. Now, using (10) - (12) for the proposed technique and (14) -(16) for the traditional SLSA technique, Figures 4(a) and 4(b) show the effect of reusing the same countrywide spectrum to each floor of SBSs of MNO 1 in a multistory building. As can be seen from Figure 4, with an increase in the number of floors, SE increases linearly, whereas EE increases negative exponentially, irrespective of the degree of CCI. Further, since SE is affected additionally by the optimal amount of countrywide spectrum, the proposed technique with the maximum CCI provides insignificant SE while noticeable EE improvement over the traditional SLSA technique because of its higher average capacity performance, as shown in Figure 3(b).

B. Performance Comparison

Future 6G mobile systems are expected to require 10 times average SE (i.e., 270-370 bps/Hz), as well as 10 times average EE (i.e., 0.3×10^{-6} Joules/bit) [22] [23], of 5G mobile systems [24] [25]. Now, using Figure 4, it can be seen that the proposed CoMSAR can satisfy both the SE of 370 bps/Hz and EE of 0.3 μJ/bit for 6G mobile systems by reusing the countrywide 28 GHz mmWave spectrum to small cells of MNO 1 of about 60% less number of floors (i.e., ω_{FL} =12) with no CCI, whereas 3.3% less number of floors (i.e., ω_{FL} =29) with the maximum CCI, than that required by the traditional SLSA technique (i.e., ω_{FL} =30) in a multistory building.

C. Offered Benefits and Implementation Complexity

The proposed technique benefits from the following. It ensures the availability of a large amount of spectrum by allocating the countrywide full (instead of a portion) mmWave spectrum to each MNO. Further, it provides an efficient spectrum utilization by allowing each MNO dynamic and flexible (instead of static and dedicated) access to the countrywide spectrum. Furthermore, it allows an MNO to pay only for the amount of spectrum that it uses to serve its user demands (i.e., in proportionate with the number of its users) at

 ISBN: 978-1-61208-828-0

any term t_{rnw}, resulting in reducing the cost per unit capacity (i.e., bps).

However, the implementation of the proposed technique warrants from the following issues, including updating the dynamic usage of the countrywide spectrum on each floor by UEs of different MNOs and enforcing CCI management. In this regard, SBSs of each MNO per floor can keep sensing using either a reactive or proactive approach to detect the status of the shared full countrywide spectrum usage and coordinate with SBSs of other MNOs on the same floor to update the CCI status and amount of the shared spectrum usage for each MNO. However, such coordination among SBSs of different MNOs generates a huge amount of control signaling overheads depending on the size of the group of the coordinated SBSs. The larger the size of the group of the coordinated SBSs, the greater the amount of generated control signaling overheads, as well as delay in updating the CCI status.

In general, coordination among SBSs can be done centrally or in a distributed manner. Central coordination of SBSs per building, for example, can contribute to achieving a global optimization in updating the CCI status and the corresponding spectrum allocation to each MNO. This, however, comes at the cost of generating high control signaling overheads. On the other hand, by limiting the size of a coordinated group of SBSs, control signaling overheads due to the coordination can be kept limited. This, however, comes at the cost of allowing a local optimization in updating the CCI status and the corresponding allocated spectrum to each MNO. Hence, a tradeoff between the optimal performance in the CCI and scheduled spectrum status updates per MNO and the generated control signaling overhead due to the coordination needs to be achieved, which asks for further studies. We consider this issue as part of our future research studies.

V. CONCLUSION

In this paper, we have proposed a countrywide millimeter-wave (mmWave) spectrum allocation and reuse (CoMSAR) technique that considers assigning each MNO with the massive 28 GHz mmWave spectrum countrywide at the cost of paying the spectrum licensing fee subject to avoiding co-channel interference (CCI). The assigned spectrum to each MNO is reused further to operate its small cells deployed on each floor in a multistory building. The amount of the spectrum licensing fee for an MNO is updated in accordance with its number of subscribers at each license renew term. Moreover, CCI has been avoided by developing a frequency-domain CCI avoidance scheme that allocates UEs of different MNOs on any floor of a building orthogonally to the countrywide 28 GHz mmWave spectrum. We have derived average capacity, Spectral Efficiency (SE), Energy Efficiency (EE), and Cost Efficiency (CE) metrics for the proposed technique. Extensive numerical and simulation results and analyses have been carried out for an example scenario of a country consisting of four MNOs, i.e., MNO 1, MNO 2, MNO 3, and MNO 4 with the number of subscribers of 40%, 30%, 20%, and 10% of the total number of subscribers of all MNOs, respectively.

It has been shown for MNO 1 that, for a single building of small cells, the proposed technique can improve the average capacity, SE, EE, and CE performances by 300%, 165%, 75%, and 60%, respectively with no CCI, whereas 60%, 6%, 37%, and 0.4%, respectively with the maximum CCI, as compared to that of the traditional Static Licensed Spectrum Allocation (SLSA) technique. Finally, we have shown that the proposed CoMSAR technique can satisfy the SE and EE requirements for 6G mobile systems by reusing the countrywide 28 GHz mmWave spectrum to small cells of MNO 1 of about 60% less number of floors with no CCI, whereas 3.3% less number of floors with the maximum CCI, than that required by the traditional SLSA technique in a multistory building.

So far, in this paper, we have restricted investigating the proposed countrywide mmWave spectrum allocation and reuse technique to indoor SBSs deployed in multistory buildings. However, the propagation characteristics of mmWave signals in outdoor environments differ greatly from that in indoor one, particularly, rain and atmospheric absorption effect, cell coverage, shadowing effect from large buildings, outage probability, user density, and speed, and mobility and handover management. All these aspects have a significant impact on the allocation and reuse of the mmWave spectrum outdoors. Hence, how to allocate the countrywide mmWave spectrum to each MNO without causing CCI to each other and reuse the same mmWave spectrum for an MNO spatially need considerable research works. We aim to address these issues, i.e., mmWave spectrum allocation and reuse, in outdoor environments in our future research studies.

REFERENCES

[1] X. Yan, S. Qijun, Z. Hongshun, and S. Lulu, "Dynamic Spectrum Allocation Based on Cognitive Radio," Proc. The 2009 5th Asia-Pacific Conference on Environmental Electromagnetics, Sep. 2009, pp. 254-257.

[2] H. Kim, Y. Lee, and S. Yun, "A Dynamic Spectrum Allocation Between Network Operators with Priority-Based Sharing and Negotiation," Proc. The 2005 IEEE 16th International Symposium on Personal, Indoor and Mobile Radio Communications, Sep. 2005, pp. 1004-1008.

[3] S. J. Kim, E. C. Kim, S. Park, and J. Y. Kim, "Dynamic Spectrum Allocation with Variable Bandwidth for Cognitive Radio Systems," Proc. The 2009 9th International Symposium on Communications and Information Technology, Sep. 2009, pp. 106-109.

[4] R. K. Saha and C. Aswakul, "A Tractable Analytical Model for Interference Characterization and Minimum Distance Enforcement to Reuse Resources in Three-Dimensional In-Building Dense Small Cell Networks," International Journal of Communication Systems, vol. 30, Art. No. e3240, Jul. 2017, doi.org/10.1002/dac.3240

[5] N. Saquib, E. Hossain, and D. Kim, "Fractional Frequency Reuse for Interference Management in LTE-Advanced Hetnets," IEEE Wireless Communications, vol. 20, pp. 113-122, Apr. 2013, doi: 10.1109/MWC.2013.6507402.

[6] R. K. Saha, "A Technique for Massive Spectrum Sharing with Ultra-Dense In-Building Small Cells in 5G Era," Proc. The 2019 IEEE 90th Vehicular Technology Conference (VTC2019-Fall), Sep. 2019, pp. 1-7.

 ISBN: 978-1-61208-828-0

[7] R. K. Saha, "A Hybrid Interweave-Underlay Countrywide Millimeter-Wave Spectrum Access and Reuse Technique for CR Indoor Small Cells in 5G/6G Era," Sensors, vol. 20, Art. No. 3979, 2020, doi.org/10.3390/s20143979.

[8] R. K. Saha, "On Exploiting Millimeter-Wave Spectrum Trading in Countrywide Mobile Network Operators for High Spectral and Energy Efficiencies in 5G/6G Era," Sensors, vol. 20, Art. No. 3495, 2020, doi.org/10.3390/s20123495.

[9] R. K. Saha, "3D Spatial Reuse of Multi-Millimeter-Wave Spectra by Ultra-Dense In-Building Small Cells for Spectral and Energy Efficiencies of Future 6G Mobile Networks," Energies, vol. 13, Art. No. 1748, 2020, doi.org/10.3390/en13071748.

[10] R. Allan, "Application of FSS Structures to Selectively Control the Propagation of Signals into and Out of Buildings – Executive Summary," ERA Technology Ltd, Cleeve Road, Leatherhead Surrey, KT22 7SA UK. Available online: https://www.ofcom.org.uk/__data/assets/pdf_file/0020/ 36155/exec_summary.pdf [retrieved: Feb. 2020]

[11] Propagation Data and Prediction Methods for The Planning of Indoor Radiocommunication Systems and Radio Local Area Networks in The Frequency Range 300 MHz to 450 GHz. Recommendation ITU-R P.1238-10, 08/2019. Available online: https://www.itu.int/rec/R-REC-P.1238 [retrieved: Feb. 2020]

[12] D. Lu and D. Rutledge, "Investigation of Indoor Radio Channels from 2.4 GHz to 24 GHz," Proc. IEEE Antennas and Propagation Society International Symposium. Digest. Held in conjunction with: USNC/CNC/URSI North American Radio Sci. Meeting (Cat. No.03CH37450), Jun. 2003, pp. 134-137.

[13] R. K. Saha, S. Nanba, and K. Nishimura, "A Technique for Cloud Based Clustering and Spatial Resource Reuse and Scheduling of 3D In-Building Small Cells Using CoMP for High Capacity CRAN," IEEE Access, vol. 6, pp. 71602-71621, Nov. 2018, doi: 10.1109/ACCESS.2018.2879835.

[14] R. K. Saha, "A Hybrid System and Technique for Sharing Multiple Spectrums of Satellite Plus Mobile Systems with Indoor Small Cells in 5G and Beyond Era," IEEE Access, vol. 7, pp. 77569-77596, 2019, doi: 10.1109/ACCESS.2019.2921723.

[15] R. K. Saha and C. Aswakul, "A Novel Frequency Reuse Technique for In-Building Small Cells in Dense Heterogeneous Networks," IEEJ Transactions on Electrical and Electronic Engineering, vol. 13, pp. 98-111, Jan. 2018, doi.org/10.1002/tee.22503.

[16] Evolved Universal Terrestrial Radio Access (E-UTRA); Radio Frequency (RF) System Scenarios. document 3GPP TR 36.942, V.1.2.0, 3rd Generation Partnership Project, Jul. 2007. Available online: https://portal.3gpp.org/ desktopmodules /Specifications/Specification Details.aspx?specificationId=2592 [retrieved: Feb. 2020]

[17] Simulation Assumptions and Parameters for FDD HeNB RF Requirements. document TSG RAN WG4 (Radio) Meeting #51, R4-092042, 3GPP, May 2009. Available online: https://www.3gpp.org/ftp/tsg_ran /WG4_Radio/TSGR4_51/Documents/ [retrieved: Feb. 2020]

[18] Guidelines for Evaluation of Radio Interface Technologies for IMT-2020. Report ITU-R M.2412-0 (10/2017), Geneva, 2017. Available online: https://www.itu.int/dms_pub/itu-r/opb/rep/R-REP-M.2412-2017-PDF-E.pdf [retrieved: Feb. 2020]

[19] R. K. Saha, P. Saengudomlert, and C. Aswakul, "Evolution Toward 5G Mobile Networks-A Survey On Enabling Technologies," Engineering Journal, vol. 20, pp. 87-119, Jan. 2016, doi.org/10.4186/ej.2016.20.1.87.

[20] G. R. Maccartney, T. S. Rappaport, S. Sun, and S. Deng, "Indoor Office Wideband Millimeter-Wave Propagation Measurements and Channel Models at 28 and 73 GHz for Ultra-Dense 5G Wireless Networks," IEEE Access, vol. 3, pp. 2388-2424, 2015, doi: 10.1109/ACCESS.2015.2486778.

[21] R. K. Saha, "Spectrum Sharing in Satellite-Mobile Multisystem Using 3D In-Building Small Cells for High Spectral and Energy Efficiencies in 5G and Beyond Era," IEEE Access, vol. 7, pp. 43846-43868, Mar. 2019, doi: 10.1109/ACCESS.2019.2908203.

[22] Z. Zhang et al., "6G Wireless Networks: Vision, Requirements, Architecture, and Key Technologies," IEEE Vehicular Technology Magazine, vol. 14, pp. 28-41, Sep. 2019, doi: 10.1109/MVT.2019.2921208.

[23] S. Chen et al., "Vision, Requirements, and Technology Trend of 6G: How to Tackle the Challenges of System Coverage, Capacity, User Data-Rate and Movement Speed," IEEE Wireless Communications, vol. 27, no. 2, pp. 218-228, Apr. 2020, doi: 10.1109/MWC.001.1900333.

[24] C.-X. Wang et al., "Cellular Architecture and Key Technologies for 5G Wireless Communication Networks," IEEE Communications Magazine, vol. 52, pp. 122-130, Feb. 2014, doi: 10.1109/MCOM.2014.6736752.

[25] G. Auer et al., "How Much Energy is Needed to Run a Wireless Network?" IEEE Wireless Communications, vol. 18, pp. 40-49, Oct. 2011, doi: 10.1109/MWC.2011.6056691.

 ISBN: 978-1-61208-828-0

Hybrid Interweave-Underlay Millimeter-Wave Spectrum Access in Multi-Operator Cognitive Radio Networks Toward 6G

Rony Kumer Saha
Radio and Spectrum Laboratory
KDDI Research, Inc.
2-1-15 Ohara, Fujimino-shi, Saitama, Japan
email: ro-saha@kddi-research.jp

***Abstract*—In this paper, we propose a hybrid interweave-underlay spectrum access technique to share the licensed 28 GHz millimeter-wave spectrum of one Mobile Network Operator (MNO), termed as primary MNO, with small cells in a building of another MNO, termed as secondary MNO, in a country. The proposed technique explores the traditional interweave spectrum access technique by operating a small cell at the maximum transmission power if no user equipment of a primary MNO exists and the traditional underlay spectrum access technique by operating a small cell at a reduced transmission power if a user equipment of a primary MNO exists within the coverage of any in-building small cell of a secondary MNO. We derive average capacity, spectral efficiency, and energy efficiency and carry out extensive numerical and simulation results and analyses for a secondary MNO of a country consisting of four MNOs. It is shown that the proposed technique can improve the spectral efficiency by about 2.82 times, and the energy efficiency by about 73% of the secondary MNO as compared to that of the traditional static licensed spectrum allocation technique that allocates each MNO an equal amount of the 28 GHz millimeter-wave spectrum. Moreover, we show that the proposed technique can satisfy the expected spectral efficiency and energy efficiency requirements for Sixth-Generation (6G) mobile systems by reusing the millimeter-wave spectrum of the secondary MNO to its small cells of roughly 31%, 36%, and 72% less number of buildings than that required by the traditional interweave, underlay, and static licensed spectrum allocation techniques, respectively.**

***Keywords*—6G; 28 GHz; cognitive radio; CRN; millimeter-wave; interweave; underlay; hybrid; mobile system; spectrum access.**

I. INTRODUCTION

Nowadays, radio spectrum scarcity has become a major issue in mobile communications due to a non-dynamic or static allocation of spectrum to Mobile Network Operators (MNOs) to serve an ever-increasing user demand for high data rates and capacity. Such static allocations of spectrum cause a great portion of the spectrum to be left unused in time, frequency, and space, resulting in poor spectrum utilization. According to the Federal Communications Commission (FCC), the spectrum utilization below 3 GHz changes considerably with an occupancy of around 15% to 85% [1]. Recently, Cognitive Radio (CR) has been considered as a key enabling technology to address this spectrum scarcity issue [2]. In CR, spectrum access is a major function [3], which prevents collisions between primary User Equipments (UEs) and Secondary UEs (SUs) in accessing any spectrum. In this regard, interweave and underlay are two major spectrum access categories in CR.

In interweave access, SUs can opportunistically access only the spectrum not used by Primary UEs (PUs). Though interweave access needs additional spectrum sensing by SUs to find an idle spectrum of PUs, SUs are allowed to transmit at the maximum power. In contrast, in underlay access, SUs can simultaneously access the spectrum of PUs subject to satisfying the interference threshold set by PUs. Though underlay access suffers from the reduced transmission power of SUs to limit Co-Channel Interference (CCI) to PUs, no spectrum sensing is needed by SUs. Hence, though both interweave and underlay have pros and cons as aforementioned, the combination of these two spectrum accesses can maximize the Spectral Efficiency (SE) and Energy Efficiency (EE) [4]. More specifically, SUs can explore the interweave access when the spectrum of PUs is idle and the underlay access when the spectrum of PUs is busy. This allows SUs to operate at the maximum power during an idle period in contrast to operating at reduced power when employing only the underlay access all the time.

A number of research works have addressed the hybrid or joint interweave-underlay spectrum access. For example, Khan et al. [5] have proposed a hybrid underlay-interweave mode enabled Cognitive Radio Network (CRN) scheme. Likewise, in [6], Zoe et al. have proposed a hybrid interweave-underlay spectrum access scheme using spectrum sensing in the 5 GHz license-exempt spectrum. Besides, for the performance analysis, Mehmeti et al. [2] have provided expressions that allow the performance comparison of the interweave and underlay modes under a unified network setup. Also, in [7], Jazaie et al. have presented the downlink capacity region of a secondary network in a multiuser spectrum sharing system for a hybrid underlay-interweave paradigm. However, a consensus about the more suitable spectrum access out of the interweave and underlay for SUs is not too obvious [2].

Besides, most data are originated in indoors, particularly in dense urban areas where the existence of a large number of multistory buildings installed with small cells is an obvious scenario [8]. Hence, addressing high capacity and data rates in such buildings is crucial. In this regard, due to the favorable propagation characteristics of high-frequency millimeter-wave (mmWave) signals, such as low interference effects and the existence of Line-of-Sight (LOS) components, operating small cells at the mmWave spectrum in such buildings can be a promising candidate to provide high data rates and capacity. In line with this, a hybrid interweave-underlay spectrum access technique for sharing the licensed mmWave spectrum of one MNO with in-building small cells of another to increase its available spectrum within multistory buildings can play a vital role in serving high capacity and data rates indoors, which, however, has not been addressed in the existing literature.

 ISBN: 978-1-61208-828-0

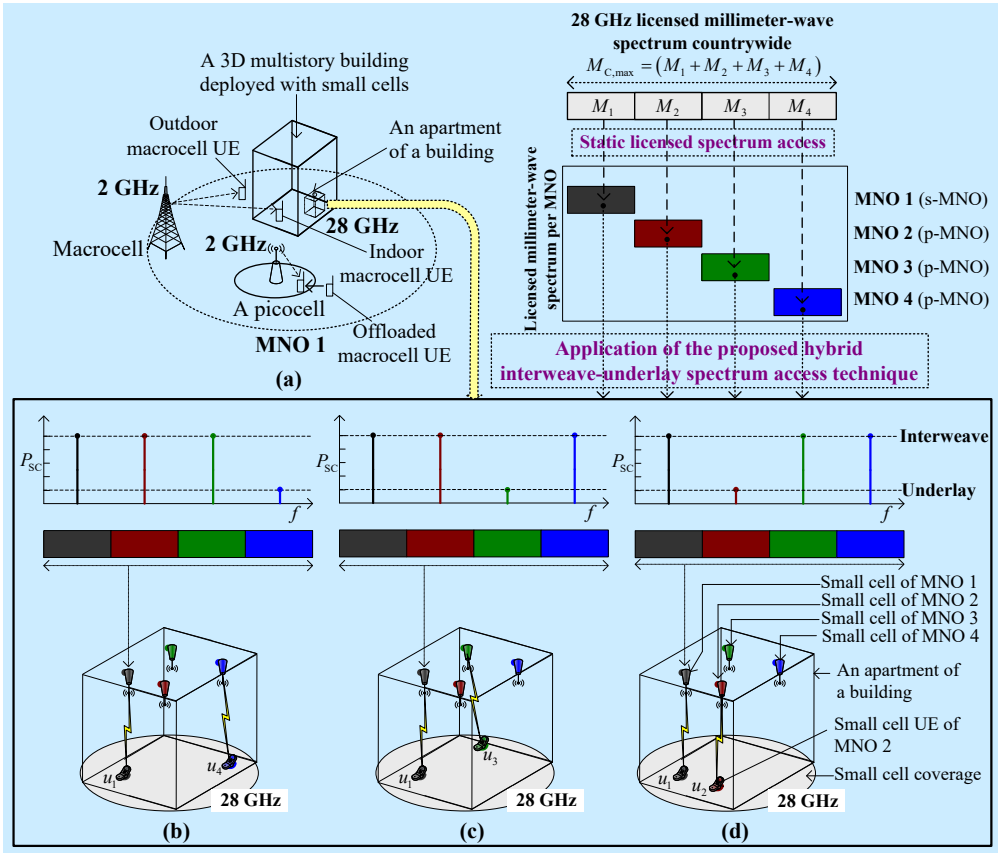

Figure 1. A system architecture consisting of four MNOs in a country. P_{SC} denotes the transmission power of an in-building small cell base station of MNO 1.

To address the issues outlined above, in this paper, we propose a hybrid interweave-underlay spectrum access technique to share the licensed 28 GHz mmWave spectrum of one MNO, referred to as primary MNO (p-MNO), with small cells in a building of another MNO, referred to as secondary MNO (s-MNO), in a country. The proposed technique explores both the traditional interweave and underlay spectrum access techniques. The following are performed section-wise to address the proposed technique. In Section II, the proposed technique along with the system architecture are presented. In Section III, we perform relevant mathematical analysis to derive average capacity, SE, and EE performance metrics for s-MNOs by employing the proposed technique. Section IV provides default simulation parameters and assumptions, as well as extensive numerical and simulation results and analyses for an s-MNO of a country consisting of four MNOs to demonstrate that the proposed technique can satisfy both the SE and EE requirements for Sixth-Generation (6G) mobile systems. We conclude the paper in Section V.

II. System Architecture and Proposed Technique

A. System Architecture

We consider that four MNOs (i.e., MNO 1, MNO 2, MNO 3, and MNO 4) are operating in a country. Assume that each MNO has a similar system architecture consisting of three types of Base Stations (BSs), namely Macrocell BSs (MBSs), Picocell BSs (PBSs), and Small Cell BSs (SBSs). For simplicity, we show the detailed architecture of only one MNO (i.e., MNO 1) in Figure 1(a). All SBSs are deployed only within 3-Dimensional (3D) multistory buildings each serving one UE at a time. Both in-building SBSs and PBSs are located within the coverage of an MBS. Each macrocell UE of an MBS is served either by the MBS itself or by any PBSs within its coverage. SBSs within each building are considered to be operating at the 28 GHz mmWave spectrum, whereas MBSs and PBSs are operating at the 2 GHz spectrum (Figure 1(a)).

We assume that each MNO is given a license for an equal amount of 28 GHz mmWave spectrum, and the spectrum of one MNO can be shared with in-building SBSs of another MNO following a hybrid interweave-underlay spectrum access technique presented in the following section. Figures 1(b)-1(d) show an example for sharing the spectra of MNO 2, MNO 3, and MNO 4 as p-MNOs with an in-building SBS of MNO 1 as an s-MNO using the proposed technique by considering that the maximum of two UEs (one from MNO 1 and the other from any p-MNO) can exist simultaneously within the coverage of the SBS.

B. Proposed Technique

We propose a hybrid interweave-underlay spectrum access technique for the dynamic spectrum access of the licensed 28-GHz mmWave spectrum of one MNO to another in a country, stated as follows.

"The licensed 28-GHz mmWave spectrum of one MNO (i.e., p-MNO) can be allowed to share with small cells in a building of another MNO (i.e., s-MNO) subject to operating each small cell of the s-MNO at the maximum transmission

 ISBN: 978-1-61208-828-0

power if no UE of the p-MNO is present, but at a reduced transmission power if a UE of the p-MNO is present. The reduced transmission power is varied in accordance with the predefined interference threshold set by the p-MNO."

As indicated above, the proposed technique takes advantage of exploring both the interweave as well as underlay spectrum access techniques. Using the interweave access, small cells of an s-MNO in a building can access opportunistically the whole licensed 28-GHz spectrum of every single p-MNO in a country in time, frequency, and space by operating them at the maximum transmission power as long as no UE of the respective p-MNO is present at the same time. But, if a UE of any p-MNO is present, following the underlay access, each small cell of the s-MNO immediately reduces its transmission power corresponding to the predefined interference threshold set by the p-MNO to limit CCI to the UE of the p-MNO. In this regard, the small cells of the s-MNO keep sensing to detect the presence of UEs for each p-MNO to update the corresponding spectrum access mode of operation to either the interweave access or the underlay access such that the CCI constraint to UEs of the respective p-MNO can be guaranteed. More specifically, each small cell of an s-MNO needs to switch only between two states of its transmission power, either the maximum or the reduced one. For switching, both reactive and proactive spectrum sensing approaches can be applied to detect the usage of the shared spectrum of any p-MNO. In the reactive approach, an s-MNO performs spectrum sensing mechanisms to detect the usage on the shared spectrum, whereas in the reactive approach, based on the knowledge of the traffic model of the UEs of a p-MNO, the arrival of UEs can be predicted [9] to reduce the transmission power beforehand.

III. MATHEMATICAL ANALYSIS

Assume that O denotes the maximum number of MNOs of a country such that $o \in \boldsymbol{O} = \{1,2,...,O\}$. Let $M_{\text{C,max}}$ denote the countrywide 28 GHz mmWave spectrum defined in terms of the number of Resource Blocks (RBs), where an RB is equal to 180 kHz. Let M_o denote the amount of 28 GHz spectrum of an MNO such that $\sum_{o=1}^{O} M_o \le M_{\text{C,max}}$. Assume that L denotes the number of buildings per macrocell such that $l \in \{1,2,...,L\}$. Let S_{F} denote the number of small cells per 3D building such that $s \in \{1,2,...,S_{\text{F}}\}$, where S_{F} is assumed the same for all buildings. Let S_{M} denote the number of macrocells and let S_{P} denote the number of picocells per macrocell of each MNO. Also, let $\boldsymbol{T}$ denote the simulation run time with the maximum time of Q (in time step each lasting 1 ms) such that $\boldsymbol{T}$= {1, 2, 3,…,Q}.

Denote P_{MC} and P_{PC}, respectively, as the transmission power of a macrocell and a picocell. Let $P_{\text{SC,lic},o}$ denote the transmission power of an SBS when operating at the licensed spectrum of its MNO o, whereas $P_{\text{SC,int},o}$ and $P_{\text{SC,und},o}$ denote, respectively, the transmission power of an SBS of MNO o when operating at the shared spectrum of other MNOs $\boldsymbol{O}\backslash o$ under the interweave and underlay spectrum access techniques. Let $P_{\text{SC,max},o}$ and $P_{\text{SC,red},o}$ denote, respectively, the maximum transmission power and the reduced transmission power of an SBS of MNO o when operating under the interweave and underlay spectrum access techniques such that $P_{\text{SC,max},o} > P_{\text{SC,red},o}$. Let $I_{\text{thr,und}}$ denote the predefined value of the maximum CCI that can be caused by an SBS to a UE of a p-MNO when operating under the underlay spectrum access technique. If κ denotes the interference channel gain, then the transmission power of an SBS of MNO o when operating under the underlay access can be adapted with $I_{\text{thr,und}}$ as follows [10].

$$P_{\text{SC,und},o} = \begin{cases} P_{\text{SC,red},o}, & \left(\kappa P_{\text{SC,red},o}\right) \le I_{\text{thr,und}} \\ \left(I_{\text{thr,und}}/\kappa\right), & \left(\kappa P_{\text{SC,red},o}\right) > I_{\text{thr,und}} \end{cases} \quad (1)$$

The received Signal-to-Interference-Plus-Noise Ratio (SINR) at RB=i in Transmission Time Interval (TTI)=t at a UE of an MNO o can be expressed as

$$\rho_{t,i,o} = \left(P_{t,i,o} / (N^{\text{s}}_{t,i,o} + I_{t,i,o})\right).H_{t,i,o} \quad (2)$$

where $P_{t,i,o}$ is the transmission power, $N^{\text{s}}_{t,i,o}$ is the noise power, $I_{t,i,o}$ is the total interference signal power, and $H_{t,i,o}$ is the link loss for a link between a UE and a BS of an MNO o at RB=i in TTI=t. $H_{t,i,o}$ can be expressed in dB as

$$H_{t,i,o}\left(\text{dB}\right) = (G_{\text{t}} + G_{\text{r}}) - (L_{\text{F}} + PL_{t,i,o}) + (LS_{t,i,o} + SS_{t,i,o}) \quad (3)$$

where $(G_{\text{t}} + G_{\text{r}})$ and L_{F} are, respectively, the total antenna gain and connector loss. $LS_{t,i,o}$, $SS_{t,i,o}$, and $PL_{t,i,o}$, respectively, denote large scale shadowing effect, small scale Rayleigh or Rician fading, and distance-dependent path loss between a BS and a UE of an MNO o at RB=i in TTI=t.

Using Shannon's capacity formula, a link throughput at RB=i in TTI=t for an MNO o in bps per Hz is given by [11] [12]

$$\sigma_{t,i,o}\left(\rho_{t,i,o}\right) = \begin{cases} 0, & \rho_{t,i,o} < -10\,\text{dB} \\ \beta \log_2\left(1 + 10^{\left(\rho_{t,i,o}(\text{dB})/10\right)}\right), & -10\,\text{dB} \le \rho_{t,i,o} \le 22\,\text{dB} \\ 4.4, & \rho_{t,i,o} > 22\,\text{dB} \end{cases} \quad (4)$$

where β denotes the implementation loss factor.

Let $M_{\text{MBS},o}$ denote the 2 GHz spectrum in RBs of a macrocell for an MNO o. Then, the total capacity of all macrocell UEs for an MNO o can be expressed as

$$\sigma_{\text{MBS},o} = \sum_{t=1}^{Q} \sum_{i=1}^{M_{\text{MBS},o}} \sigma_{t,i,o}\left(\rho_{t,i,o}\right) \quad (5)$$

where σ and ρ are responses over $M_{\text{MBS},o}$ RBs of all macro UEs in $t \in \boldsymbol{T}$ for an MNO o.

Assume that each MNO o has an SBS in each apartment, and each SBS can serve the maximum of one UE at a time. Assume that there are 4 MNOs in a country such that $o \in \boldsymbol{O} = \{1,2,3,4\}$. So, a maximum of four different UEs each from one MNO may exist at once in an apartment. Each UE has two states for existence (i.e., a UE of an MNO may either exist or not) in an apartment. Let the binary digits 1 and 0 denote, respectively, the existence and nonexistence of a UE of an MNO o in an apartment such that four UEs can coexist in an

 ISBN: 978-1-61208-828-0

apartment in a maximum of 2^4 possible ways, as shown in Table I.

Assume that the existence of four UEs in an apartment for each possible way shown in Table I is equally likely. Hence, given the existence (i.e., the binary state 1) of a UE of an MNO o (i.e., an s-MNO) over the observation time of $|\boldsymbol{T}| = Q$, UEs of other MNOs $\boldsymbol{O}\backslash o$ (i.e., p-MNOs) can coexist with the UE of MNO o in a maximum of eight possible ways, as shown in Table I, each occurs with a probability of 1/8 and, hence, persisting for $Q/8$ during the observation time Q in an apartment.

For example, for a UE u_1 of MNO 1 as an s-MNO, all the possible combinations in which u_1 can coexist with other UEs u_2, u_3, and u_4 of MNO 2, MNO 3, and MNO 4 as p-MNOs, respectively, are the following $\{u_1\}$, $\{u_1,u_2\}$, $\{u_1,u_3\}$, $\{u_1,u_4\}$, $\{u_1,u_2,u_3\}$, $\{u_1,u_2,u_4\}$, $\{u_1,u_3,u_4\}$, and $\{u_1,u_2,u_3,u_4\}$, where each occurs with a probability of 1/8 in an apartment. Assume that each MNO is allocated to an equal amount of spectrum of M RBs. Then, the above possible combinations for the coexistence of u_1 with other UEs (i.e., u_2, u_3, and u_4) in an apartment correspond to the amount of shared spectrum for u_1 of 3M, 2M, 2M, 2M, M, M, M, and 0, respectively, for the interweave access, and of 0, M, M, M, 2M, 2M, 2M, and 3M for the underlay access, as shown in Table I. These correspond to the total spectrum for u_1 of 4M, 3M, 3M, 3M, 2M, 2M, 2M, and M, respectively, for the interweave access, and of M, 2M, 2M, 2M, 3M, 3M, and 4M for the underlay access.

Now, if all SBSs in each building serve simultaneously in $t \in \boldsymbol{T}$, using Table I, the aggregate capacity served by an SBS of an MNO o (i.e., an s-MNO) can be found as follows. Let $P_{\mathrm{SC,int,RB}}$ and $P_{\mathrm{SC,und,RB}}$ denote, respectively, the transmission power per RB of an SBS of an MNO o when operating under the interweave and underlay spectrum access techniques. Assume that $\rho_{t,i,o,\mathrm{int}}$ and $\rho_{t,i,o,\mathrm{und}}$ denote, respectively, the received SINR at RB=i in TTI=t at a UE of an MNO o when operating at the power of $P_{t,i,o} = P_{\mathrm{SC,int,RB}}$ under the interweave access and $P_{t,i,o} = P_{\mathrm{SC,und,RB}}$ under the underlay access. Let $\sigma_{t,i,o,\mathrm{int}}$ and $\sigma_{t,i,o,\mathrm{und}}$ denote, respectively, the link throughput corresponding to $\rho_{t,i,o,\mathrm{int}}$ and $\rho_{t,i,o,\mathrm{und}}$. Using (2) and (4), the capacity served by an SBS of an MNO o using the interweave access at the shared spectrum of MNOs $\boldsymbol{O}\backslash o$ in $t \in \boldsymbol{T}$ is given by

$$\sigma_{s,o,\mathrm{int}} = \begin{pmatrix} \left(3\sum_{t=1}^{(Q/8)}\sum_{i=1}^{M}\sigma_{t,i,o,\mathrm{int}}\left(\rho_{t,i,o,\mathrm{int}}\right)\right) \\ +\left(3\sum_{t=1}^{(Q/8)}\sum_{i=1}^{2M}\sigma_{t,i,o,\mathrm{int}}\left(\rho_{t,i,o,\mathrm{int}}\right)\right) \\ +\sum_{t=1}^{(Q/8)}\sum_{i=1}^{3M}\sigma_{t,i,o,\mathrm{int}}\left(\rho_{t,i,o,\mathrm{int}}\right) \end{pmatrix} \quad (6)$$

Also, the capacity served by an SBS of an MNO o using the underlay access at the shared spectrum in $t \in \boldsymbol{T}$ is given by

$$\sigma_{s,o,\mathrm{und}} = \begin{pmatrix} \left(3\sum_{t=1}^{(Q/8)}\sum_{i=1}^{M}\sigma_{t,i,o,\mathrm{und}}\left(\rho_{t,i,o,\mathrm{und}}\right)\right) \\ +\left(3\sum_{t=1}^{(Q/8)}\sum_{i=1}^{2M}\sigma_{t,i,o,\mathrm{und}}\left(\rho_{t,i,o,\mathrm{und}}\right)\right) \\ +\sum_{t=1}^{(Q/8)}\sum_{i=1}^{3M}\sigma_{t,i,o,\mathrm{und}}\left(\rho_{t,i,o,\mathrm{und}}\right) \end{pmatrix} \quad (7)$$

Now, the capacity served by an SBS of an MNO o at the licensed spectrum of M of MNO o itself in $t \in \boldsymbol{T}$ is given by

$$\sigma_{s,o,\mathrm{lic}} = \sum_{t=1}^{Q}\sum_{i=1}^{M}\sigma_{t,i,o,\mathrm{lic}}\left(\rho_{t,i,o,\mathrm{lic}}\right) \quad (8)$$

TABLE I. CO-EXISTENCE AND SHARED SPECTRUM FOR UE u_1 OF MNO 1 USING THE PROPOSED TECHNIQUE.

u_1	u_2	u_3	u_4	Shared spectrum for u_1		Licensed spectrum for u_1
				Interweave	Underlay	Both interweave and underlay
0	0	0	0	Not applicable due to the nonexistence of u_1		
0	0	0	1			
0	0	1	0			
0	0	1	1			
0	1	0	0			
0	1	0	1			
0	1	1	0			
0	1	1	1			
1	0	0	0	3M	0	M
1	0	0	1	2M	M	M
1	0	1	0	2M	M	M
1	0	1	1	M	2M	M
1	1	0	0	2M	M	M
1	1	0	1	M	2M	M
1	1	1	0	M	2M	M
1	1	1	1	0	3M	M

Based on the above, the overall aggregate capacity served by an SBS of an MNO o using the proposed technique at the licensed spectrum of M of MNO o itself, as well as the shared spectrum of MNOs $\boldsymbol{O}\backslash o$, in $t \in \boldsymbol{T}$ is given by

$$\sigma_{s,o,\mathrm{prop}} = \left(\sigma_{s,o,\mathrm{lic}} + \sigma_{s,o,\mathrm{int}} + \sigma_{s,o,\mathrm{und}}\right) \quad (9)$$

Now, the aggregate capacity served by all SBSs of an MNO o in a building using the proposed technique in $t \in \boldsymbol{T}$ is given by

$$\sigma_{S_{\mathrm{F}},o,\mathrm{prop}} = \sum_{s=1}^{S_{\mathrm{F}}}\sigma_{s,o,\mathrm{prop}} \quad (10)$$

However, due to the short distance between a small cell UE and its SBS and a low transmission power of an SBS, we assume similar indoor signal propagation characteristics for all L buildings per macrocell for an MNO o. Then, by linear approximation, the system-level average capacity, SE, and EE for an MNO o are given for L>1, respectively as follows.

$$\sigma^{\mathrm{sys}}_{\mathrm{cap},o,\mathrm{prop}}\left(L\right) = \sigma_{\mathrm{MBS},o} + \left(L\,\sigma_{S_{\mathrm{F}},o,\mathrm{prop}}\right) \quad (11)$$

$$\sigma^{\mathrm{sys}}_{\mathrm{SE},o,\mathrm{prop}}\left(L\right) = \sigma^{\mathrm{sys}}_{\mathrm{cap},o,\mathrm{prop}}\left(L\right) \Big/ \left(\left(M_{\mathrm{MBS},o} + M\right)Q\right) \quad (12)$$

 ISBN: 978-1-61208-828-0

$$\sigma^{\text{sys}}_{\text{EE},o,\text{prop}}(L) = \left(\begin{pmatrix} \begin{pmatrix} (L S_{\text{F}}) \\ \begin{pmatrix} P_{\text{SC,lic},o} + \\ \left(1.5\left(P_{\text{SC,int},o} + P_{\text{SC,und},o}\right)\right) \end{pmatrix} \end{pmatrix} \\ +\left(S_{\text{P}} P_{\text{PC}}\right) + \left(S_{\text{M}} P_{\text{MC}}\right) \end{pmatrix} \right) \Big/ \left(\sigma^{\text{sys}}_{\text{cap},o,\text{prop}}(L)/Q\right) \quad (13)$$

Also, in the traditional Static Licensed Spectrum Allocation (SLSA) technique, each MNO is licensed exclusively for an equal amount of the 28 GHz mmWave spectrum of M RBs. Then, for SLSA, the system-level average capacity, SE, and EE for an MNO o for $L>1$ are given, respectively by

$$\sigma^{\text{sys}}_{\text{cap},o,\text{SLSA}}(L) = \sigma_{\text{MBS},o} + \left(L \sigma_{S_{\text{F}},o,\text{SLSA}}\right) \quad (14)$$

$$\text{where } \sigma_{S_{\text{F}},o,\text{SLSA}} = \sum\nolimits_{s=1}^{S_{\text{F}}} \sum_{t \in \boldsymbol{\mathcal{T}}} \sum\nolimits_{i=1}^{M} \sigma_{s,t,i,o}\left(\rho_{s,t,i,o}\right) \quad (15)$$

$$\sigma^{\text{sys}}_{\text{SE},o,\text{SLSA}}(L) = \sigma^{\text{sys}}_{\text{cap},o,\text{SLSA}}(L) \Big/ \left(\left(M_{\text{MBS},o} + M\right)Q\right) \quad (16)$$

$$\sigma^{\text{sys}}_{\text{EE},o}(L) = \left(\begin{pmatrix} (L S_{\text{F}} P_{\text{SC}}) \\ +\left(S_{\text{P}} P_{\text{PC}}\right) + \left(S_{\text{M}} P_{\text{MC}}\right) \end{pmatrix} \right) \Big/ \left(\sigma^{\text{sys}}_{\text{cap},o,\text{SLSA}}(L)/Q\right) \quad (17)$$

From here, the improvement factors for capacity, SE, and EE performances due to applying the proposed technique for an MNO o (i.e., an s-MNO) with respect to that due to applying the SLSA technique can be expressed, respectively as follows.

$$\sigma^{\text{sys}}_{\text{cap},o,\text{IF}}(L) = \sigma^{\text{sys}}_{\text{cap},o,\text{prop}}(L) \Big/ \sigma^{\text{sys}}_{\text{cap},o,\text{SLSA}}(L) \quad (18)$$

$$\sigma^{\text{sys}}_{\text{SE},o,\text{IF}}(L) = \sigma^{\text{sys}}_{\text{SE},o,\text{prop}}(L) \Big/ \sigma^{\text{sys}}_{\text{SE},o,\text{SLSA}}(L) \quad (19)$$

$$\sigma^{\text{sys}}_{\text{EE},o,\text{IF}}(L) = \sigma^{\text{sys}}_{\text{EE},o,\text{prop}}(L) \Big/ \sigma^{\text{sys}}_{\text{EE},o,\text{SLSA}}(L) \quad (20)$$

IV. Performance Result and Analysis

Table II shows the default simulation parameters and assumptions used for evaluating the performance of the proposed technique for MNO 1, as an s-MNO. For the underlay access, we assume that the transmission power of an SBS is upper limited by 20% of its maximum power. To allow flexibility in switching between the interweave and underlay accesses, for each SBS, a separate transceiver is assumed to operate at the shared spectrum of M RBs of each p-MNO.

Figure 2 shows improvement factors in terms of SE and EE performances for MNO 1 due to applying the proposed hybrid interweave-underlay technique, as well as the traditional interweave and underlay techniques. It can be found that the proposed hybrid technique improves both the SE and EE metrics of MNO 1 considerably as compared to that of the traditional interweave and underlay techniques when applied separately. This is because, using Table I, the maximum amount of the shared spectrum obtained by employing the proposed technique is 3 times (interweave and underlay techniques each contributing 1.5 times) the spectrum of MNO 1 of M RBs for any observation time Q. This causes the proposed technique to increase the licensed spectrum of M RBs to $4M$ RBs for MNO 1 in time Q. Since the capacity, and hence SE, is directly proportional, whereas the EE is inversely proportional, to the spectrum, the proposed technique improves SE by about 2.82 times, whereas EE by about 73%, of MNO 1, as shown in Figure 2.

Figures 3(a) and 3(b) show, respectively, the SE and EE responses for MNO 1 by reusing the mmWave spectrum of MNO 1 to its small cells in each building due to applying the proposed technique, as well as the traditional interweave, underlay, and SLSA techniques for a number of buildings of small cells. It can be found that, with an increase in l, SE increases linearly, whereas EE improves negative exponentially for all techniques, and the proposed technique outperforms all techniques in terms of SE and EE.

TABLE II. DEFAULT PARAMETERS AND ASSUMPTIONS

Parameters and Assumptions			Value
Countrywide 28 GHz spectrum and number of MNOs			200 MHz and 4
28 GHz and 2 GHz spectra per MNO			50 MHz and 10 MHz
For each MNO			
E-UTRA simulation case[1,6]			3GPP case 3
Cellular layout[2], Inter-Site Distance (ISD)[1,2,6], transmission direction			Hexagonal grid, dense urban, 3 sectors per macrocell site, 1732 m, downlink
Carrier frequency[2,5,6]			2 GHz non-LOS (NLOS) for macrocells and picocells, 28 GHz LOS for all small cells
Number of cells			1 macrocell, 2 picocells, 8 small cells per building
Total BS transmission power[1] (dBm)			46 for macrocell[1,4], 37 for picocells[1], 19 (interweave) for small cells[1,3,4], and 12.01 (underlay) for small cells
Co-channel small-scale fading model[1,3,5]			Frequency selective Rayleigh for 2 GHz NLOS, none for 28 GHz LOS
Path loss	MBS and a UE[1]	Outdoor macrocell UE	PL(dB)=15.3 + 37.6 $\log_{10}R$, R is in m
		Indoor macrocell UE	PL(dB)=15.3 + 37.6 $\log_{10}R$ + L_{ow}, R is in m and L_{ow}=20 dB
	PBS and a UE[1]		PL(dB)=140.7+36.7 $\log_{10}R$, R is in km
	SBS and a UE[1,2,5]		PL(dB)=61.38+17.97 $\log_{10}R$, R is in m
Lognormal shadowing standard deviation (dB)			8 for MBS[2], 10 for PBS[1], and 9.9 for SBS[2,5]
Antenna configuration			Single-input single-output for all BSs and UEs
Antenna pattern (horizontal)			Directional (120^0) for MBS[1], omnidirectional for PBS[1] and SBS[1]
Antenna gain plus connector loss (dBi)			14 for MBS[2], 5 for PBS[1], 5 for SBS[1,3]
UE antenna gain[2,3]; Indoor macrocell UE[1]			0 dBi (for 2 GHz), 5 dBi (for 28 GHz, Biconical horn); 35%
UE noise figure[2,3] and UE speed[1]			9 dB (for 2 GHz) and 10 dB (for 28 GHz), 3 km/hr
Picocell coverage, the total number of macrocell UEs, and macrocell UEs offloaded to all picocells[1]			40 m (radius), 30, 2/15
3D multistory building and SBS models (square-grid apartments): number of buildings, number of floors per building, number of apartments per floor, number of SBSs per apartment, area of an apartment			L, 2, 4,1, 10×10 m^2
Scheduler and traffic model[2]			Proportional Fair and full buffer
Type of SBSs			Closed Subscriber Group femtocell BSs
TTI[1] and scheduler time constant[6] (t_c)			1 ms and 100 ms
Total simulation run time			8 ms

taken [1]from [13], [2]from [14], [3]from [15], [4]from [16], from [5][17], from [6][18].

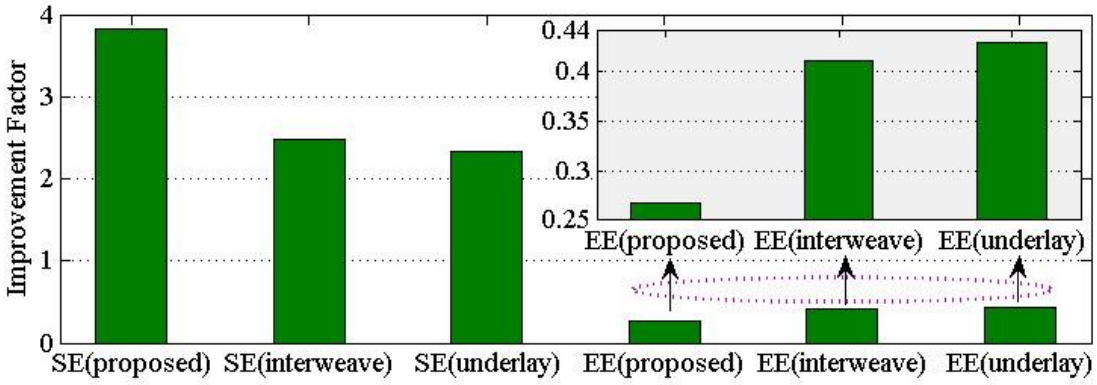

Figure 2. SE and EE improvement factors for an s-MNO (i.e., MNO 1) due to applying different techniques for a single building of SBSs.

Moreover, according to [19] [20], it is expected that the 6G mobile systems will require 10 times average SE (i.e., 270-370 bps/Hz), as well as 10 times average EE (i.e., 0.3μJ/bit), of 5G mobile systems [21]-[23]. Using Figure 3, the values of l that satisfy both SE and EE requirements for 6G mobile systems are 9, 13, 14, and 32, respectively, for the proposed hybrid, interweave, underlay, and SLSA techniques.

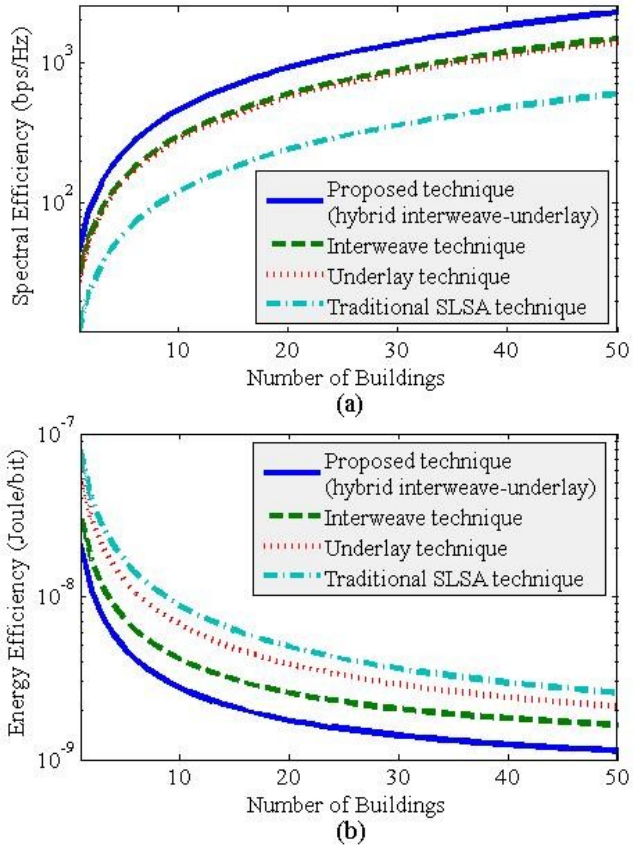

Figure 3. (a) SE and (b) EE performances for MNO 1 due to applying different techniques for multiple buildings of SBSs.

According to the evidence above, the proposed hybrid interweave-underlay technique can satisfy both SE and EE requirements for 6G mobile systems by reusing the whole mmWave spectrum of MNO 1 to its small cells of roughly 31%, 36%, and 72% less number of buildings than that required by the traditional interweave, underlay, and SLSA techniques, respectively.

V. Conclusion

In this paper, we have proposed a hybrid interweave-underlay spectrum access technique to share the licensed 28 GHz millimeter-wave (mmWave) spectrum of one MNO with small cells in a building of another MNO in a country. We have derived average capacity, Spectral Efficiency (SE), and Energy Efficiency (EE) performance metrics for the proposed technique and carried out extensive numerical and simulation results and analyses for MNO 1 of a country consisting of four MNOs. It has been shown that the proposed technique can improve the SE by about 2.82 times and the EE by about 73% of MNO 1 as compared to that of the traditional Static Licensed Spectrum Allocation (SLSA) technique. Further, we have shown that the proposed technique can satisfy both SE and EE requirements for 6G mobile systems by reusing the mmWave spectrum of MNO 1 to its small cells of roughly 31%, 36%, and 72% less number of buildings than that required by the traditional interweave, underlay, and SLSA techniques, respectively.

The proposed technique can be investigated further for a complete analysis to address numerous crucial issues, including millimeter-wave bands other than 28 GHz, such as 26 GHz, 38 GHz, and 60 GHz, non-LOS path loss models, directional millimeter-wave antennas, spectrum sensing mechanisms and control signaling overhead, implementation complexity analysis, burst traffic characteristics, random deployments of indoor UEs, as well as serving more than one UE simultaneously by a single small cell in a building.

References

[1] Spectrum Policy Task Force Report. Federal Communications Commission, Washington, DC, USA, Tech. Rep. 02-155, Nov. 2002. Available Online: https://www.fcc.gov/document/spectrum-policy-task-force. [retrieved: August, 2020].

[2] F. Mehmeti and T. Spyropoulos, "Performance Analysis, Comparison, and Optimization of Interweave and Underlay Spectrum Access in Cognitive Radio Networks," IEEE Transactions on Vehicular Technology, vol. 67, pp. 7143-7157, Aug. 2018, doi: 10.1109/TVT.2018.2828090.

 ISBN: 978-1-61208-828-0

[3] I. F. Akiyildiz, W. Y. Lee, M. C. Vuran, and S. Mohanty, "A Survey on Spectrum Management in Cognitive Radio Networks," IEEE Communications Magazine, vol. 46, pp. 40-48, Apr. 2008, doi: 10.1109/MCOM.2008.4481339.

[4] A. Sharmila and P. Dananjayan, "Spectrum Sharing Techniques in Cognitive Radio Networks - A Survey," Proc. The 2019 IEEE International Conference on System, Computation, Automation and Networking (ICSCAN), Pondicherry, India, 2019, pp. 1-4.

[5] A. U. Khan et al., "HBLP: A Hybrid Underlay-Interweave Mode CRN for the Future 5G-based Internet of Things," IEEE Access, vol. 8, pp. 63403-63420, 2020, doi: 10.1109/ACCESS.2020.2981413.

[6] P. Zuo, T. Peng, W. Linghu and W. Wang, "Optimal Resource Allocation for Hybrid Interweave-Underlay Cognitive Satcom Uplink," Proc. The 2018 IEEE Wireless Communications and Networking Conference (WCNC), IEEE Press, 2018, pp. 1-6.

[7] M. Jazaie and A. R. Sharafat, "Downlink Capacity and Optimal Power Allocation in Hybrid Underlay–Interweave Secondary Networks," IEEE Transactions on Wireless Communications, vol. 14, pp. 2562-2570, May 2015, doi: 10.1109/TWC.2014.2388222.

[8] R. K. Saha, "Countrywide Mobile Spectrum Sharing with Small Indoor Cells for Massive Spectral and Energy Efficiencies in 5G and Beyond Mobile Networks," Energies, vol. 12, Art. No. 3825, Oct. 2019, doi.org/10.3390/en12203825.

[9] A. Ali and W. Hamouda, "Advances on Spectrum Sensing for Cognitive Radio Networks: Theory and Applications," IEEE Communications Surveys & Tutorials, vol. 19, pp. 1277-1304, Second quarter 2017, doi: 10.1109/COMST.2016.2631080.

[10] J. Oh and W. Choi, "A Hybrid Cognitive Radio System: A Combination of Underlay and Overlay Approaches," Proc. 2010 IEEE 72nd Vehicular Technology Conference - Fall, Sept. 2010, pp. 1-5.

[11] R. K. Saha, "A Hybrid System and Technique for Sharing Multiple Spectrums of Satellite Plus Mobile Systems with Indoor Small Cells in 5G and Beyond Era," IEEE Access, vol. 7, pp. 77569-77596, 2019, doi: 10.1109/ACCESS.2019.2921723.

[12] R. K. Saha and C. Aswakul, "A Novel Frequency Reuse Technique for In-Building Small Cells in Dense Heterogeneous Networks," IEEJ Transactions on Electrical and Electronic Engineering, vol. 13, pp. 98-111, Jan. 2018, doi.org/10.1002/tee.22503.

[13] Evolved Universal Terrestrial Radio Access (E-UTRA); Radio Frequency (RF) System Scenarios. document 3GPP TR 36.942, V.1.2.0, 3rd Generation Partnership Project, Jul. 2007. Available online: https://portal.3gpp.org/ desktopmodules /Specifications/Specification Details.aspx?specificationId=2592 [retrieved: February, 2020]

[14] Simulation Assumptions and Parameters for FDD HeNB RF Requirements. document TSG RAN WG4 (Radio) Meeting #51, R4-092042, 3GPP, May 2009. Available online: https://www.3gpp.org/ftp/tsg_ran /WG4_Radio/TSGR4_51/Documents/ [retrieved: February, 2020].

[15] Guidelines for Evaluation of Radio Interface Technologies for IMT-2020. Report ITU-R M.2412-0 (10/2017), Geneva, 2017. Available online: https://www.itu.int/dms_pub/itu-r/opb/rep/R-REP-M.2412-2017-PDF-E.pdf [retrieved: February, 2020]

[16] R. K. Saha, P. Saengudomlert, and C. Aswakul, "Evolution Toward 5G Mobile Networks-A Survey On Enabling Technologies," Engineering Journal, vol. 20, pp. 87-119, Jan. 2016, doi.org/10.4186/ej.2016.20.1.87.

[17] G. R. Maccartney, T. S. Rappaport, S. Sun, and S. Deng, "Indoor Office Wideband Millimeter-Wave Propagation Measurements and Channel Models at 28 and 73 GHz for Ultra-Dense 5G Wireless Networks," IEEE Access, vol. 3, pp. 2388-2424, 2015, doi: 10.1109/ACCESS.2015.2486778.

[18] R. K. Saha, S. Nanba, and K. Nishimura, "A Technique for Cloud Based Clustering and Spatial Resource Reuse and Scheduling of 3D In-Building Small Cells Using CoMP for High Capacity CRAN," IEEE Access, vol. 6, pp. 71602-71621, Nov. 2018, doi: 10.1109/ACCESS.2018.2879835.

[19] Z. Zhang et al., "6G Wireless Networks: Vision, Requirements, Architecture, and Key Technologies," IEEE Vehicular Technology Magazine, vol. 14, pp. 28-41, Sept. 2019, doi: 10.1109/MVT.2019.2921208.

[20] S. Chen et al., "Vision, Requirements, and Technology Trend of 6G: How to Tackle the Challenges of System Coverage, Capacity, User Data-Rate and Movement Speed," IEEE Wireless Communications, vol. 27, no. 2, pp. 218-228, Apr. 2020, doi: 10.1109/MWC.001.1900333.

[21] C.-X. Wang et al., "Cellular Architecture and Key Technologies for 5G Wireless Communication Networks," IEEE Communications Magazine, vol. 52, pp. 122-130, Feb. 2014, doi: 10.1109/MCOM.2014.6736752.

[22] G. Auer et al., "How Much Energy is Needed to Run a Wireless Network?" IEEE Wireless Communications, vol. 18, pp. 40-49, Oct. 2011, doi: 10.1109/MWC.2011.6056691.

[23] R. K. Saha, "3D Spatial Reuse of Multi-Millimeter-Wave Spectra by Ultra-Dense In-Building Small Cells for Spectral and Energy Efficiencies of Future 6G Mobile Networks," Energies, vol. 13, Art. No. 1748, Apr. 2020, doi.org/10.3390/en13071748.

 ISBN: 978-1-61208-828-0

Exploiting Multi-Path for Safeguarding mmWave Communications Against Randomly Located Eavesdroppers

Rohith Talwar, Nancy Amala, George Medina, Akshadeep Singh Jida, and Mohammed E. Eltayeb
Department of Electrical & Electronic Engineering
California State University, Sacramento, USA
Emails: {rohithtalwar, nancyamalajosephraj, gm739, asjida, mohammed.eltayeb}@csus.edu

***Abstract*—Communication in the millimeter-wave (mmWave) band has recently been proposed to enable giga-bit-per-second data rates for next generation wireless systems. Physical layer security techniques have emerged as a simple and yet effective way to safeguard these systems against eavesdropping attacks. These techniques make use of the large antenna arrays available in mmWave systems to provide an array gain at the target receiver and degrade the signal quality at the eavesdropper. Despite their effectiveness, the majority of these techniques are based on line-of-sight communication links between the transmitter and the receiver, and may fail in the presence of blockages or non-line-of-sight links. This paper builds upon previous work and extends physical layer security to the non-line-of-sight communication case and randomly located eavesdroppers. Specifically, the large dimensional antenna arrays in mmWave systems and the intrinsic characteristics of wireless channel are exploited to induce noise-like signals that jam eavesdroppers with sensitive receivers. Numerical results show that the proposed techniques provide higher secrecy rate when compared to conventional array and physical layer techniques based on line-of-sight links.**

Keywords–Millimeter-Wave; Physical layer security; Beamforming.

I. INTRODUCTION

The abundance of bandwidth in the millimeter-wave (mmWave) band enables high-speed, low latency, communication to support next generation systems [1]-[3]. These systems rely on directional communication with large antenna arrays to achieve sufficient link budget [4][5]. Securing these systems against eavesdropping and privacy attacks is one major challenge [6]-[8].

Security in wireless communications can be mainly grouped into cryptographic and Physical Layer Security (PLS) strategies, where the previous incorporates key-based approaches normally applied at higher system layers. The limited transmit RF-chains, higher path-loss, and directional communication requirement of mmWave systems, however, makes the implementation of classical cryptographic techniques inefficient for these systems [4][8][9]. For this reason, physical layer security has emerged as a simple but yet effective way to secure these systems and complement key-based cryptographic techniques [6][8][10]. Further, the implementation of PLS in mmWave is considered a productive strategy as it can result in higher communication speed, narrow communication beam and shorter transmission separation [11]. Physical layer security techniques utilize the large antenna arrays to enhance the communication signal (via beamforming) at the target receiver and degrade the signal quality at the eavesdropper. Directional beamforming, however, relies on Line-of-Sight (LoS) communication, and assumes the eavesdropper is not along the direction of communication. In practice, the passive eavesdropper could be located in the direction of communication, and, in the case of Non-Light-of-Sight (NLoS) communication, scatters can enable the eavesdropper to intercept the communication signal via multipath, hence rendering PHY layer security techniques ineffective. Therefore, it is critical to develop PHY layer security techniques that preserve privacy in both the LoS and NLoS cases.

Several strategies have been adopted in the literature to enhance the secrecy of mmWave wireless systems. Switched array based schemes [8] [12]-[14] employ random antenna subsets to induce artificial noise that jams potential eavesdroppers in non-receiver directions. In addition to this, the work in [8] proposed the use of prior information obtained from sensors to opportunistically inject noise in potential eavesdropper locations. In [15] and [16], low-complexity PLS techniques based on analog cooperative beamforming are proposed. These techniques enhanced the secrecy rate as distributed antenna nodes result in narrower beamwidth and increased artificial noise. The work in [17] built upon the techniques in [15] and [16] and proposed a beamforming solution with null steering. This solution is shown to improve the secrecy performance when the eavesdropper is in close proximity to the target receiver. Despite their capability in enhancing the transmission secrecy, those techniques require a LoS link to the target receiver and fail if the eavesdropper and the target receiver paths overlap. For instance, path overlap can occur if the eavesdropper is located along the transmission direction of the receiver or it is in close proximity to the receiver. Scatters close to the transmitter can cause blockages and lead to NLoS links. Overlapped common channel paths (as a result of NLoS links) between the receiver and the eavesdropper increase the risk of information leakage to the eavesdropper. To safeguard mmWave systems with possible overlapped common channel paths with the eavesdropper, the work in [18]-[21] considered the problem of aligned transmitter, eavesdropper, and target receiver in the mainlobe path, i.e., mainlobe security. In [18], a dual beam transmission technique that ensures the mainlobe is coherent only at the target receiver's location is proposed. The work in [19] proposed a dynamic rotated angular beamforming technique which uses a set of frequency offset modulator to

 ISBN: 978-1-61208-828-0

generate angle and range based transmission. The work in [21] utilized channel knowledge of eavesdroppers to enhance the secrecy rate of the target receiver. It should be noted that eavesdroppers in general are passive and their presence is unknown. The work in [20] proposed the use of maximum ratio combining and artificial noise injection in the null space of the receiver's channel to safeguard transmission. Maximum ratio combining, however, only increases the Signal-to-Noise Ratio (SNR) at the target receiver, but does not safeguard the communication link against an eavesdropper with a sensitive receiver. Moreover, noise injection requires complex antenna architectures which might be impractical to implement in mmWave systems.

In this paper, we address the problem of overlapped communication channel paths between the receiver and an arbitrary eavesdropper and propose two transmission techniques that enhance the security of mmWave systems with NLoS channels. Unlike [18]-[21], the proposed techniques do not necessarily require a LoS channel path between the transmitter and the receiver, and can be applied using a simple analog antenna architecture with a single RF chain at the transmitter. The first technique enhances secrecy by employing a path hopping technique, while the second technique uses random antenna subsets to beamform along multiple transmission paths. The proposed techniques facilitate secure transmission to the receiver without the need for complex antenna architectures and reduce the likelihood of information leakage to potential eavesdropper with common receiver communication paths.

The rest of the paper is structured as follows. In Section II, we introduce the system model. In Section III, we describe the proposed PLS techniques and analyze their performance in Section IV. We present some numerical results in Section V and conclude the work in Section VI.

II. System Model

We consider a mmWave system where the transmitter communicates with a receiver via NLoS communications paths $L > 1$ in the presence of an eavesdropper. The transmitter consists of one RF chain and N antennas and the receiver is equipped with N_{R} antennas. To transmit the kth information symbol $s(k)$, where $E[|s(k)|^2] = 1$, to the receiver, the transmitter multiplies $s(k)$ by unit norm transmit vector $\mathbf{f} = [f_1, f_2, f_3, \dots f_N] \in \mathcal{C}^N$, where f_n denotes the complex weight (or phase-shift) associated with the nth transmitting antenna. At the receiver, the received signals on all receive antennas are combined using a combining vector $\mathbf{w} \in \mathcal{C}^{N_{\mathrm{R}}}$. Assuming a narrowband block fading channel, the received signal at the receiver is given by

$$y(k) = \mathbf{w}^* \mathbf{H} \mathbf{f} s(k) + z(k), \tag{1}$$

where $\mathbf{H}$ represents the mmWave channel matrix between the transmitter and the receiver, and $z(k) \sim \mathcal{CN}(0, \sigma^2)$ is the additive noise at the receiver. Adopting a geometric channel model with L scatters, where each scatter is assumed to contribute to a single channel path between the transmitter and the receiver, the channel $\mathbf{H}$ is given by [4]

$$\mathbf{H} = \sqrt{\frac{N N_{\mathrm{R}}}{L}} \sum_{l=1}^{L} \alpha_l \mathbf{a}_{\mathrm{R}}(\phi_l) \mathbf{a}_{\mathrm{T}}^*(\theta_l) \tag{2}$$

where ϕ_l is Angle-of-Arrival (AoA) at the receiver associated with the lth Angle-of-Departure (AoD) θ_l from the transmitter, α_l is the complex gain of the lth path and $\mathbf{a}_{\mathrm{R}}(\phi_l)$ and $\mathbf{a}_{\mathrm{T}}(\theta_l)$ represent the receiver's and transmitter's array response defined in [4]. For ease of exposition, we assume a uniform linear array at the transmitter and a single antenna at the receiver. Hence, the the channel in (2) becomes

$$\mathbf{h} = \sqrt{\frac{N}{L}} \sum_{l=1}^{L} \alpha_l \mathbf{a}_{\mathrm{T}}(\theta_l), \tag{3}$$

where $\mathbf{a}_{\mathrm{T}}(\theta_l) = \frac{1}{\sqrt{N}}[e^{-j(\frac{N-1}{2})2\pi \frac{d}{\lambda}\cos(\theta_l)}, ..., e^{j(\frac{N-1}{2})2\pi \frac{d}{\lambda}\cos(\theta_l)}]$ and the signal in (1) simplifies to

$$y(k) = \mathbf{h}^* \mathbf{f} s(k) + z(k). \tag{4}$$

III. Millimeter Wave Secure Transmission

In this section, we introduce simple transmission techniques suitable for mmWave systems with analog antenna architecture (single RF chain). Nonetheless, the proposed techniques can also be applied in systems with advanced antenna architectures. The key idea is to exploit the intrinsic randomness of the wireless channel to distort transmission to eavesdroppers, with possible overlapping channels with the receiver, without the need for a fully digital array or prior channel information of eavesdroppers. With the assumption of local scatters at both the transmitter and receiver, the receiver's channel becomes unique at the transmitter, i.e.,, function of its location and scatters. This property has been exploited in finger-printing and localization techniques, see example [22]-[24] and references therein, to uniquely identify the location of the receiver. In this paper, with the assumption of full channel knowledge at the both the transmitter and the receiver, we exploit this property to jam an eavesdropper with an overlapping communication channel, i.e.,, eavesdropper shares a communication path with the target receiver. Instead of transmitting data symbols using the strongest channel path, the proposed transmission techniques select a random set of paths to transmit each data symbol (or data packet) to the target receiver. With the assumption that the receiver knows a-priori the selected transmission paths (this could be preprogrammed in the system) the receiver receives coherent signal, whereas, the eavesdropper receives a noise-like signal. This noise-like signal, which we term artificial noise, is a result of the randomized beam pattern observed at the eavesdropper. In the following sections, we further elaborate on those transmission techniques.

A. Enhancing secrecy with random path selection

In this technique, the transmitter transmits each data symbol along a random path (or AoD). Specifically, let $\theta_l \in \Phi$ be the lth AoD towards the target receiver and the set Φ represents all possible AoDs towards the target receiver. The transmitter's inter-antenna phase shifts are set as [13]

$$\Upsilon_n(k) = \left(\frac{N-1}{2} - n\right) 2\pi \frac{d}{\lambda} \cos(\theta_l) \tag{5}$$

where θ_l represents the lth selected AoD for the kth data symbol. Based on this, the nth entry of the beamforming vector $\mathbf{f}(k)$ (i.e., nth antenna weight) becomes $f_n(k) = \frac{1}{\sqrt{N}} e^{j\Upsilon_n(k)}$.

 ISBN: 978-1-61208-828-0

Using (4), the received signal at the receiver along AoD θ_l becomes

$$y_{\mathrm{R}}(k,\theta_l) = \mathbf{h}^*\mathbf{f}(k)s(k) + z_{\mathrm{R}}(k)$$
$$= \sqrt{\frac{N}{L}}\alpha_l \mathbf{a}_{\mathrm{T}}^*(\theta_l)\mathbf{f}(k)s(k) + z_{\mathrm{R}}(k) = \frac{1}{\sqrt{LN}}\alpha_l s(k)\times$$
$$\left(\sum_{n=0}^{N-1} e^{-j\left(\frac{N-1}{2}-n\right)\frac{2\pi d}{\lambda}\cos\theta_l} e^{j\left(\frac{N-1}{2}-n\right)\frac{2\pi d}{\lambda}\cos\theta_l}\right) + z_{\mathrm{R}}(k), \quad (6)$$
$$= \underbrace{s(k)}_{\substack{\text{information}\\ \text{symbol}}} \quad \underbrace{\alpha_l\sqrt{\frac{N}{L}}}_{\substack{\text{effective channel}\\ \text{and array gain}}} + \underbrace{z_{\mathrm{R}}(k)}_{\substack{\text{additive}\\ \text{noise}}}.$$

where α_l is the lth path gain gain at the receiver, and $z_{\mathrm{R}}(k) \sim \mathcal{CN}(0,\sigma_{\mathrm{R}}^2)$ is the additive noise at the receiver.

Similarly, the received signal at an eavesdropper along an AoD θ_{E} is given by

$$y_{\mathrm{E}}(k,\theta_{\mathrm{E}}) = \mathbf{h}^*\mathbf{f}(k)s(k) + z_{\mathrm{E}}(k)$$
$$= \sqrt{\frac{N}{L}}\alpha_l \mathbf{a}_{\mathrm{T}}^*(\theta_{\mathrm{E}})\mathbf{f}(k)s(k) + z_{\mathrm{E}}(k) = \frac{1}{\sqrt{LN}}\alpha_{\mathrm{E}} s(k)\times$$
$$\left(\sum_{n=0}^{N-1} e^{-j\left(\frac{N-1}{2}-n\right)\frac{2\pi d}{\lambda}\cos\theta_{\mathrm{E}}} e^{j\left(\frac{N-1}{2}-n\right)\frac{2\pi d}{\lambda}\cos\theta_l}\right) + z_{\mathrm{E}}(k) \quad (7)$$
$$= \underbrace{s(k)}_{\substack{\text{information}\\ \text{symbol}}} \quad \underbrace{\alpha_{\mathrm{E}}}_{\substack{\text{channel}\\ \text{gain}}} \quad \underbrace{\sqrt{1/LN}B(\theta_l)}_{\substack{\text{artifical}\\ \text{noise}}} + \underbrace{z_{\mathrm{E}}(k)}_{\substack{\text{additive}\\ \text{noise}}},$$

where $\theta_l \in \Phi$, $z_{\mathrm{E}}(k) \sim \mathcal{CN}(0,\sigma_{\mathrm{E}}^2)$ is the additive noise at the eavesdropper and the random variable $B(\theta_l)$ (due to random selection of θ_l) is

$$B(\theta_l) = \sum_{n=0}^{N-1} e^{-j\left(\frac{N-1}{2}-n\right)\frac{2\pi d}{\lambda}\cos\theta_{\mathrm{E}}} e^{j\left(\frac{N-1}{2}-n\right)\frac{2\pi d}{\lambda}\cos\theta_l} \quad (8)$$
$$= \sum_{n=0}^{N-1} e^{-j\left(\frac{N-1}{2}-n\right)\frac{2\pi d}{\lambda}(\cos(\theta_{\mathrm{E}})-\cos(\theta_l))} \quad (9)$$
$$= N\frac{\sin(N(\frac{\pi d}{\lambda}(\cos(\theta_{\mathrm{E}})-\cos(\theta_l))))}{\sin((\frac{\pi d}{\lambda}(\cos(\theta_{\mathrm{E}})-\cos(\theta_l))))}. \quad (10)$$

Observe when the eavesdropper is located along one of the AoDs in the set Φ, i.e., $\theta_{\mathrm{E}} = \theta_l$, then $B(\theta_l)$ becomes deterministic with the value of N. Note this event occurs with probability $\frac{1}{L}$, where L is the number of paths. Hence, it is important to have large number of paths L for this technique to be efficient.

B. Enhancing secrecy with joint path and antenna selection

The secrecy performance of the random path selection technique deteriorates with limited number of scatters, i.e., low number of transmit path L. To improve the secrecy in a low scattering environment, we propose a joint antenna selection and path selection technique. The idea is to associate a set of M antennas for the strongest transmission path and the remaining $N-M$ antennas for another randomly selected path. For each transmit symbol (or packet), different sets of antennas are associated with the strongest path and a random secondary transmit path. Selecting the strongest path maximizes the receive SNR at the receiver. This dual antenna and path selection technique results in controlled interference in both the main and secondary transmission paths. The interference results from the contribution of the side-lobes of each transmit beam in all paths. The random antenna selection ensures that the side-lobe levels are perturbed for each transmit symbol. As the target receiver is aware of its channel, the transmit path identity, and the set of selected antennas for each path (can be preprogrammed a priori), it is able to decode the received symbol. As the eavesdropper does not have knowledge of these parameters, it can not precancel the interference due to the perturbed side-lobes. This reduces its rate and enhances the overall secrecy rate.

Let $\mathcal{I}_M(k)$ be a random subset of M antennas used to transmit the kth symbol along the strongest path (AoD θ_{S}), and $\mathcal{I}_L(k)$ be subset that contains the indices of the remaining antennas used to transmit the kth symbol along a secondary path (AoD θ_i). The nth antenna phase shift is set as

$$\Upsilon_n(k) = \begin{cases} \left(\frac{N-1}{2}-n\right)2\pi\frac{d}{\lambda}\cos(\theta_{\mathrm{S}}), & n \in \mathcal{I}_M(k) \\ \left(\frac{N-1}{2}-n\right)2\pi\frac{d}{\lambda}\cos(\theta_i), & n \in \mathcal{I}_L(k) \end{cases} \quad (11)$$

and the received signal at the target receiver becomes

$$y_{\mathrm{R}}(k,\theta_{\mathrm{S}},\theta_i) = \mathbf{h}^*\mathbf{f}(k)s(k) + z_{\mathrm{R}}(k) = \frac{1}{\sqrt{LN}}s(k)\times$$
$$\Bigg(\sum_{n\in\mathcal{I}_M(k)} \alpha_{\mathrm{S}} e^{-j\left(\frac{N-1}{2}-n\right)\frac{2\pi d}{\lambda}\cos\theta_{\mathrm{S}}} e^{j\left(\frac{N-1}{2}-n\right)\frac{2\pi d}{\lambda}\cos\theta_{\mathrm{S}}}$$
$$+ \sum_{n\in\mathcal{I}_L(k)} \alpha_{\mathrm{S}} e^{-j\left(\frac{N-1}{2}-n\right)\frac{2\pi d}{\lambda}\cos\theta_{\mathrm{S}}} e^{j\left(\frac{N-1}{2}-n\right)\frac{2\pi d}{\lambda}\cos\theta_i}$$
$$+ \sum_{n\in\mathcal{I}_L(k)} \alpha_i e^{-j\left(\frac{N-1}{2}-n\right)\frac{2\pi d}{\lambda}\cos\theta_i} e^{j\left(\frac{N-1}{2}-n\right)\frac{2\pi d}{\lambda}\cos\theta_i}$$
$$+ \sum_{n\in\mathcal{I}_M(k)} \alpha_i e^{-j\left(\frac{N-1}{2}-n\right)\frac{2\pi d}{\lambda}\cos\theta_i} e^{j\left(\frac{N-1}{2}-n\right)\frac{2\pi d}{\lambda}\cos\theta_{\mathrm{S}}}\Bigg)$$
$$+ z_{\mathrm{R}}(k)$$
$$= \underbrace{s(k)}_{\substack{\text{information}\\ \text{symbol}}} \underbrace{\frac{1}{\sqrt{LN}}\Big(\alpha_{\mathrm{S}}M + \alpha_{\mathrm{i}}(N-M) + \beta_{\mathrm{R}}\Big)}_{\substack{\text{effective beamforming and}\\ \text{channel gain}}} + \underbrace{z_{\mathrm{R}}(k)}_{\substack{\text{additive}\\ \text{noise}}}, \quad (12)$$

where β_{R} is given by

$$\beta_{\mathrm{R}} = \sum_{n\in\mathcal{I}_L(k)} \alpha_{\mathrm{S}} e^{j\left(\frac{N-1}{2}-n\right)\frac{2\pi d}{\lambda}(\cos\theta_i-\cos\theta_{\mathrm{S}})} + \sum_{n\in\mathcal{I}_M(k)} \alpha_i e^{j\left(\frac{N-1}{2}-n\right)\frac{2\pi d}{\lambda}(\cos\theta_{\mathrm{S}}-\cos\theta_i)}. \quad (13)$$

Note β_{R} can be precalculated at the receiver since it has prior knowledge of the channel and the transmit antenna set along each path.

The eavesdropper can intercept the transmitted signal via the transmitter's side lobe or main lobe (this occurs when the eavesdropper is located along the the transmitter's main lobe). We will investigate these two scenarios separately. Assuming the eavesdropper can only intercept communication via the side lobe, the received signal at the eavesdropper along its

AoD $\theta_{\mathrm{E}} \notin \Phi$ is given by

$$y_{\mathrm{E}}(k,\theta_{\mathrm{S}},\theta_i,\theta_{\mathrm{E}}) = \mathbf{h}^{*}\mathbf{f}(k)s(k) + z_{\mathrm{E}}(k) = \frac{1}{\sqrt{LN}}s(k)\alpha_{\mathrm{E}}\times \Bigg(\sum_{n\in\mathcal{I}_M(k)} e^{-j\left(\frac{N-1}{2}-n\right)\frac{2\pi d}{\lambda}\cos\theta_{\mathrm{E}}} e^{j\left(\frac{N-1}{2}-n\right)\frac{2\pi d}{\lambda}\cos\theta_{\mathrm{S}}} + \sum_{n\in\mathcal{I}_L(k)} e^{-j\left(\frac{N-1}{2}-n\right)\frac{2\pi d}{\lambda}\cos\theta_{\mathrm{E}}} e^{j\left(\frac{N-1}{2}-n\right)\frac{2\pi d}{\lambda}\cos\theta_i} \Bigg) + z_{\mathrm{E}}(k)$$

$$= \underbrace{s(k)}_{\substack{\text{information}\\ \text{symbol}}} \quad \underbrace{\alpha_{\mathrm{E}}\beta_{\mathrm{E}}}_{\substack{\text{effective artificial}\\ \text{noise}}} \quad + \underbrace{z(k)}_{\substack{\text{additive}\\ \text{noise}}}, \tag{14}$$

where the noise term β_{E} is given by

$$\beta_{\mathrm{E}} = \frac{1}{\sqrt{LN}} \sum_{n\in\mathcal{I}_L(k)} e^{j\left(\frac{N-1}{2}-n\right)\frac{2\pi d}{\lambda}(\cos\theta_{\mathrm{S}}-\cos\theta_{\mathrm{E}})} + \sum_{n\in\mathcal{I}_M(k)} e^{j\left(\frac{N-1}{2}-n\right)\frac{2\pi d}{\lambda}(\cos\theta_i-\cos\theta_{\mathrm{E}})}. \tag{15}$$

From (15) we observe that the noise term β_{E} is random since the eavesdropper is unaware of the transmit angles θ_i and θ_{s} and the associated transmit antenna sets $\mathcal{I}_L(k)$ and $\mathcal{I}_M(k)$. This induces artificial noise that jams the eavesdropper. We also observe from (14) that high channel gain α_{E} increases the artificial noise at the eavesdropper, hence, no significant rate gain is expected with high channel gain.

Considering the second scenario, where we assume the eavesdropper can only intercept the communication link via the main lobe, the received signal at the eavesdropper along an AoD $\theta_{\mathrm{E}} = \theta_{\mathrm{S}}$ becomes

$$y_{\mathrm{E}}(k,\theta_{\mathrm{S}},\theta_i,\theta_{\mathrm{E}}) = \mathbf{h}^{*}\mathbf{f}(k)s(k) + z_{\mathrm{E}}(k) = \frac{1}{\sqrt{LN}}s(k)\alpha_{\mathrm{E}}\times \Bigg(\sum_{n\in\mathcal{I}_M(k)} e^{-j\left(\frac{N-1}{2}-n\right)\frac{2\pi d}{\lambda}\cos\theta_{\mathrm{E}}} e^{j\left(\frac{N-1}{2}-n\right)\frac{2\pi d}{\lambda}\cos\theta_{\mathrm{S}}} + \sum_{n\in\mathcal{I}_L(k)} e^{-j\left(\frac{N-1}{2}-n\right)\frac{2\pi d}{\lambda}\cos\theta_{\mathrm{E}}} e^{j\left(\frac{N-1}{2}-n\right)\frac{2\pi d}{\lambda}\cos\theta_i} \Bigg) + z_{\mathrm{E}}(k)$$

$$= \underbrace{s(k)}_{\substack{\text{information}\\ \text{symbol}}} \quad \underbrace{\frac{\alpha_{\mathrm{E}}\hat{\beta}_{\mathrm{E}}}{\sqrt{LN}}}_{\substack{\text{effective artificial}\\ \text{noise}}} \quad + \underbrace{z_{\mathrm{E}}(k)}_{\substack{\text{additive}\\ \text{noise}}}, \tag{16}$$

where the noise term $\hat{\beta}_{\mathrm{E}}$ is given by

$$\hat{\beta}_{\mathrm{E}} = \begin{cases} M + \sum_{n\in\mathcal{I}_L(k)} e^{-j\left(\frac{N-1}{2}-n\right)\gamma(\theta_i,\theta_{\mathrm{E}})}, & \text{if } \theta_{\mathrm{E}} = \theta_{\mathrm{S}} \\ N - M + \sum_{n\in\mathcal{I}_M(k)} e^{-j\left(\frac{N-1}{2}-n\right)\gamma(\theta_{\mathrm{S}},\theta_{\mathrm{E}})}, & \text{if } \theta_{\mathrm{E}} = \theta_i \end{cases} \tag{17}$$

and $\gamma(\theta_x,\theta_{\mathrm{E}}) = \frac{2\pi d}{\lambda}(\cos\theta_x - \cos\theta_{\mathrm{E}})$. From (17) we observe that the noise term $\hat{\beta}_{\mathrm{E}}$ consists of a constant term and a random term (function of transmit antenna sets and AoD). Hence, to maintain the randomness of the term $\hat{\beta}_{\mathrm{E}}$ both transmit subsets should be sufficiently large. This maximizes the randomness of $\hat{\beta}_{\mathrm{E}}$ and, as a result, the artificial noise at the eavesdropper.

IV. Performance Evaluation

In this section, we evaluate the performance of the proposed transmission techniques in terms of the achievable secrecy rate R (bits/s/Hz). It is assumed that all communication takes place during a fixed coherence interval in which the channel is assumed to known to both the transmitter and target receiver. Furthermore, for ease of exposition, we take a pessimistic approach and assumed that the eavesdropper is aligned with one of the transmitter's L paths.

The secrecy rate R is defined as

$$R = [\log_2(1+\mathrm{SNR}_{\mathrm{R}}) - \log_2(1+\mathrm{SNR}_{\mathrm{E}})]^{+}, \tag{18}$$

where $\mathrm{SNR}_{\mathrm{R}}$ is the SNR at the target receiver, $\mathrm{SNR}_{\mathrm{E}}$ is the SNR at the eavesdropper, and a^{+} denotes $\max\{0,a\}$. In the following, we derive the average SNR expressions for the proposed transmission techniques.

A. Random path selection

From (6), the SNR at the receiver can be expressed as

$$\mathrm{SNR}_{\mathrm{R}} = \frac{(\mathbb{E}[\alpha_i\sqrt{N/L}])^2}{\sigma_{\mathrm{R}}^2} = \frac{N\bar{\alpha}^2}{L\sigma_{\mathrm{R}}^2} = \frac{N\rho_{\mathrm{R}}}{L}, \tag{19}$$

where $\bar{\alpha}$ is the average channel gain of all transmit paths, and $\rho_{\mathrm{R}} = \frac{(\mathbb{E}[\alpha_i])^2}{\sigma_{\mathrm{R}}^2}$. From (19) we observe that the SNR at the target receiver deteriorates with increasing number of paths. This results as the total transmit power is spread among all L paths and weaker links will be utilized for transmission. However, as we will show in the derivation of the $\mathrm{SNR}_{\mathrm{E}}$ (see (20)), increasing the number of paths increases the artificial noise at the eavesdropper. Hence there is an optimal number of paths L that enhances the secrecy rate.

Similar to (19), the SNR at an eavesdropper can be expressed as (see (7))

$$\begin{aligned} \mathrm{SNR}_{\mathrm{E}} &= \frac{1}{L}\left(\frac{\alpha_{\mathrm{E}}^2 N}{L\sigma_{\mathrm{E}}^2}\right) + \left(1-\frac{1}{L}\right)\left(\frac{\alpha_{\mathrm{E}}^2(\mathbb{E}[B(\theta_l)])^2/LN}{\alpha_{\mathrm{E}}^2\mathrm{var}[B(\theta_l)]/LN + \sigma_{\mathrm{E}}^2}\right) \\ &= \frac{\rho_{\mathrm{E}}N}{L^2} + \left(1-\frac{1}{L}\right)\left(\frac{\rho_{\mathrm{E}}(\mathbb{E}[B(\theta_l)])^2}{\rho_{\mathrm{E}}\mathrm{var}[B(\theta_l)] + LN}\right) \end{aligned} \tag{20}$$

where $\rho_{\mathrm{E}} = \frac{\alpha_{\mathrm{E}}^2}{\sigma_{\mathrm{E}}^2}$, $\mathrm{var}[\alpha_{\mathrm{E}}B(\theta_l)/\sqrt{LN}] = \alpha_{\mathrm{E}}^2/LN\,\mathrm{var}[B(\theta_l)]$ represents the artificial noise variance, $\theta_l \in \Phi$, and

$$\mathbb{E}[B(\theta_l)] = \frac{N}{L}\sum_{l=1}^{L}\frac{\sin(N(\frac{\pi d}{\lambda}(\cos(\theta_{\mathrm{E}}) - \cos(\theta_l))))}{\sin((\frac{\pi d}{\lambda}(\cos(\theta_{\mathrm{E}}) - \cos(\theta_l))))}, \tag{21}$$

and

$$\mathrm{var}[B(\theta_l)] = \mathbb{E}[B(\theta_l)^2] - (\mathbb{E}[B(\theta_l)])^2. \tag{22}$$

The first term of (20) captures the eavesdropper SNR when it is aligned with one of the transmitter's AoD, i.e., $\theta_{\mathrm{E}} = \theta_l$. This occurs with probability $1/L$ as it is assumed that θ_{E} overlaps with one of the receiver's AoDs, and there are a total of L AoDs. The second term of (20) captures the eavesdropper SNR when it is not aligned with the transmitter's AoD, i.e., $\theta_{\mathrm{E}} \neq \theta_l$. This occurs with probability $1 - 1/L$. It is not difficult to observe from (20) that the eavesdropper's SNR deteriorates with increasing number of transmission paths.

 ISBN: 978-1-61208-828-0

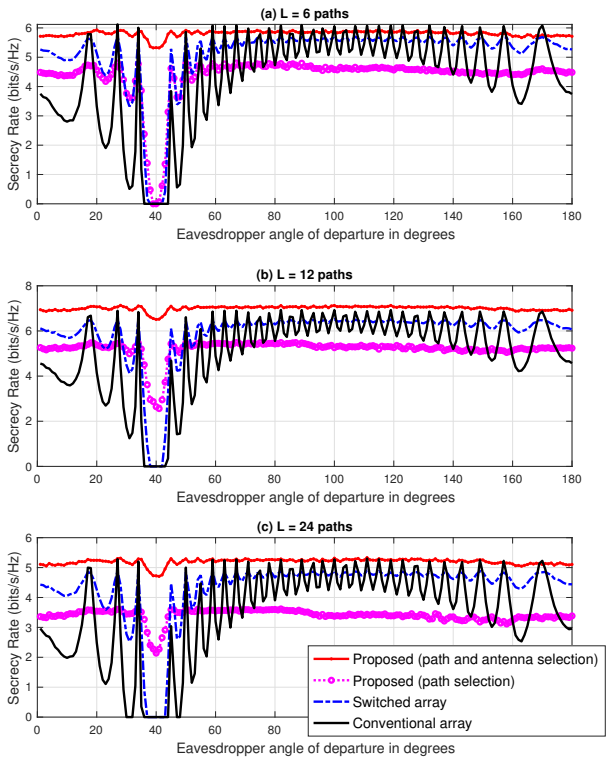

Figure 1. Secrecy rate versus the eavesdropper's angle of departure $\theta_{\rm E}$ for different number of transmission paths; $N = 32$ transmit antennas, $\rho_{\rm R} = 10$ dB, and $\rho_{\rm E} = 15$ dB.

B. Joint path and antenna selection

Using (12), the SNR at the target receiver can be expressed as

$$\text{SNR}_{\rm R} = \frac{(\mathbb{E}[\alpha_{\rm s} M + \alpha_i (N-M) + \beta_{\rm R}])^2}{LN\sigma_{\rm R}^2} \quad (23)$$

$$= \frac{\alpha_{\rm s}^2 M^2}{LN\sigma_{\rm R}^2} + \frac{(\bar{\bar{\alpha}}(N-M)^2}{LN\sigma_{\rm R}^2} + \frac{(\mathbb{E}[\beta_{\rm R}])^2}{LN\sigma_{\rm R}^2}, \quad (24)$$

where $\bar{\bar{\alpha}}$ is the average channel gain of all transmit paths, excluding the strongest path.

Similarly, using (14) and (16), the SNR at the eavesdropper can be expressed as

$$\text{SNR}_{\rm E} = \frac{2}{L}\left(\frac{\alpha_{\rm E}^2(\mathbb{E}[\hat{\beta}_{\rm E}])^2}{LN\sigma_{\rm E}^2}\right) + \left(1-\frac{2}{L}\right)\left(\frac{\alpha_{\rm E}^2(\mathbb{E}[\beta_{\rm E}])^2}{\alpha_{\rm E}^2 \text{var}[\beta_{\rm E}] + LN\sigma_{\rm E}^2}\right)$$

$$= \frac{2\rho_{\rm E}(\mathbb{E}[\hat{\beta}_{\rm E}])^2}{L^2 N} + \left(1-\frac{2}{L}\right)\left(\frac{\rho_{\rm E}(\mathbb{E}[\beta_{\rm E}])^2}{\rho_{\rm E}\text{var}[\beta_{\rm E}] + LN}\right), \quad (25)$$

where the expectation is over all transmit antennas and AoDs. The first term of (25) captures the eavesdropper SNR when it is aligned with one of the transmitter AoDs, i.e., $\theta_{\rm E} = \theta_{\rm s}$ or $\theta_{\rm E} = \theta_i$, and $\theta_i, \theta_{\rm s} \in \Phi$. This occurs with probability $2/L$. The second term of (25) captures the eavesdropper SNR when it is not aligned with the transmitter's AoD, i.e., $\theta_{\rm E} \neq \theta_i, \theta_{\rm s}$. This occurs with probability $1 - 2/L$. It is not difficult to see that $(\mathbb{E}[\hat{\beta}_{\rm E}])^2 < N^2$ in (25), and hence the first SNR term is lower than the first SNR term in (20).

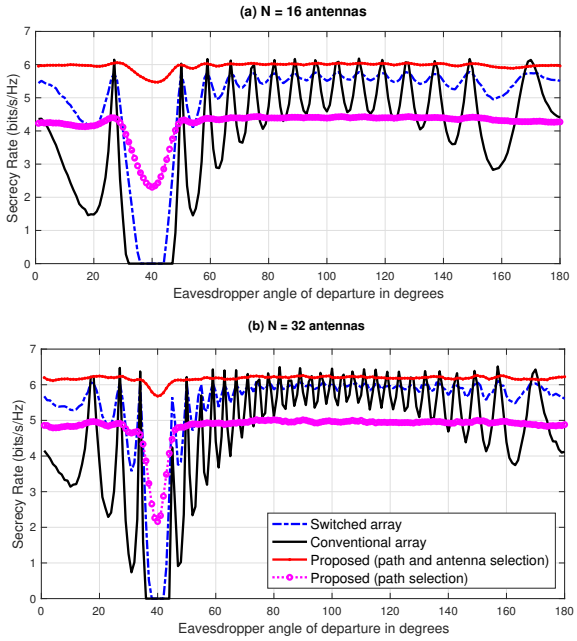

Figure 2. Secrecy rate versus the eavesdropper's angle of departure $\theta_{\rm E}$; $L = 12$ transmit path, $\rho_{\rm R} = 10$ dB, and $\rho_{\rm E} = 15$ dB.

V. Numerical Results and Discussions

In this section, we conduct numerical simulations to evaluate the efficacy of the proposed techniques. We consider a setup where a transmitter is communicating with a receiver in the presence of an eavesdropper. Both the transmitter and receiver are unaware of the eavesdropper's location. In this setup, the transmitter is equipped with a uniform linear array, with half wavelength separation, and the transmitter, receiver and eavesdropper have perfect knowledge of their channels. To benchmark the performance of the proposed techniques, we compare the secrecy rate achieved by the proposed techniques with the secrecy rate achieved when using conventional transmit antenna array, i.e., no action is taken at the transmitter, and the switched array technique proposed in [13] since it can be applied on analog antenna architectures. For all setups, we assume that the strongest transmit path to the target receiver is along a fixed AoD $\theta_{\rm R} = 40$ degrees, i.e., $\theta_{\rm R} = 40 \in \Phi$, and the remaining entries of Φ are randomly selected from the set $[1, 180]$ degrees. The channel gains are assumed to be normally distributed with zero mean and unit variance. Both the conventional array and switch antenna techniques always transmit along AoD $\theta_{\rm R} = 40$ degrees. When simulating the joint angle and antenna selection techniques, we assume that the secondary link is selected from the set of $L_{\rm S} = 5$ strongest paths and $M = N/2$.

To examine the performance of the proposed techniques, we plot the achievable secrecy rate when using the proposed techniques versus the eavesdropper AoD $\theta_{\rm E}$ in Figure 1. For all cases, we observe that the secrecy rate is higher when the eavesdropper AoD $\theta_{\rm E}$ does not overlap with the transmission AoD $\theta_{\rm R} = 40$ degrees. However, when $\theta_{\rm E} = 40$ degrees, i.e., the eavesdropper is located along one of the transmission path to the target receiver, we observe that all techniques suffer

 ISBN: 978-1-61208-828-0

a performance hit, with the conventional technique and the switched array technique achieving zero secrecy rate for all values of L. The proposed path selection technique is shown to achieve higher secrecy rate for higher number of paths while the proposed path and antenna selection technique achieves the best performance for all cases. The reason for this is that for low number of paths, the probability of intercepting a direct link when using the path selection technique is higher. This reduces the secrecy rate. The proposed path and antenna selection technique achieves the best performance as it randomizes both the transmit angle and antennas associated with each angle, thereby resulting in higher artificial noise at the eavesdropper.

In Figure 2, we examine the effect of the number of transmit antennas on the secrecy rate. For all techniques, we observe that increasing the number of antennas increases the secrecy rate and the proposed techniques achieve non-zero secrecy rates at $\theta_{\mathrm{E}} = 40$ degrees. This is achieved as higher number of antennas result in narrower beams and increased number of sidelobes. The increased number of sidelobe levels increases the variance of the artificial noise. The path selection technique is shown to achieve lower secrecy rate when the eavesdropper is not located along the main transmission path $\theta_{\mathrm{E}} \neq 40$ degrees. This rate loss is experienced as the path selection technique does not always use the best transmission path, but rather, it transmits along a set of paths, which contain weaker paths, to enhance the secrecy rate of the system.

To investigate the effect of the eavesdropper channel strength on the secrecy rate, we plot the secrecy rate versus the eavesdropper's average channel gain to noise ratio ρ_{E} when the eavesdropper is located along the transmitter's AoD $\theta_{\mathrm{E}} = \theta_{\mathrm{R}} = 40$ degrees in Figure 3, and when the eavesdropper is located along the transmitters sidelobe, i.e., $\theta_{\mathrm{E}} \neq \theta_{\mathrm{R}}$ in Figure 4. When the eavesdropper's communication link is weak, Figure 3 shows that all techniques achieve high secrecy rate. However, when the eavesdropper channel is stronger, the performance of both the switched-array and conventional array techniques plummet to zero, while the performance of the path selection technique deteriorates at a slower rate and the joint path and antenna selection technique deteriorates at a much slower rate as it achieves a higher artificial noise. When the eavesdropper is not located along the transmitter's AoD, Figure 4 shows that all techniques, except the conventional array technique, achieve high secrecy rate. The proposed joint path and antenna selection technique achieves the highest secrecy rate as it randomizes both the transmit AoD and transmit antenna sets, followed by the switched-array technique, and the proposed path selection technique. The path selection technique achieves a lower secrecy rate as it uses all paths (with potentially weaker paths) for communications, while the path and antenna selection technique always uses the strongest path and an auxiliary path for transmission. This results in a higher secrecy rate.

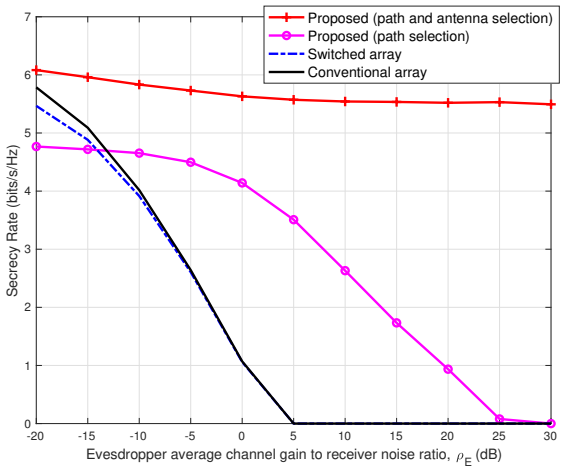

Figure 3. Secrecy rate versus ρ_{E}; $N = 32$ transmit antennas, $\rho_{\mathrm{R}} = 10$ dB, and $L = 12$ paths. Eavesdropper is located along AoD $\theta_{\mathrm{E}} = 40$ degrees.

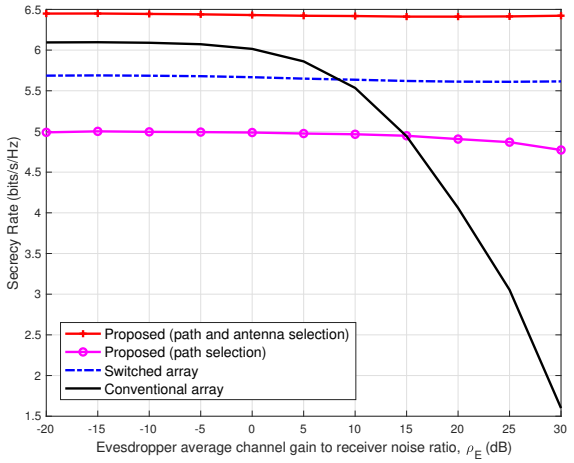

Figure 4. Secrecy rate versus ρ_{E}; $N = 32$ transmit antennas, $\rho_{\mathrm{R}} = 10$ dB, and $L = 12$ paths. Eavesdropper is located along AoD $\theta_{\mathrm{E}} = 55$ degrees.

VI. Conclusion

This paper addressed the problem of PLS in the presence of an eavesdropper with overlapped channel paths with the target receiver. Two transmission techniques suitable for mmWave systems with analog antenna architectures are proposed. Both techniques use random transmission paths, instead of a single or all paths, for data transmission. This results in noise-like signals at an arbitrary eavesdropper and improves the secrecy of the communication system. Numerical results show that in the presence of scatters, the proposed techniques achieve significantly higher secrecy rate when compared to conventional and switched array techniques. Note that the proposed techniques require the number of paths $L > 1$. For single path, i.e., LoS link, passive relays can be used to increase the number of transmission paths and induce randomness in the communication channel. Future work would focus on implementing a hardware prototype to investigate the efficacy of the proposed techniques.

Acknowledgment

This material is based upon work supported in part by the Sacramento State Research and Creative Activity Faculty Awards Program, California, USA.

 ISBN: 978-1-61208-828-0

REFERENCES

[1] F. Boccardi, R. Heath, A. Lozano, T. Marzetta, and P. Popovski, "Five disruptive technology directions for 5G," *IEEE Commun. Mag., vol. 52, no. 2, pp. 74-80, Feb. 2014.*

[2] Z. Pi and F. Khan, "An introduction to millimeter-wave mobile broadband systems", *IEEE Commun. Mag.,* vol. 49, no. 6, pp. 101-107, 2011.

[3] S. Pulipati et al., "Xilinx RF-SoC-based Digital Multi-Beam Array Processors for 28/60 GHz Wireless Testbeds," *2020 Moratuwa Engineering Research Conference (MERCon)*, Srilanka, Jul. 2020, pp. 1-6

[4] A. Alkhateeb, O. Ayach, and R. W. Heath Jr., "Channel estimation and hybrid precoding for millimeter wave cellular systems," *IEEE J. on Select. Areas in Commun.*, vol. 8, no. 5, pp. 831-846, Oct. 2014.

[5] M. E. Eltayeb, A. Alkhateeb, R. W. Heath Jr., and T. Y. Al-Naffouri, "Opportunistic Beam Training with Hybrid Analog/Digital Codebooks for mmWave Systems," *in IEEE Global Conference on Signal and Information Processing (GlobalSIP),* Dec. 2015, Orlando, Florida, USA.

[6] R. Khan, P. Kumar, D. N. K. Jayakody and M. Liyanage, "A Survey on Security and Privacy of 5G Technologies: Potential Solutions, Recent Advancements, and Future Directions," *in IEEE Communications Surveys & Tutorials,* vol. 22, no. 1, pp. 196-248, 2020.

[7] X. Wang et al., "Privacy-Preserving Content Dissemination for Vehicular Social Networks: Challenges and Solutions," *in IEEE Communications Surveys & Tutorials,* vol. 21, no. 2, pp. 1314-1345, 2019.

[8] M. E. Eltayeb, J. Choi, T. Y. Al-Naffouri, and R. W. Heath Jr., "Enhancing Secrecy With Multiantenna Transmission in Millimeter Wave Vehicular Communication Systems," *in IEEE Transactions on Vehicular Technology*, vol. 66, no. 9, pp. 8139-8151, Sept. 2017.

[9] A. N. Mohammed, M. E. Eltayeb, and I. Kostanic, "Channel Estimation in Millimeter Wave Systems with Inter Cell Interference," *in the 2019 IEEE 90th Vehicular Technology Conference,* Honolulu, HI, USA, 2019, pp. 1-5.

[10] H. M. Madni, M. S. Solaija, and H. Arslan, "Intelligent Physical Layer Security Approach for V2X Communication," arXiv:1905.05075, 2019.

[11] X. Sun, W. Yang, Y. Cai, L. Tao, and C. Cai, "Physical Layer Security in Wireless Information and Power Transfer Millimeter Wave Systems," *in the 2018 24th Asia-Pacific Conference on Communications (APCC),* Ningbo, China, 2018, pp. 83-87.

[12] M. E. Eltayeb, J. Choi, T. Y. Al-Naffouri, and R. W. Heath Jr., "On the Security of Millimeter Wave Vehicular Communication Systems Using Random Antenna Subsets," *in the 2016 IEEE 84th Vehicular Technology Conference*, Montreal, QC, 2016, pp. 1-5.

[13] N. Valliappan, A. Lozano, and R. W. Heath, "Antenna Subset Modulation for Secure Millimeter-Wave Wireless Communication," *in IEEE Transactions on Communications,* vol. 61, no. 8, pp. 3231-3245, August 2013.

[14] Y. Hong, X. Jing, and H. Gao, "Programmable Weight Phased-Array Transmission for Secure Millimeter-Wave Wireless Communications," *in IEEE Journal of Selected Topics in Signal Processing,* vol. 12, no. 2, pp. 399-413, May 2018.

[15] H. Jung and I. Lee, "Secrecy Rate of Analog Collaborative Beamforming With Virtual Antenna Array Following Spatial Random Distributions," *in IEEE Wireless Communications Letters,* vol. 7, no. 4, pp. 626-629, Aug. 2018.

[16] H. Jung and I. Lee, "Secrecy Performance Analysis of Analog Cooperative Beamforming in Three-Dimensional Gaussian Distributed Wireless Sensor Networks," *in IEEE Transactions on Wireless Communications,* vol. 18, no. 3, pp. 1860-1873, Mar. 2019.

[17] H. Jung and I. Lee, "Distributed Null-Steering Beamformer Design for Physical Layer Security Enhancement in Internet-of-Things Networks," *in IEEE Systems Journal*, doi: 10.1109/JSYST.2020.2967404.

[18] M. E. Eltayeb and R. W. Heath Jr., "Securing mmWave Vehicular Communication Links with Multiple Transmit Antennas," *in the 2018 IEEE International Conference on Communications Workshops (ICC Workshops)*, Kansas City, MO, 2018, pp. 1-6.

[19] Y. Hong, X. Jing, Y. He, and J. Mu, "Dynamic Rotated Angular Beamforming Using Frequency Diverse Phased-Array for Secure MmWave Wireless Communications," Electronics 2020.

[20] Y. Ju, H. Wang, T. Zheng, Q. Yin, and M. H. Lee, "Safeguarding Millimeter Wave Communications Against Randomly Located Eavesdroppers," *in IEEE Transactions on Wireless Communications,* vol. 17, no. 4, pp. 2675-2689, April 2018.

[21] Y. R. Ramadan and H. Minn, "Artificial Noise Aided Hybrid Precoding Design for Secure mmWave MISO Systems With Partial Channel Knowledge," *in IEEE Signal Processing Letters,* vol. 24, no. 11, pp. 1729-1733, Nov. 2017.

[22] P. Bahl and V. N. Padmanabhan, "RADAR: an in-building RF-based user location and tracking system," *in Proc. of the IEEE INFOCOM,* Mar. 2000, pp. 775-784.

[23] A. Alkhateeb, "DeepMIMO: A Generic Deep Learning Dataset for Millimeter Wave and Massive MIMO Applications", arXiv:1902.06435, Feb. 2019.

[24] V. Va, J. Choi, T. Shimizu, G. Bansal, and R. W. Heath, "Inverse Multipath Fingerprinting for Millimeter Wave V2I Beam Alignment," *in IEEE Transactions on Vehicular Technology,* vol. 67, no. 5, pp. 4042-4058, May 2018.

 ISBN: 978-1-61208-828-0